HEAT REMOVAL FROM A LARGE SCALE WARM WATER STORAGE

A THESIS SUBMITTED TO
THE GRADUATE SCHOOL OF NATURAL AND APPLIED SCIENCES
OF
MIDDLE EAST TECHNICAL UNIVERSITY

BY

YAVUZ SELİM KAYSERİLİOĞLU

IN PARTIAL FULFILLMENT OF THE REQUIREMENTS
FOR
THE DEGREE OF MASTER OF SCIENCE
IN
MECHANICAL ENGINEERING

AUGUST 2004

Approval of the Graduate School of Natural and Applied Sciences

_____

Prof. Dr. Canan Özgen
Director

I certify that this thesis satisfies all the requirements as a thesis for the degree of Master of Science.

_____

Prof. Dr. Kemal İder
Head of Department

This is to certify that we have read this thesis and that in our opinion it is fully adequate, in scope and quality, as a thesis for the degree of Master of Science.

_____

Prof. Dr. Rüknettin Oskay
Supervisor

Examining Committee Members

Prof. Dr. Faruk Arınç (METU, ME)_____

Prof. Dr. Rüknettin Oskay (METU, ME)_____

Prof. Dr. Zafer Dursunkaya (METU, ME)_____

Assoc. Prof. Dr. Cemil Yamalı (METU, ME)_____

Prof. Dr. Canan Özgen (METU, ChE)_____

I hereby declare that all information in this document has been obtained and presented in accordance with academic rules and ethical conduct. I also declare that, as required by these rules and conduct, I have fully cited and referenced all material and results that are not original to this work.

Name, Last name :Yavuz Selim KAYSERİLİOĞLU

Signature :

ABSTRACT

HEAT REMOVAL FROM A LARGE SCALE WARM WATER STORAGE

Kayserilioğlu, Yavuz Selim
M.S., Department of Mechanical Engineering
Supervisor: Prof. Dr. Rüknettin Oskay
August 2004, 88 Pages

A preliminary experimental study was performed in order to investigate the charging and heat removal characteristics of a sensible heat storage. Two sets of experiments were performed at two aspect ratios. Heat removal processes of these two sets were different while the charging processes were similar. In the first set of experiments, after the charging of the storage unit with relatively warm water was complete, heat removal process was started with simple heat exchangers from different elevations within the storage while the charging of the storage unit was continued. In the second set of experiments, after the charging of the storage unit was complete, heat removal from the storage unit was started without further charging of the storage unit.

Charging water was fed into the storage from the top of one side and relatively colder water was drained from the bottom of the opposite side. Internal heat exchangers were used for the heat removal. Vertical temperature profile developments during the charging and heat removal periods were investigated. Thermal stratification was observed in all experiments. Heat exchangers extracted heat from different elevations in different experiments and the trend was that more heat can be extracted in upper elevations. Comparable heat can be extracted from the same elevation of lower and higher aspect ratio.

Keywords: Sensible Heat Storage, Heat Removal, Thermal Stratification, Warm Water Storage

ÖZ

BÜYÜK ÖLÇEKLİ SICAK SU DEPOSUNDAN ISI ÇEKME

Kayserilioğlu, Yavuz Selim
Yüksek Lisans, Makine Mühendisliği Bölümü
Tez Yöneticisi: Prof. Dr. Rüknettin Oskay
Ağustos 2004, 88 Sayfa

Bir duyulur ısı deposunun depolama ve ısı çekme özellikleri başlangıç niteliğindeki bir deneysel çalışmada incelendi. İki tür deney iki ayrı boyut oranında yapıldı. Bu iki tür deneyde birimin depolanması eşken ısı çekme süreçleri farklıdır. İlk tür deneyde depolama biriminin tam beslenmesi bittiğinde sıcak su beslemesi kesilmeden basit ısı geçirgeçlerinin kullanımı ile değişik seviyelerden ısı çekme başlatıldı. İkinci tür deneyde ısı çekme, ısı depolamasının bitiminde sıcak su beslemesinin kesilmesi ile başlatıldı.

Besleme suyu birime birimin bir yüzeyinin tepesinden verilirken soğuk boşaltma suyu karşı yüzeyin dibinden alındı. Isı çekme için birim içi ısı geçirgeçleri kullanıldı. Dikey sıcaklık profillerinin depolama ve ısı çekme süreçlerindeki gelişimi incelendi. Her deneyde ısıl tabakalanma görüldü. Isı geçirgeçleri değişik deneylerde farklı seviyelerden ısı çekti. Deponun üst seviyelerinden daha çok ısı çekilebileceğine dair bir eğilim gözlendi. Düşük ve yüksek boyut oranlarında eşit derinlikten denk ısı çekilebilmektedir.

Anahtar Kelimeler: Duyulur Isı Depolama, Isı Çekme, Isıl Tabakalanma, Sıcak Su Deposu

To My Parents

ACKNOWLEDGEMENTS

I am deeply grateful to my supervisor, Prof. Dr. Rüknettin OSKAY, for his guidance, inspiration, and invaluable help all throughout the study.

I wish to express my sincere appreciation to Mustafa YALÇIN for his qualified work during the preparation of the set-up and his continual help and friendship during the experiments.

I am grateful to my colleague Nagihan TOPCU for her practical help during the writing of this thesis.

Finally, I express my deepest gratitude to my family, for their continuous encouragement, understanding, and support.

TABLE OF CONTENTS

LIST OF TABLES

LIST OF FIGURES

NOMENCLATURE

A	area, m^2
A	aspect ratio, H/L
B	width of storage medium, m
c_p	constant pressure specific heat, J/kgK
c_v	constant volume specific heat, J/kgK
D_{aw}	binary diffusion coefficient, m^2/s
d	relative location of heat removal tubes from free surface, m
E	energy, J
e	specific energy, J/kg
H	height of storage medium, m
H	enthalpy, J
$\dot{H}$	enthalpy flow rate, W
h	specific enthalpy, J/kg
h	convective heat transfer coefficient, W/m^2K
h_{fg}	latent heat of vaporization, J/kg
k	thermal conductivity, W/mK
L	length of storage medium, m
Le	Lewis number, α / D_{ab}
m	mass, kg
$\dot{m}$	mass flow rate, kg/s
Nu	Nusselt number, hL / k
P	pressure, mmHg
Pr	Prandtl number, ν / α
Q	heat transfer, J
$\dot{Q}$	rate of heat transfer, W
Ra	Rayleigh number, $g\beta(T_s - T_\infty) L_{ch}^{\ 3} / \nu\alpha$
T	temperature, °C

t	time, s
U	internal energy, J
u	specific internal energy, J/kg
V	velocity, m/s
V	volume, m^3
$\mathbf{v}$	velocity vector, m/s
W	work, J
w	specific humidity ratio, kg_w/kg_a
x	Cartesian coordinate along length
y	Cartesian coordinate along width
z	Cartesian coordinate along depth

Greek Symbols

α	thermal diffusivity, m^2/s
β	thermal expansion coefficient, 1/K
ε	effectiveness of storage unit, $\Delta U_{stored}/\Delta H_{net}$
ϕ	relative humidity, %
ν	kinematic viscosity, m^2/s
ρ	density, kg/m^3
θ	dimensionless bulk temperature, $(T_b\text{-}T_0)/(T_i\text{-}T_0)$

Subscripts

a	air
amb	ambient
b	bulk
ch	characteristic
$conv$	convective
e	exit

evap	evaporative
f	film
i	inlet
L	limiting value
m	mass transfer
o	outlet
rem	removed
s	surface
w	water
ws	water at saturation
0	initial
∞	free stream

Abbreviations

c.s.	control surface
c.v. or CV	control volume

CHAPTER 1

INTRODUCTION

Energy storage systems involve the collection and retention of readily available energy for later use. There are four main modes of energy storage; electrical, mechanical, chemical, and thermal. Among these, thermal energy storage is attractive for the applications related to waste heat recovery, solar energy utilization, and peak electricity.

Thermal energy can be stored as sensible heat, as latent heat of phase change, or in a reversible chemical reaction. Latent heat can be stored within a medium undergoing a phase change. For example, during boiling of a liquid, heat of vaporization is stored in its vapour and this stored energy can be released during the condensation of the vapour. Thermal energy can be stored in a reversible chemical reaction. During an endothermic reaction, energy is stored and when the reaction is reversed, the exothermic reaction releases the stored energy.

Sensible heat storage systems utilize materials that store energy as sensible heat, thus the temperature of storage medium changes as it stores or discharges thermal energy. The sensible heat gained or lost by a material during a change in temperature from T_1 to T_2 can be written as;

$$Q = V \int_{T_1}^{T_2} \rho c dT$$

where Q : sensible heat gained or lost

T : temperature of the material

ρ : density of the material

V : volume of the material

Liquids and solids are used as the storage media. Most commonly used solids as the solid storage media are rocks and pebble beds. Water is the most common liquid used as liquid storage media.

Some of the adventages of using water as the sensible heat storage medium are:

- it is cheap and abundant
- has relatively high heat capacity (more than five times that of granite)
- has lower density compared to rocks
- non-toxic, non-combustible.

General operational problems of sensible heat storage systems can be summarized as [1]:

- Temperature of the storage continually rises during charging which results in greater heat loss.
- Temperature of the storage continually drops during heat discharge which results smaller heat flux deliveries.
- Heat storage occurs at temperatures higher than ambient temperature. Therefore insulation is required, and adding to system cost.

The temperature distribution within the sensible liquid storage medium can be isothermal as it is in a well-mixed liquid storage or can be non-uniform as it is in thermally stratified storage.

Thermal stratification is a kind of non-uniform temperature distribution in a body. It occurs especially in the vertical direction within a water storage tank. The relatively warmer water entering the storage unit is lighter than the relatively colder water inside the storage tank and remains on top of the relatively cold water of the storage, resulting in non-uniform temperature distribution in the vertical direction. The benefit of thermal stratification in a water storage is that

liquid at a higher temperature than the overall mixed temperature can be stored at the top of the storage medium.

The main objective of the present study is the utilization of an energy storage facility, i.e. water reservoir, under varying storage and load conditions. The experiments were performed on the set-up in Heat Transfer Laboratory of ME Department of METU. It is actually a sensible heat storage unit utilizing water as the storage medium. Two sets of experiments were performed. Heat removal processes of these two sets were different while the charging processes were similar.

In the first set of experiments, after the charging of the storage unit with relatively warm water was complete, heat removal process was started with simple heat exchangers from different elevations within the storage while the charging of the storage unit was continued. This resembles the utilization of a storage unit under the continuous energy charging from a waste heat source.

In the second set of experiments, after the charging of the storage unit was complete, heat removal from the storage unit was started without further charging of the storage unit. This was done to simulate the day-time charging by the hot water coming from solar collectors and at night discharging of the stored energy.

CHAPTER 2

LITERATURE REVIEW

Some of the aspects that are important in the evaluation of storage performance of a sensible storage may be classified as follows; the velocity and temperature of the inlet flow charging the storage medium, relative locations of the inlet and outlet channels or ports with respect to the storage geometry, boundary conditions of the storage medium, especially at the surface if there is a free surface with the ambient, aspect ratio dictated by the storage medium (*L/D* for cylindrical geometries, *L/H* for rectangular geometries) and the thermal stratification inside the the storage medium. Following is a review of some of the papers available in the literature dealing with these aspects.

Oberkampf and Crow [2] simulated the velocity and temperature fields in a reservoir by using a finite difference procedure. They assumed the flow inside the reservoir to be two-dimensional in a vertical plane. The inflow was set at a temperature value and velocity to simulate thermal discharge from a power plant and occured at the surface at one end of the reservoir and outflow occured on the opposite end at different depths. Wind shear, thermal radiation, evaporation, convection at the surface of the reservoir were considered. They discussed the effects of inflow-outflow, wind shear and heat transfer on the reservoir.

Lavan and Thompson [3] studied thermal stratification in hot water storage systems. Cylindrical plastic vessels with various length to diameter ratios were charged with varying inlet-outlet temperature differences and mass flow rates. They also studied inlet and exit port configuration on thermal stratification. They concluded that, even at very large flow rates, thermal stratification could be maintained in cylindrical water tanks. Increasing *L/D* and inlet and outlet port diameter, decreasing mass flow rate improved thermal stratification. They

obtained best results when the inlet and outlet ports were near the end walls of the storage tank.

Çömez [4] designed and constructed a sensible heat storage unit as part of his M.S. Study. The same set-up was used in the current study with major alterations and component additions.

Author observed the development of temperature and velocity profiles experimentally within the storage unit. The main parameters investigated for the evaluation of performance of the storage unit were the charging flow rate, charging temperature and aspect ratio ($A = H/L$) of the water body.

Two dimensionless parameters were defined, the effectiveness, ε, was related to the percentage of input energy which could be stored inside the storage unit and a dimensionless temperature θ, represented a mean bulk temperature for the storage medium.

The main conclusions that the author derived were as follows. The storage medium could be thermally stratified for all of the charging mass flow rates. Better stratification was observed at lower charging rates. Aspect ratio was an important parameter affecting the performance of the storage unit. Lower aspect ratios gave better storage performance. Slow moving convective currents were observed during the flow visualization tests.

Jaluria and Gupta [5] carried out an experimental study of the temperature decay in a thermally stratified water body. Water body was initially stratified by the recirculating flow of hot water discharge and by the addition of hot water at the top of the colder fluid. After the fluid was stratified, it was allowed to cool without any external charging of the storage. They also investigated the cooling of an isothermal water region. Greater buoyancy-induced mixing was observed in isothermal case, since stratified region inhibited mixing currents and energy

transfer in this region was mainly by thermal diffusion. They concluded that stratified medium was a better energy storage system compared to the isothermal one. Experimental results indicated that the temperature field was largely one-dimensional and they formulated a simple analytical model. Analytical results were in good agreement with the experimental results.

Jaluria and O'Mara [6] studied experimentally the recirculating flow in an enclosed water region due to the discharge of heated, buoyant, surface jets, coupled with withdrawal of cold fluid at the other end of the region. They determined both the transient and steady-state temperature fields. Effects of inflow conditions, flow configuration, enclosure dimensions and the outlet location on the temperature field were examined. They investigated the downward penetration of the flow and thermal stratification in the region. They found that the temperature field in the water body undergoes a rapid transient behaviour at the beginning of the flow, followed by a gradual variation to steady-state conditions. Inlet conditions and outlet location determined the transient behaviour. An interesting finding was that the temperature field they obtained was mainly two-dimensional, only a small variation was observed in the transverse direction. Buoyancy affected mainly the temperature distribution inside the water body. It was the cause of a fairly good horizontal temperature homogeneity except the proximity of inlet and outlet channels.

Yoo and Pak [7] studied a theoretical model of the charging process to provide an upper limit of the performance for stratified thermal storage tanks. They reached a closed-form solution for the transient temperature as a function of Peclet number, Pe, assuming perfect piston flow together with appropriate boundary conditions and applying Laplace transform. They compared the model with those from heat conduction between two semi-infinite regions in contact with the moving interface. They concluded that the model could be used for a wider range of Pe, and predicted the thermal behaviour of storage tank better compared to the semi-infinite case.

Safi and Loc [8] performed a numerical study for the determination of thermal stratification in an open cavity with one heated discharge. Hot laminar jet entered horizontally into the square cavity at the top of one end, the outlet was at the bottom of the opposite end. They used a finite difference scheme to solve two-dimensional flow described by the Navier-Stokes and energy equations. The influences of nondimensional parameters of Reynolds, Peclet and Richardson numbers on the flow and thermal stratification were observed. Authors concluded that the flow was strongly dependent on Richardson and Peclet numbers.

Eames and Norton [9] performed a theoretical and experimental study to investigate the thermal performance of stratified hot water stores. They compared their transient three-dimensional finite volume model with the experiments they performed. Variations in inlet velocities, temperatures and initial store stratification were the main concerns. Authors reported that store charging was more efficient when *H/D* of the store increased and inlet port located near to the top of the store.

Spall [10] studied numerically the natural stratification of turbulent flows in an axisymmetric, cylindrical, chilled-water storage tank. Turbulence models were k-ε and full Reynolds stress turbulence closure. In the calculations, cold water injected through a slot in the base of the insulated tank, within which isothermal water was initially at rest. The calculations were based on inlet Reynolds number in the range 500-3000, and Archimedes number in the range 0.5-5.0. Author concluded that stratified flow within the storage could be achieved when Archimedes number was greater than two, independent of inlet Reynolds number.

Hahne and Chen [11] investigated numerically the flow and heat transfer characteristics of a cylindrical store during charging under adiabatic conditions. The study is concentrated on the effects of charging temperature differences, charging velocities, charging flow rates and length to diameter ratios on the charging efficiency. The conclusions were; charging efficiency depended mainly on Richardson number, Peclet number and aspect ratio of the storage. An increase

in Richardson number or aspect ratio revealed an increase in charging efficiency. An increase in Peclet number when Richardson number kept constant, increased charging efficiency.

Alizadeh [12] studied experimentally and numerically the thermal behaviour of a horizontal cylindrical storage tank. Cold water was injected from the bottom of the storage tank, within which three different initial temperature fields existed. In the first set of experiments, the storage tank was stratified and the temperature at the bottom of the tank was the same as the inflow temperature. In the second set, the tank was again initially stratified while the bottom temperature was relatively higher than the inflow temperature. Third set included an initially heated isothermal storage. The conclusion on the experiments was that the second set of experiments gave slightly better performance. Two different types of one-dimensional numerical models were developed. It was concluded that the two numerical models, Turbulent Mixing Model and Displacement Mixing Model, were in good agreement with the experiments.

Yoo et al. [13] proposed an approximate analytical solution to the two-region one-dimensional model describing the charging process of stratified thermal storage tanks with variable inlet temperature as well as momentum induced mixing. They decomposed an arbitrarily varying inlet temperature into a number of continuous changes. Each continuous interval was approximated as a set of piecewise linear functions. They ended up an analytical solution to the temperature of the perfectly mixed region. Three different types of function were found. The linear combination of these constant, linear and exponential functions were used to determine the temperature profile of the plug flow region.

According to Bouhdjar and Harhad [14], thermal stratification generated in the sensible heat storage should be promoted in order to improve thermodynamic system efficiency of the storage. They presented a numerical study of transient mixed convection. The use of different fluids (Torada oil, ethylene glycol, and water) as a heat storage medium in cylindrical cavities with different aspect ratios

(3 to 1/3) were examined. The effect of different fluids was observed by changing the physical properties represented by the Prandtl number. Fluid was injected from the top and discharged from the bottom. They solved conservation equations for laminar natural convection flow with Boussinesq approximation and superimposed forced convection using finite volume method. They presented the performances of the thermal energy storage through the transient thermal storage efficiency.

In the study of Shin et al. [15], a series of numerical investigation with bench scale experiments was performed in order to figure out the flow characteristics and thermal stratification of a vertical cylindrical storage tank. The major parameters were the size of the storage tank, charging water rate, temperature difference between charging water and colder reservoir.

CHAPTER 3

EXPERIMENTAL SET-UP

3.1 Description of the Experimental Set-up

A schematic view of the set-up is shown in Figure 3.1. It consists of:

i. Warm water production unit

ii. Warm water storage unit and heat removal tubes

iii. Discharge unit.

i.1. Main storage tank: has a volume of 1 m^3, located 2.25 m above the floor. This head drives the main water flow through the system. Water level inside the main storage tank is kept nearly constant by supplying tap water into it either during the experiments or before the experiments.

i.2. Warm water production chamber: is a cylindrical tank 50 cm in diameter and 60 cm in height. It consists of 4 electric heaters. The capacity of each heater is 1.5 kW and each heater has its own thermostat. The heaters are horizontally placed at different levels inside the warm water production chamber. A rheostat is connected to one of the electric heaters to compensate for potential variations in electricity. Relatively cold water coming from the main storage tank is fed at the bottom of the chamber, is heated inside the chamber, and leaves the chamber from the top. Warm water production chamber is insulated.

i.3. Mixing chamber: warm water from the warm water production chamber is mixed inside the mixing chamber in order to eliminate local temperature variations and air bubbles. There is an overflow piping for the mixing chamber, hence a constant water level inside the chamber can be maintained by allowing a small amount of water to be drained through the overflow piping. Mixing chamber is insulated against losses.

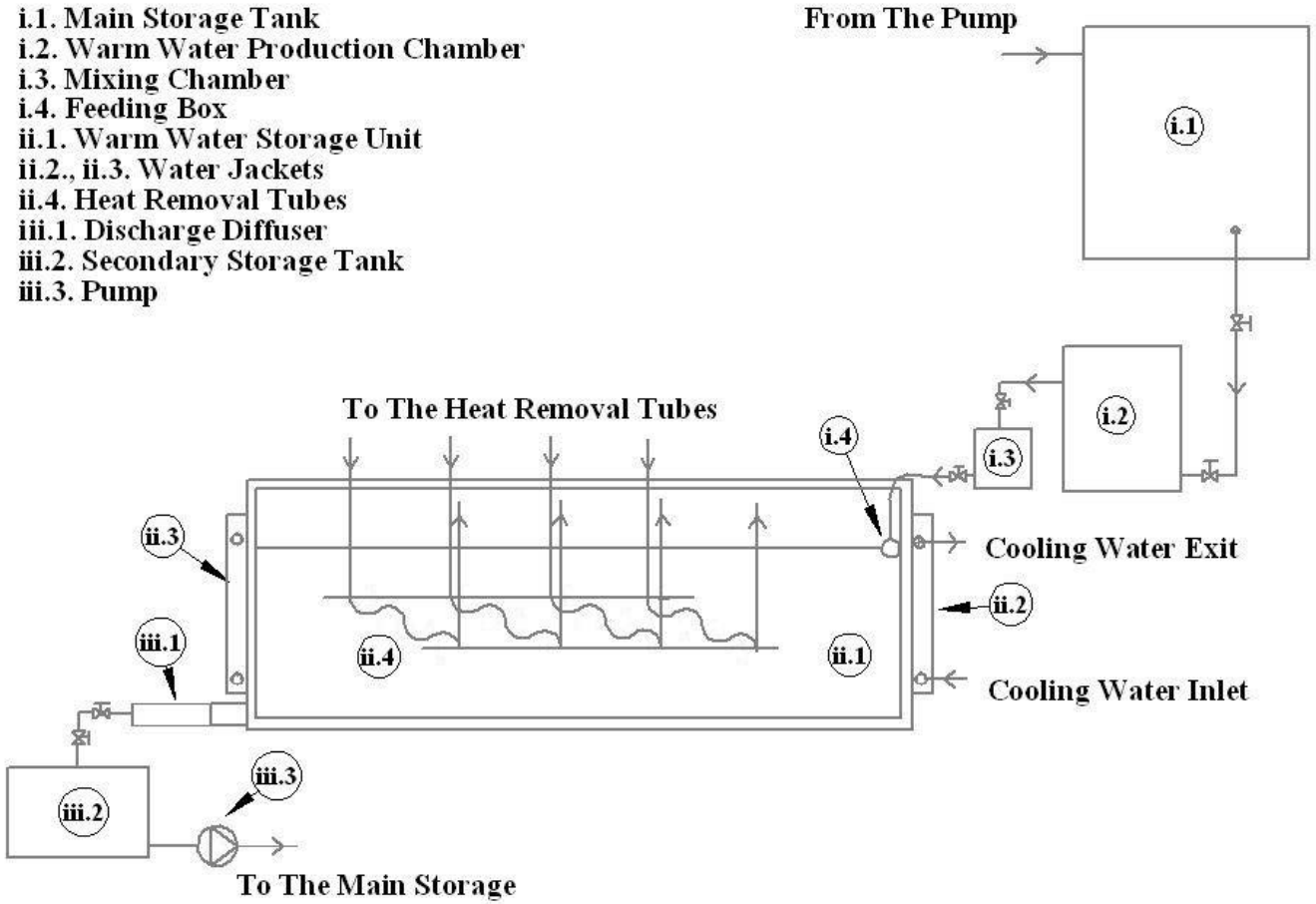

Figure 3.1 Schematic Drawing of the Set-up

i.4. Feeding box: is the inlet of the warm water storage unit manufactured from a 2 in galvanized steel 0.95 m long, closed at both ends. It enhances 1-D (horizontal) charging flow to the storage unit. To achieve this, feeding box has a 15 mm height slit extending parallel to the axis of the pipe. 19 rubber hoses carry the water from the mixing chamber to the feeding box. Every hose has its own valve, and during the experiments at least 6 of the hoses (distributed evenly through the feeding box) were open and were adjusted evenly to further enhance 1-D charging flow to the storage unit. The valves serve a mean for fine adjustment of the mass flow rate of charging water to the storage unit. Two power screws are welded to the two closed sides of the feeding box. With these power screws, the feeding box can be suspended from the frame of the storage tank at different elevations. The height of the inlet of the storage tank can be varied, thus different aspect ratios could be tried.

ii.1. Warm water storage unit: is the model of large scale warm water storage. The dimensions are ($0.975 \times 1.99 \times 0.75$) m, first one being the width, second one the length, and the third one the height. Inlet and exit surfaces are covered with water jackets. The other two side surfaces are from glass for flow visualization. The bottom surface is insulated, while the top surface is exposed to ambient air. Charging water enters the warm water storage tank from the feeding box located at the top of one side of the storage tank, while relatively colder fluid leaves the storage tank from the bottom of the opposite side into the discharge diffuser. A photograph of warm water storage unit is given in Figure 3.3.

ii. 2, ii.3. Water jackets: These are two heat exchangers attached to the inlet and exit sides of the storage tank. Tap water is circulated through the water jackets to simulate side losses from the storage tank. Tap water enters from the bottom of the heat exchangers, extracts heat from the storage unit, and leaves from the top of the exchangers with a few degrees elevated temperature. Without the side loss effect of these two heat exchangers, only weak thermal stratification inside the warm water storage tank could be achieved.

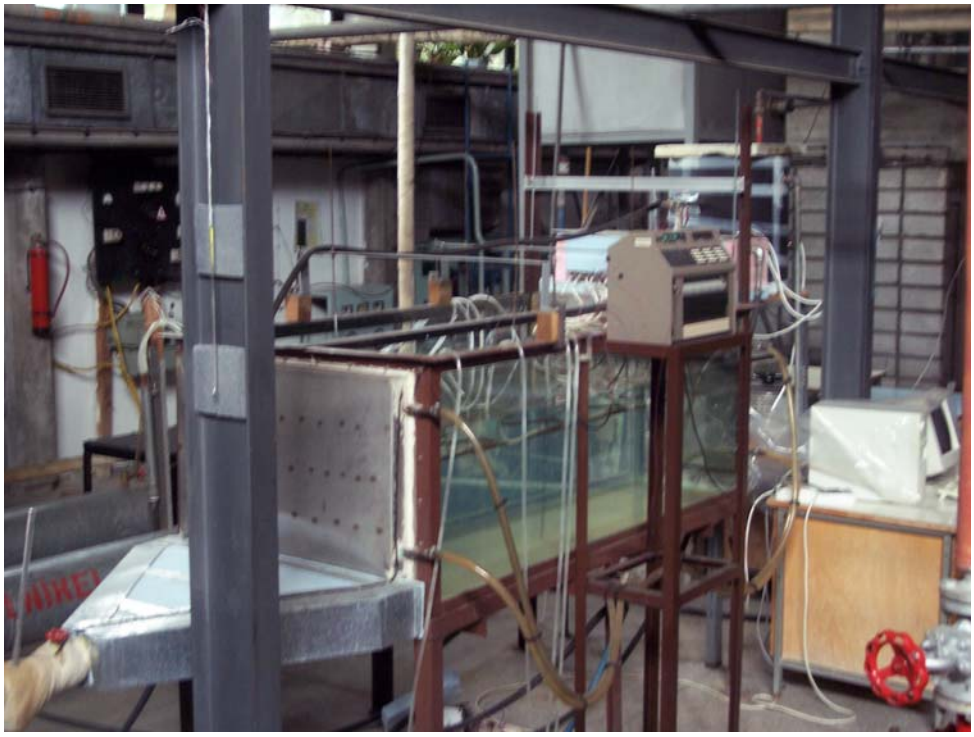

Figure 3.2 A View of the Set-up

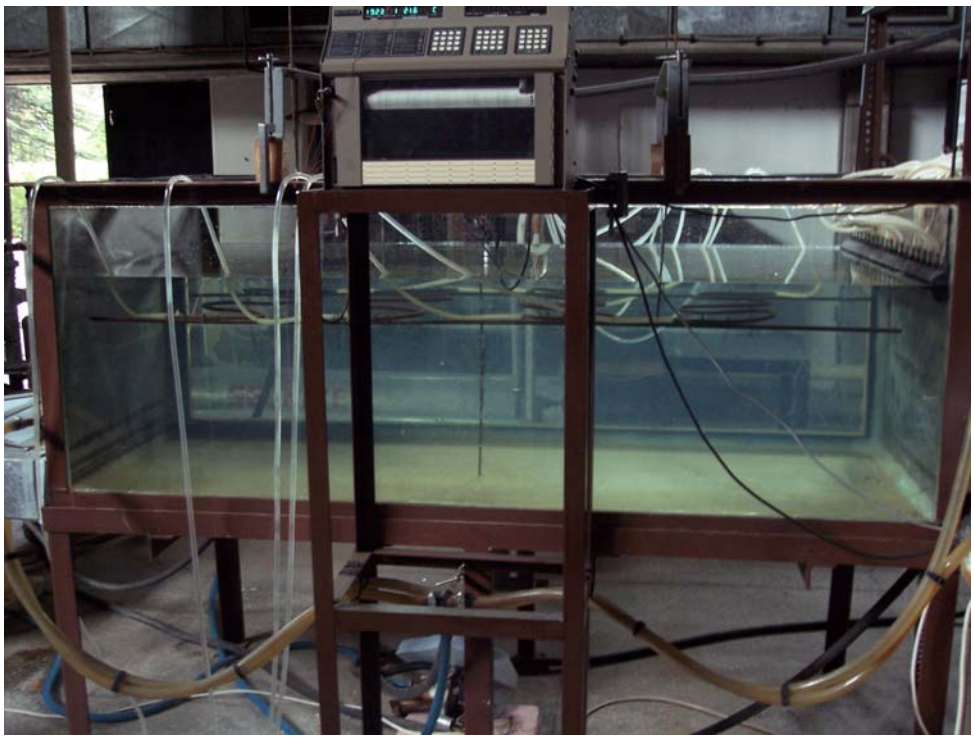

Figure 3.3 Warm Water Storage Unit and Heat Removal Tubes

ii. 4. Heat removal tubes: there are 4 copper heat removal tubes to extract heat from the warm water storage unit. Outer diameter of the tubes is 1 cm and the length of each tube is 140 cm. Heat removal tubes are suspended inside water at the same level with two brass rods. Brass rods are suspended with 4 power screws to the frame of the storage unit. Power screws are utilized to change the depth of the heat removal tubes to extract heat at different levels of the storage unit. Once a steady-state thermal stratification inside the storage unit is achieved, tap water is circulated through the heat removal tubes to extract thermal energy from the storage medium.

iii. 1. Discharge diffuser: is utilized to maintain a regulated outflow from the storage tank. There is a valve at the end of the diffuser to adjust the mass flow rate of discharged water. Discharged water temperature is measured at the end of the diffuser, so it is insulated against losses.

iii. 2. Secondary storage tank: water discharged from the storage unit is collected inside the secondary storage tank. A float is mounted inside this tank to drive the pump.

iii. 3. Pump: A 150 Watt pump is used to pump up the water collected inside the secondary storage tank back to the main storage tank.

3.2 Measurement Techniques

3.2.1 Flow Rate Measurements

Flow rate of charging water is adjusted by changing the number of open rubber hoses between the mixing chamber and feeding box. Fine tuning is then made with the help of the valves that each rubber hose has. Water level inside the mixing chamber is tried to be kept constant in order to have a constant head for the charging water. Flow rate of discharged water is measured and the water level

inside the warm water storage unit is tried to be kept constant by tuning the discharged water flow rate with the valve at the end of the discharge diffuser. Total flow rate of water passing through the four heat removal tubes is measured by summing up the four water streams at one location. Flow rate of cooling water passing through the water jackets is also measured.

3.2.2 Temperature Measurements

23 copper-constantan thermocouples and 3 thermometers are used during the experiments. The locations that the thermocouple measurements recorded are:

- one thermocouple measures the charging water temperature inside the mixing chamber before it is fed to the feeding box.
- one thermocouple measures the discharged water temperature at the end of the discharge diffuser.
- two thermocouples measure the cooling water temperatures at the inlets of the water jackets.
- two thermocouples measure the cooling water temperatures at the outlets of the water jackets.
- one thermocouple measures the common water temperature at the inlets of the heat removal tubes.
- four thermocouples measure the water temperatures at the outlets of the heat removal tubes.
- twelve thermocouples on a temperature probe (Figure 3.4) measure the water temperature inside the warm water storage unit along the depth of the storage unit.

Ambient temperature is measured by a precision thermometer. Charging water and discharged water temperatures are also measured by precision thermometers in order to check the thermocouple readings at those locations.

Temperature probe (made of copper) is used to suspend twelve thermocouples inside the warm water storage unit. The probe can be traveled inside the warm

water storage tank. It can be moved along the slot of the slot-carriage so that it can travel between the inlet and exit side surfaces of the storage unit. The slot carriage itself can be moved so that the temperature probe can travel between the other two side surfaces made of glass. The locations of the 12 thermocouple hot junctions from the bottom tip of the probe are shown in Table 3.1. During the experiments, 5 mm offset is given between the bottom tip of the probe and the bottom surface of the storage unit.

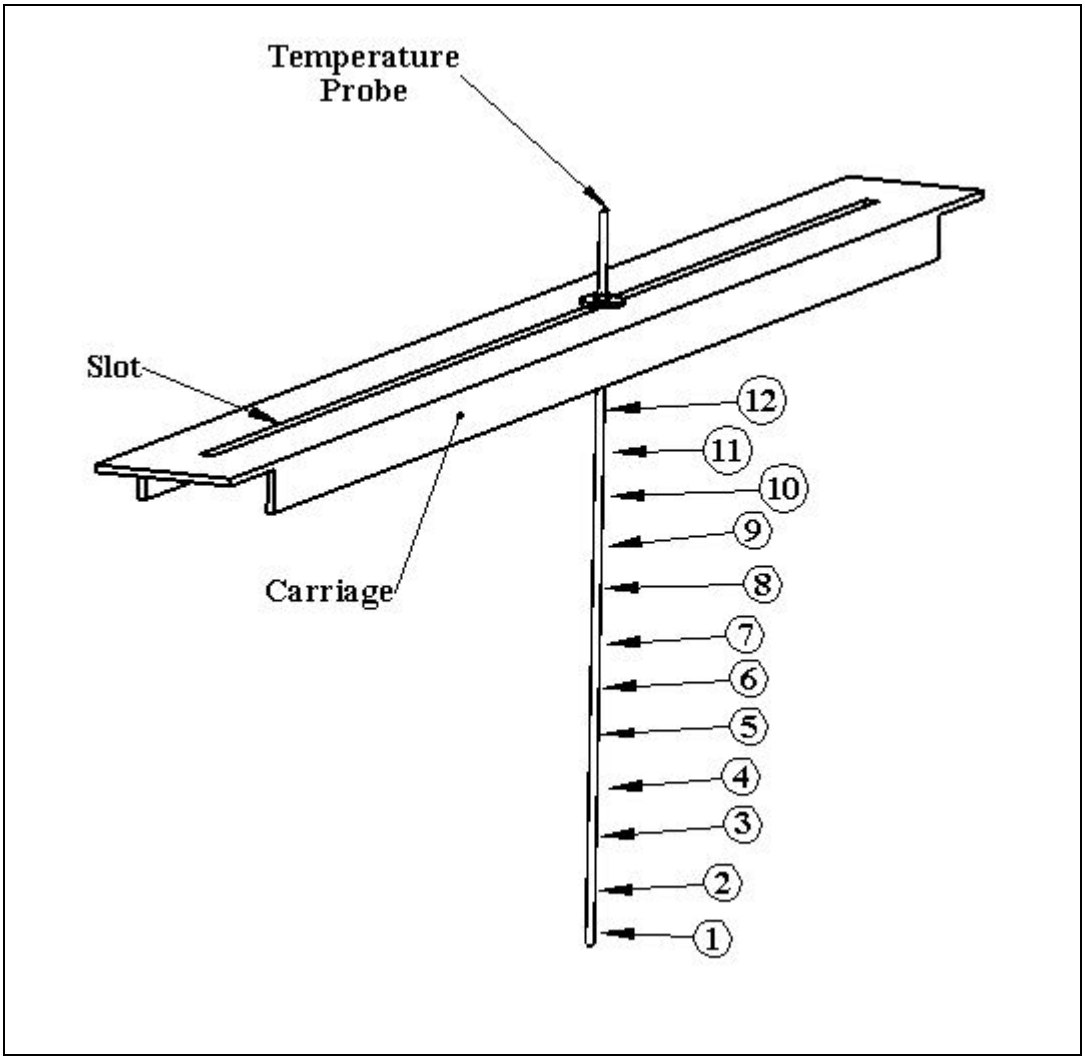

Figure 3.4 Temperature Probe and Slot-Carriage

All 23 thermocouples are connected to a 32 channel data logger. The data logger, Molytek Model 3702 [16], is capable of sending the temperature readings to a PC through a serial port. Windmill Logger software is used to read the output of the data logger and write the data into text files on the PC's harddisk in specified time intervals.

Table 3.1 Locations of Thermocouples on the Temperature Probe

Thermocouple Number	Location (mm) from bottom tip of probe
1	3
2	40
3	80
4	120
5	150
6	187
7	249
8	287
9	348
10	387
11	447
12	485

3.2.3 Other Measurements

The top surface of the warm water storage unit is exposed to ambient air. This free surface results in high convective and evaporative losses from the storage medium to the ambient air. Ambient temperature, pressure, and relative humidity are measured during the experiments to calculate the surface heat and mass transfer losses.

Figure 3.5 Data Logger

CHAPTER 4

EXPERIMENTAL PROCEDURE

The duration of the experiments were long. Data collection was started in the morning and usually ended in the evening or at night. An experiment can be classified into two parts. First part is storing thermal energy inside the storage unit until a steady-state thermal stratification inside the storage unit is achieved. Second part is extracting the stored thermal energy with the aid of heat removal tubes. The following outlines the experimental procedure followed during the experiments.

- Main storage tank was filled with tap water to have a constant head for the charging water.
- The storage unit was filled with water up to the desired level to satisfy the intended aspect ratio ($A = H/L$) inside the storage unit.
- Heat removal tubes were moved with the power screws to the depth where heat extraction from the storage unit was intended to take place.
- Electric heaters inside the warm water production chamber were operated to heat up the water to the intended charging temperature. Valve between the main storage tank and warm water production chamber was opened to feed relatively cold water to the chamber while the exiting water from the chamber was fed back to the main storage tank by by-passing the mixing chamber and warm water storage unit. This was done in order to have a steady-state water temperature inside the warm water production chamber before the charging of the storage unit started.
- Circulation of cooling water through the water jackets was started. Tap water was used as the cooling water.

- Thermocouple connections were checked. Data logger, PC and data logging software were set open to measure the initial temperature distribution inside the storage unit.
- Charging water was fed to the mixing chamber. Mass flow rate of charging water to the feeding box was fine tuned by adjusting the valves of the rubber hoses.
- The valve at the end of the discharge diffuser was opened. Discharged water flow rate was adjusted in order to have a constant water level inside the warm water storage unit.
- Until reaching steady-state thermal stratification, the following data were measured and recorded:

    i. discharged mass flow rate of water
    ii. mass flow rate of cooling water circulating the water jackets
    iii. temperatures of charging and discharged water
    iv. inlet and outlet temperatures of the cooling water circulating the water jackets
    v. thermal stratification inside the storage unit with the aid of the temperature probe
    vi. temperature, pressure, and relative humidity of ambient air

  Items (i), (ii), and (vi) were measured in 60 min periods while the measurement period of items (iii), (iv), and (v) was 5 min.

- Upon reaching steady-state thermal stratification inside the storage unit, in some of the experiments heat extraction from the storage unit was started with circulating tap water through the heat removal tubes. In addition to the previously mentioned 6 items, followings were measured and recorded:

vii. total mass flow rate of water passing through the heat removal tubes

viii. common water temperature at the inlet of the heat removal tubes and water temperatures at the each outlet of the heat removal tubes

Item (vii) was measured every 60 min and item (viii) was measured every 5 min.

- In some of the experiments, upon reaching steady-state thermal stratification inside the storage unit, heat extraction was started without further charging of the storage unit. Thus all the items accept items (i) and (iii) were measured and recorded.
- For each aspect ratio, one experiment was conducted by ceasing the charging of the storage unit without starting any heat extraction to observe the stand-by period of the storage unit. All the items accept items (i), (iii), (vii), and (viii) were measured and recorded.

CHAPTER 5

REDUCTION OF TEST DATA

5.1 The Storage Unit as a Thermodynamic Control Volume

The storage unit could be treated as a thermodynamic control volume with the parameters shown in Figure 5.1.

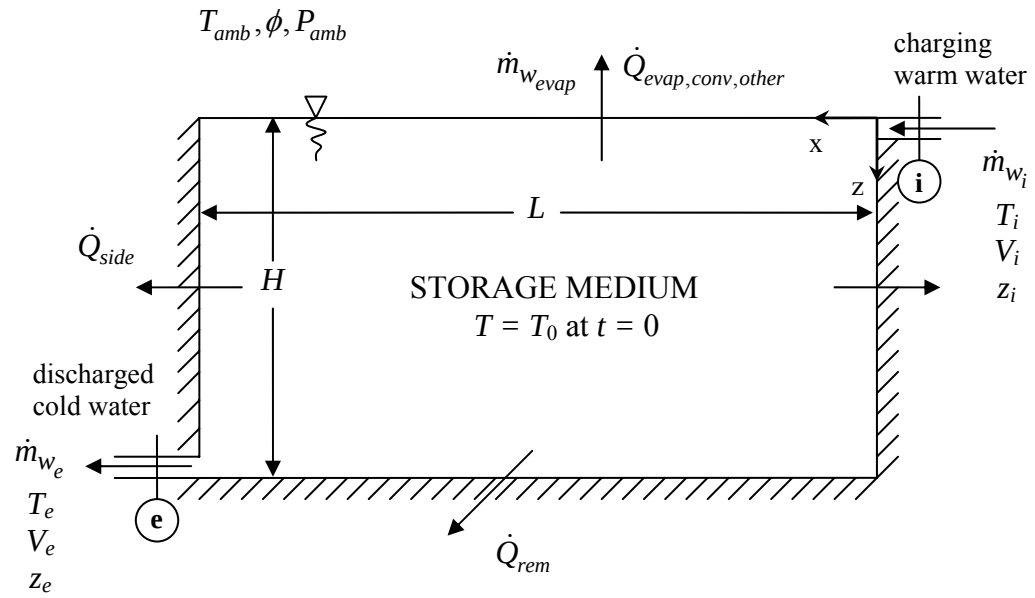

Figure 5.1 The Storage Unit as a Thermodynamic Control Volume

Continuity equation for the storage medium is:

$$\dot{m}_{w_i} = \dot{m}_{w_e} + \dot{m}_{w_{evap}} \tag{5.1}$$

Rate of evaporation from the free surface is negligible compared to the discharged water flow rate. Omitting rate of evaporation, continuity equation turns out to be:

$$\dot{m}_{w_i} \cong \dot{m}_{w_e} \cong \dot{m}_w \tag{5.2}$$

From the first law of thermodynamics:

$$\frac{\delta Q}{dt} = \frac{dE}{dt} + \frac{\delta W}{dt} \tag{5.3}$$

There is no work done on or by the control volume, hence Equation 5.3 becomes:

$$\frac{\delta Q}{dt} = \frac{dE}{dt} \tag{5.4}$$

$\frac{dE}{dt}$ term in Equation 5.4 can be written as:

$$\frac{dE}{dt} = \left(\frac{dE}{dt}\right)_{c.v.} + \oint_{c.s.} \rho e \mathbf{v} \cdot dA \tag{5.5}$$

Subtituting Equation 5.5 into Equation 5.4 and rearranging the terms:

$$-\oint_{c.s.} \rho e \mathbf{v} \cdot dA + \frac{\delta Q}{dt} = \left(\frac{dE}{dt}\right)_{c.v.} \tag{5.6}$$

First term in the left hand side of Equation 5.6 is the difference between the entering and leaving energy fluxes for the storage medium. Energy of the entering stream is higher than the energy of the leaving stream, thus evaluation of the surface integral gives a negative quantity. Minus sign in front of the surface integral makes the first term in the LHS of Equation 5.6 a positive quantity.

If the direction of heat transfer is from the CV to the surroundings, that is to say if there is heat loss from the storage unit, the sign of $\frac{\delta Q}{dt}$ term is negative. Equation 5.6 can then be described in words as:

rate of net energy input	-	rate of heat loss to the surroundings	=	rate of energy stored in the CV

First term of the LHS of Equation 5.6 can be written as:

$$-\oint_{c.s.} \rho e\mathbf{v}\cdot dA = -\oint_{c.s.} \rho(h+\frac{V^2}{2}+gz)\cdot dA \tag{5.7}$$

neglecting $\frac{V^2}{2}$ and gz terms compared to h,

$$-\oint_{c.s.} \rho e\mathbf{v}\cdot dA = -\oint_{c.s.} \rho h\mathbf{v}\cdot dA \tag{5.8}$$

Substitution of continuity equation (Equation 5.2) after the evaluation of the surface integral yields:

$$-\oint_{c.s.} \rho h\mathbf{v}\cdot dA = \dot{m}_w(h_i - h_e) = \dot{m}_w\Delta h \tag{5.9}$$

by assuming constant specific heats, Δh becomes,

$$\Delta h = h_i - h_e = c_p(T_i - T_e) \tag{5.10}$$

Rate of net energy input then becomes:

$$\dot{H}_{net} = \dot{H}_i - \dot{H}_e = \oint_{c.s.} \rho h \mathbf{v} \cdot dA = \dot{m}_w c_p (T_i - T_e) \tag{5.11}$$

Equation 5.11 can be integrated with respect to time in order to find the net energy input to the storage medium for the time interval Δt

$$\Delta H_{net} = \int_0^t \dot{H}_{net} d\tau = \dot{m}_w c_p \int_0^t (T_i - T_e) d\tau \tag{5.12}$$

$\dot{H}_{net}$ and ΔH_{net} can be found at any time *t* from the start of the experiment by the experimental data.

$\left(\frac{dE}{dt}\right)_{c.v.}$ term in Equation 5.6 can be written as:

$$\left(\frac{dE}{dt}\right)_{c.v.} = \left(\frac{dU}{dt}\right)_{c.v.} \tag{5.13}$$

by neglecting the rate of changes of KE and PE in time.

Since the storage medium contains a fluid that is incompressible:

$$du = c_v dT \tag{5.14}$$

For a thermally stratified fluid:

$$dU = \int_{\forall} (\rho c_v dT) d\forall \tag{5.15}$$

Change of internal energy of CV with respect to time becomes,

$$\left(\frac{dU}{dt}\right)_{c.v.} = \int_{\forall} (\rho c_v \frac{dT}{dt}) d\forall \tag{5.16}$$

Equation 5.16 can be integrated from 0 to time *t* to find the net energy stored in the CV up to time *t*.

$$\Delta U_{stored} = \int_{\forall} d\forall \int_{0}^{t} \rho c_v \frac{dT}{dt} d\tau \tag{5.17}$$

After the evaluation of the integral with respect to time;

$$\Delta U_{stored} = \int_{\forall} \rho c_v \left[T(t) - T(0)\right] d\forall \tag{5.18}$$

$d\forall = dxdydz$ in Cartesian coordinates system,

$$\Delta U_{stored} = \int_{0}^{H} \int_{0}^{B} \int_{0}^{L} \rho c_v \left[T(x,y,z,t) - T(x,y,z,0)\right] dxdydz \tag{5.19}$$

where *H*, *B*, and *L* are the height, width, and length of the CV.

Equation 5.19 can be simplified with the following assumptions and observations:

- $\rho \cong constant \quad c_v \cong constant$

- Temperature distribution inside the storage medium is mainly dependent upon depth, see Figures C.1 and C.2

  $$T(x,y,z,t) \cong T(z,t)$$

- Although slightly stratified, initial temperature distribution in the storage medium is assumed to be isothermal

$$T(x, y, z, 0) \cong T_0$$

Thus, Equation 5.19 becomes,

$$\Delta U_{stored} = \rho c_v BL \int_0^H [T(z,t) - T_0] dz \tag{5.20}$$

Equation 5.20 is used to find the total energy stored in the storage medium in a time interval Δt starting from the beginning of the charging process. It is also used to determine the remaining energy stored in the CV once heat extraction started. The integral is performed by the suitable numerical integration of the experimental data.

5.2 Heat Losses from the Control Volume

The last term in Equation 5.6 is $\frac{\delta Q}{dt}$. It may be written in the following form:

$$-\frac{\delta Q}{dt} = \dot{Q}_{rem} + \sum \dot{Q}_{loss} = \dot{Q}_{rem} + \dot{Q}_{side} + \dot{Q}_{evap} + \dot{Q}_{conv} + \dot{Q}_{other} \tag{5.21}$$

where

$\sum \dot{Q}_{loss}$: total rate of heat loss from the C.V.

$\dot{Q}_{rem}$: rate of heat extracted from the heat removal tubes

$\dot{Q}_{side}$: rate of heat loss through the two water jackets

$\dot{Q}_{evap}$: rate of evaporative heat loss from the free surface

$\dot{Q}_{conv}$: rate of convective heat loss from the free surface

$\dot{Q}_{other}$: rate of heat losses from the two glass surfaces and the bottom surface.

Bottom surface of the storage medium is insulated. Heat loss through the two glass surfaces is also negligible compared to the other loss terms (see APPENDIX B). Hence,

$$\dot{Q}_{other} \cong 0$$

$\dot{Q}_{rem}$ could be written as,

$$\dot{Q}_{rem} = \dot{m}_{w_{rem}} c_p (\overline{T}_{wo} - T_{wi}) \tag{5.22}$$

where $\dot{m}_{w_{rem}}$: total mass flow rate of water passing through heat removal tubes

T_{wi} : common water temperature entering heat removal tubes

$\overline{T}_{wo}$: arithmetic mean of the four water temperatures at the outlets of heat removal tubes.

Equal amount of water is tried to be circulated through the four heat removal tubes in order to use $\overline{T}_{wo}$.

Rate of side loss, $\dot{Q}_{side}$, could be computed by,

$$\dot{Q}_{side} = \dot{m}_{w_{waterjackets}} c_p (\overline{T}_{we_{waterjackets}} - \overline{T}_{wi_{waterjackets}}) \tag{5.23}$$

where $\dot{m}_{w_{waterjackets}}$: total mass flow rate of cooling water circulating the two water jackets

$\overline{T}_{we_{waterjackets}}$, $\overline{T}_{wi_{waterjackets}}$: arithmetic mean temperatures of cooling water at the outlet and inlet of the water jackets.

Convective and evaporative heat losses from the storage medium to the ambient air through the free surface can be calculated with the following equations:

$$\dot{Q}_{conv} = \overline{h}_{conv} A_{freesurface} (T_s - T_\infty) \tag{5.24}$$

$$\dot{Q}_{evap} = \bar{h}_m A_{freesurface}(\rho_{ws}|_{T_s} - \rho_w|_{T_\infty})h_{fg} \tag{5.25}$$

where $\bar{h}_{conv}$: convective heat transfer coefficient between water and ambient air

$\bar{h}_m$: mass transfer convection coefficient

$A_{freesurface}$: area of the free surface

T_s : free surface temperature

T_∞ : temperature of ambient air

h_{fg} : latent heat of vaporization.

$\bar{h}_{conv}$ and $\bar{h}_m$ can be correlated by the heat and mass transfer analogy,

$$\frac{\bar{h}_{conv}}{\bar{h}_m} = \rho_{air} c_{p_{air}} \mathrm{Le}^{2/3} \tag{5.26}$$

Calculation of $\bar{h}_{conv}$ is sufficient in order to find $\bar{h}_m$ with the heat and mass transfer analogy. External free convection occurs at the free surface. Rayleigh number should be calculated in order to determine whether the flow is laminar or turbulent,

$$\mathrm{Ra} = \frac{g\beta(T_s - T_\infty)L_{ch}^{\ 3}}{\nu_{air}\alpha_{air}} \tag{5.27}$$

where the characteristic lenght of the free surface is:

$$L_{ch} = \left(\frac{Area}{Perimeter}\right)_{freesurface} = \frac{BL}{2(B+L)} \tag{5.28}$$

A suitable correlation is used to find the average Nusselt number [17];

$$\overline{\mathrm{Nu}} = 0.15\mathrm{Ra}^{1/3} \tag{5.29}$$

and this average Nusselt number can be used to find the average convective heat transfer coefficient between the free surface of the storage medium and ambient air

$$\overline{\mathrm{Nu}} = \frac{\bar{h}_{conv} L_{ch}}{k_{air}} \tag{5.30}$$

Total energy lost as heat from the CV within a time interval Δt is:

$$\sum Q_{loss} = -\int_0^t \frac{\delta Q}{dt} d\tau = \int_0^t \left(\sum \dot{Q}_{loss} \right) d\tau \tag{5.31}$$

Taking the integral of Equation 5.6 for a time interval from 0 to *t*, and plugging in Equations 5.12, 5.20, and 5.31, energy equation becomes:

$$\dot{m}_w c_p \int_0^t (T_i - T_e) d\tau - \int_0^t \left(\sum \dot{Q}_{loss} \right) d\tau = \rho c_v BL \int_0^H \left[T(z,t) - T_0 \right] dz \tag{5.32}$$

The closed form is:

$$\Delta H_{net} = \Delta U_{stored} + \sum Q_{loss} \tag{5.33}$$

5.3 Performance Parameters

5.3.1 Dimensionless Bulk Temperature, θ

Dimensionless Bulk Temperature, θ, is defined as the ratio of the difference of bulk temperature, T_b, of the storage medium at any time *t* and initial temperature T_0, to the difference between inlet charging temperature, T_i, and initial water temperature T_0.

$$\theta(t) = \frac{T_b(t) - T_0}{T_i(t) - T_0} \tag{5.34}$$

Bulk temperature at any time can be defined as;

$$T_b(t) = \frac{\Delta U_{stored}(t)}{\rho c_v BHL} + T_0 \tag{5.35}$$

Substituting Equation 5.20 into Equation 5.35 gives;

$$T_b(t) = \frac{1}{H}\int_0^H \left[T(z,t) - T_0\right] dz + T_0 \tag{5.36}$$

Dimensionless bulk temperature is bounded by unity from above. It gets its maximum value, θ_L, after the charging of the storage unit is complete.

Dimensionless bulk temperature represents the available energy that can be stored within the storage unit. When θ reaches its maximum value of θ_L during the charging process, no further energy storage within the storage unit is possible. A steady-state temperature distribution is achieved in the storage unit at this time and heat removal process can be started. During the heat removal process, if

simultaneous charging of the storage unit is stopped, the calculation of θ becomes meaningless by its definition, since charging temperature, T_i, is undefined. On the other hand, if simultaneous charging of the storage unit is continued during the heat removal process, θ decreases asymptotically to another steady value. From this time on energy input rate to the storage unit becomes equal to the heat removal rate from the storage unit plus the rate of total heat loss.

5.3.2 Effectiveness of the Storage Unit, ε

Effectiveness, ε, is defined as the ratio of total energy stored within a time interval Δt beginning at $t = 0$, ΔU_{stored}, to the net enthalpy added to the storage medium during the same period, ΔH_{net}.

$$\varepsilon = \frac{\Delta U_{stored}}{\Delta H_{net}} \tag{5.37}$$

Effectiveness is a parameter to determine the performance of the storage unit especially during charging. The limiting value of effectiveness, ε_L, the value at the end of the charging period, can be used as a comparison criteria of different experiments. Effectiveness at any time of an experiment (provided that charging of the storage is present) can be computed by Equation 5.37 since both the numerator and denominator can be calculated by experimental data.

CHAPTER 6

RESULTS AND DISCUSSIONS

Aspect ratio is the ratio of the height of water inside the storage unit to the length of the storage unit ($A = H/L$). The experiments were performed for 2 aspect ratios, namely, $A = 0.26$ and $A = 0.16$.

Two different sets of experiments were performed with these aspect ratios. In the first set, after the storage unit was charged, heat removal was started while charging of the storage unit continued. In the second set of experiments, after charging of the storage was complete, heat removal was started in the absence of further charging of the storage unit. The charging periods for the two sets were identical.

In all of the experiments, charging rates and charging temperatures intended to be similar in order to observe the heat removal characteristics from different depths of similar storage media.

Two important approximations were made about the nature of the temperature field within the storage unit. Temperature is assumed to be only dependent upon the depth of the storage medium and time.

$$T(x, y, z, t) \cong T(z, t)$$

In order to validate this assumption, temperature measuring probe was traveled across the length and width of the storage in a time interval while energy input into the storage tank was equal to the heat removal rate from the heat removal tubes plus the total losses, i.e. when there was a steady-state temperature distribution within the storage unit. Figures C.1 and C.2 show the variation of temperature within the storage medium across the width and length respectively. Heat removal in this experiment (Exp. 23) was from a depth of 13 cm and the

thermocouple which indicated the only significant variation (third thermocouple from the top) was the one located 12.8 cm away from the free surface, near the heat removal tubes.

The second approximation is that, upper surface temperature of the storage medium was assumed to be equal to the charging water temperature, although the charging water cools down during its entrainment through the free surface by combined convection and evaporation to the ambient.

6.1 Analysis of the Charging Period

6.1.1 Temperature Profiles within the Storage Unit

Figure 6.1 and Figure 6.2 show the vertical temperature profile development within the storage unit when $A = 0.26$. The development is quite rapid during the first half of the charging period, and rate of development decreases in the second half due to the increase in the heat loss items (from the side walls and from the free surface) as the mean bulk temperature of the storage medium increases.

When the initial temperature of the storage unit is relatively high, the temperature of lower layers decreases as a result of comparatevely higher side losses at the beginning. As the heating effect of charging water penetrates deeper through the storage, this trend is reversed and temperature of lower layers also start to increase. The overall temperature increase at the bottom of the storage unit during charging is only a few degrees, thus energy input cannot affect the bottom of the storage unit at this aspect ratio ($A = 0.26$).

The temperature profile at the end of the charging period is strongly stratified and almost linear. Time to reach this steady-state temperature distribution was found between 400 and 420 min for all of the experiments performed at $A = 0.26$, Exp. 11 and Exp. 14 being the two exceptions (Table 6.1).

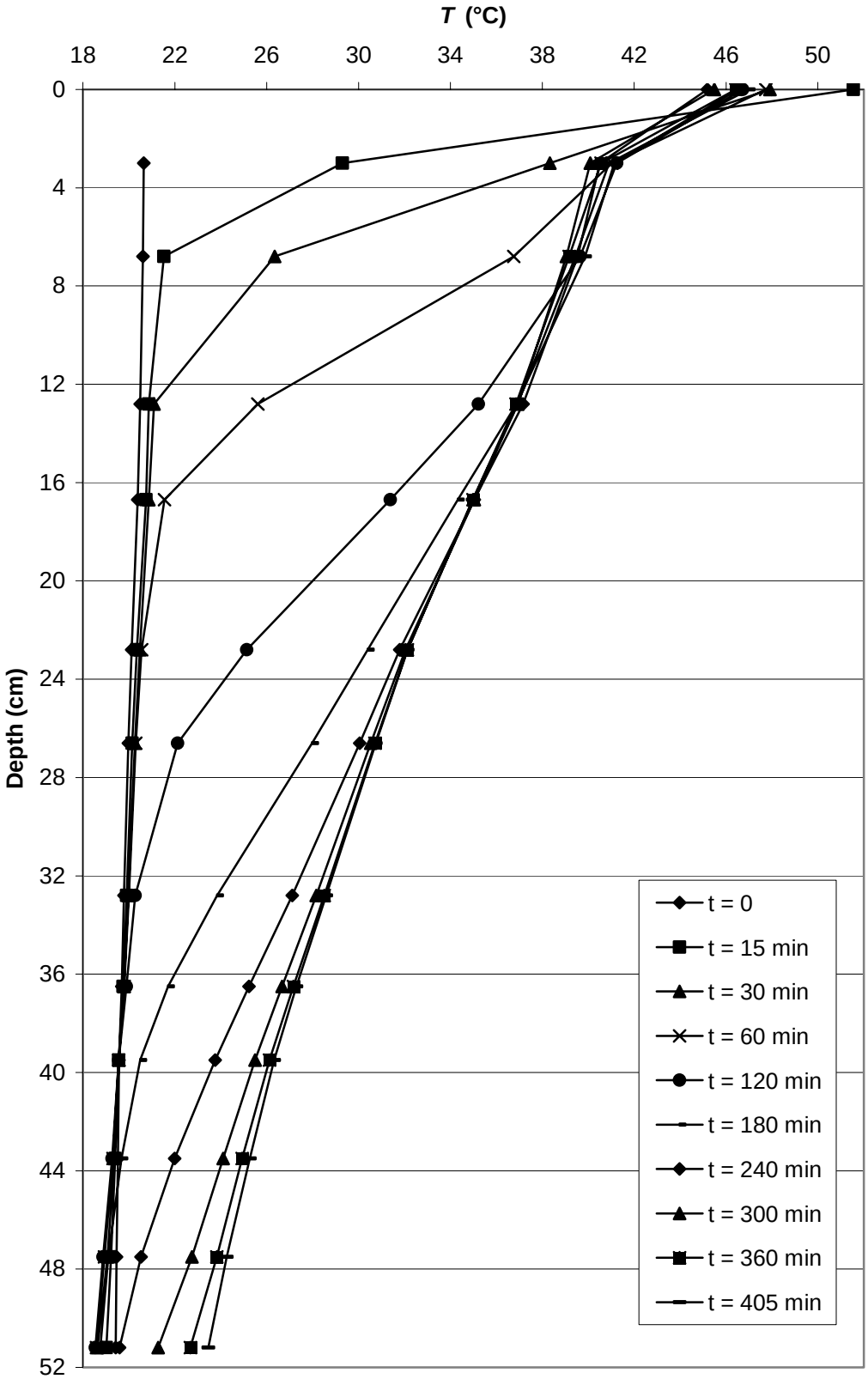

Figure 6.1 Development of Vertical Temperature Profile within the Storage Unit during Charging (Exp. 8, $A = 0.26$)

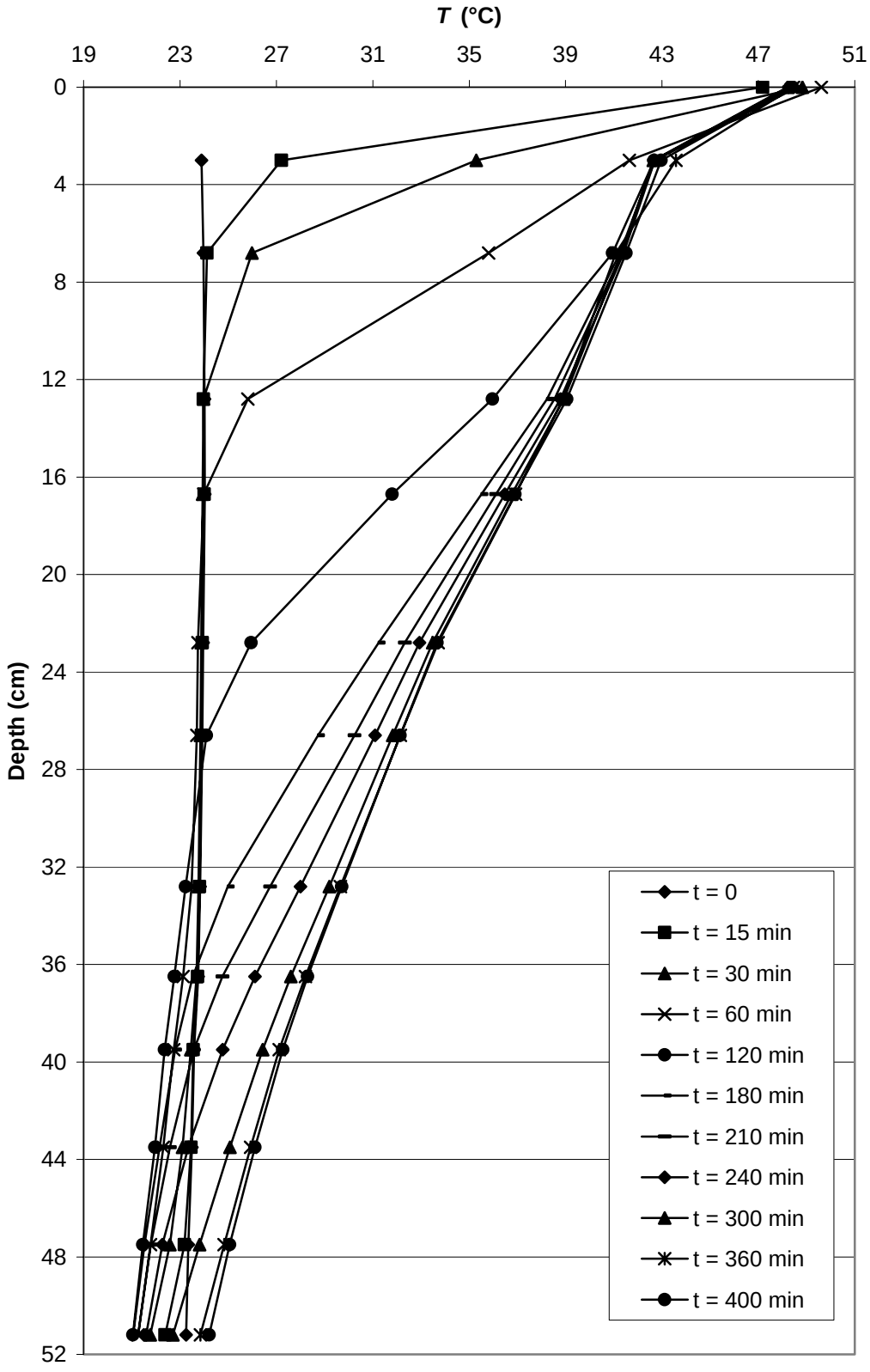

Figure 6.2 Development of Vertical Temperature Profile within the Storage Unit during Charging (Exp. 4, $A = 0.26$)

Table 6.1 Summary of Data and Results for Charging Process

Exp. No	*A=H/L*	$\dot{m}_w$ (kg/hr)	T_i (°C)	T_0 (°C)	T_{amb} (°C)	*Charging Period* (min)	ε_L	θ_L
9	0.26	221	45.9	16.2	23.5	420	0.37	0.50
11		229	43.0	16.6	23	450	0.36	0.51
8		221	46.5	20.0	23.5	405	0.30	0.44
13		229	45.9	20.9	24	395	0.30	0.44
7		226	47.0	21.0	25	420	0.29	0.44
2		214	48.4	21.5	23.5	395	0.29	0.41
14		223	44.8	23.0	24.5	370	0.27	0.38
4		219	48.4	23.8	25	400	0.24	0.38
10		201	49.5	24.6	23	420	0.19	0.29
3		230	45.8	24.7	25	420	0.23	0.36
12		218	49.3	25.2	23.5	415	0.20	0.33
5		216	47.7	25.2	24.5	400	0.20	0.30
1		206	47.5	25.2	24	405	0.19	0.30
6		222	48.5	26.0	25	420	0.18	0.32
20	0.16	234	47.3	17.5	24.5	330	0.38	0.61
17		227	49.1	20.4	22	315	0.33	0.54
21		209	50.6	21.0	22	325	0.32	0.53
16		231	49.3	22.2	24	350	0.30	0.54
22		222	48.7	23.9	21.5	330	0.27	0.49
18		229	49.8	24.0	21.5	320	0.26	0.48
19		238	47.4	24.5	21.5	300	0.28	0.50

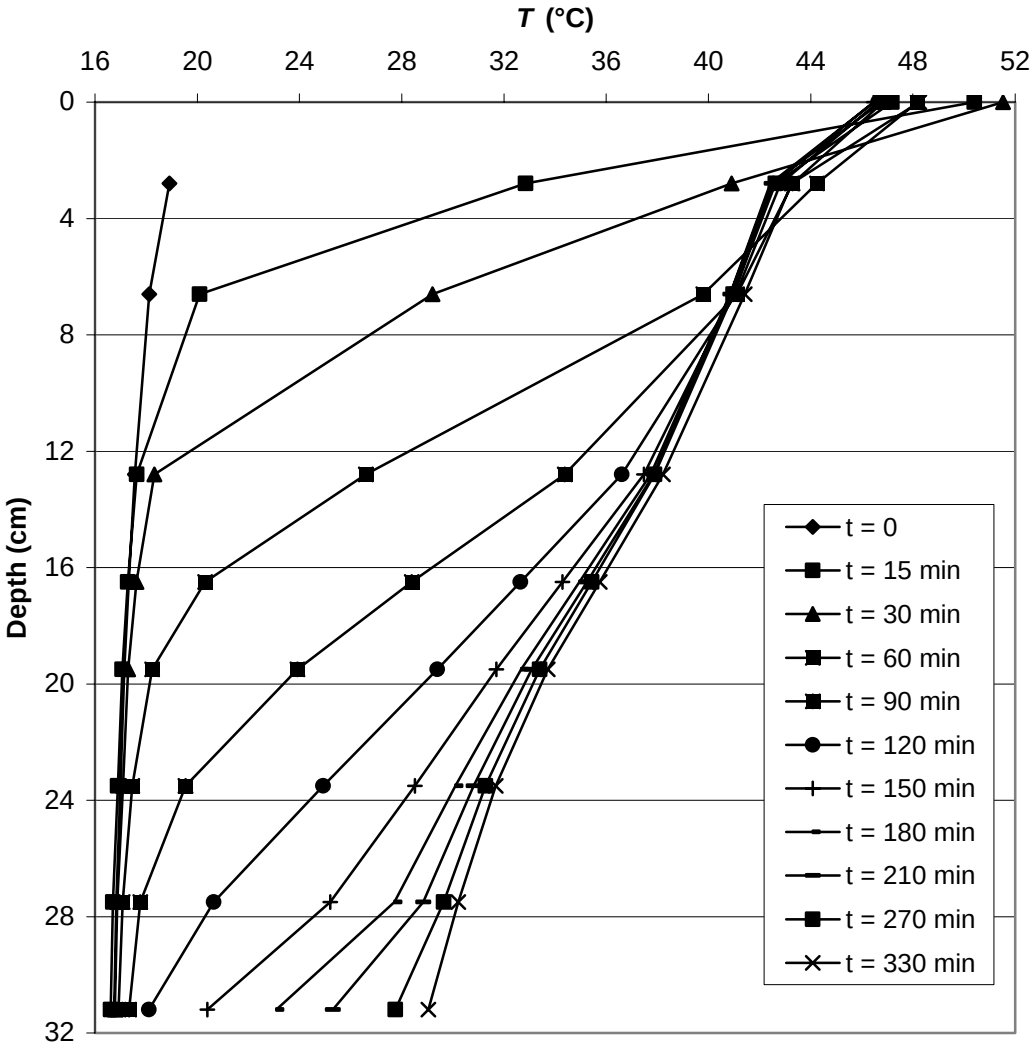

Figure 6.3 Development of Vertical Temperature Profile within the Storage Unit during Charging (Exp. 20, $A = 0.16$)

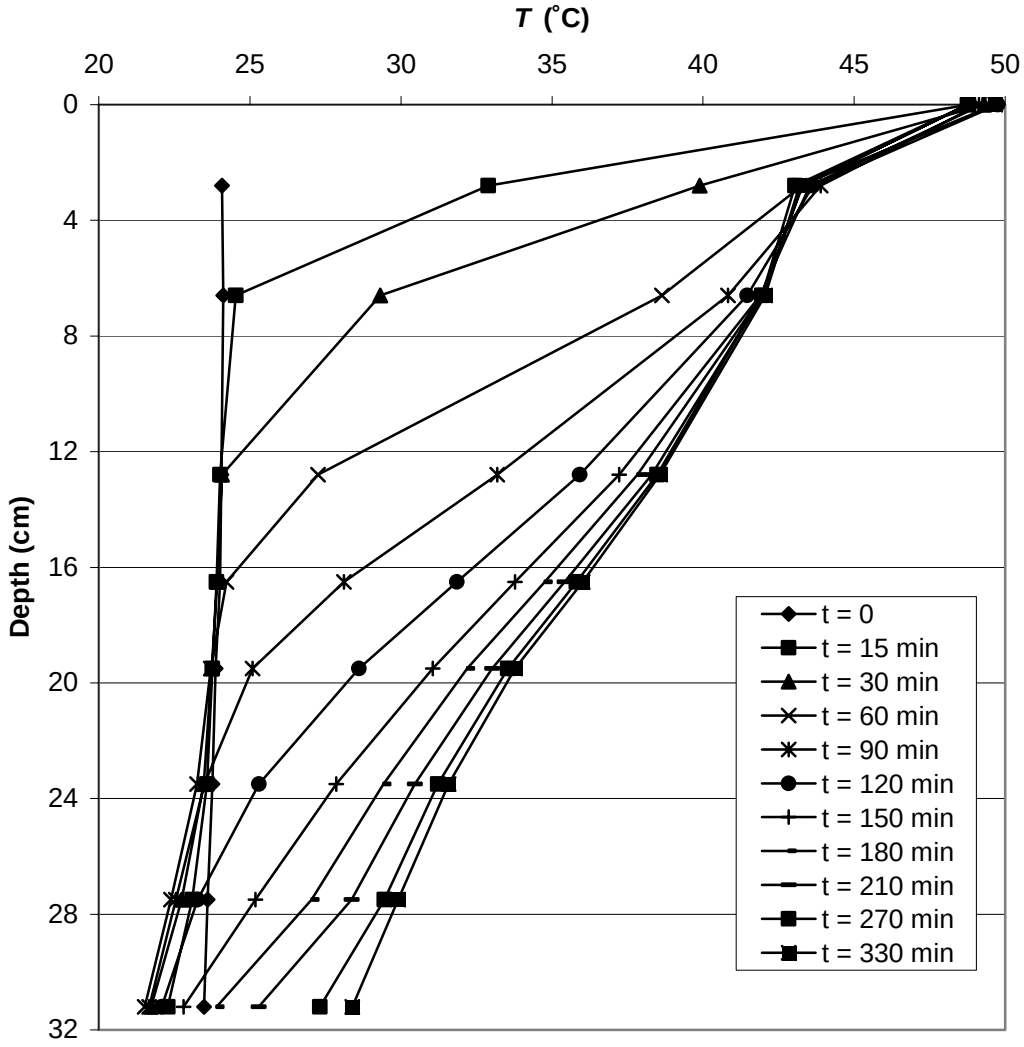

Figure 6.4 Development of Vertical Temperature Profile within the Storage Unit during Charging (Exp. 22, $A = 0.16$)

Temperature profile developments within the storage medium for $A = 0.16$ are shown in Figure 6.3 and 6.4. The major difference from the higher aspect ratio is that since the depth of the storage medium is lower for this aspect ratio, the heating effect of charging penetrates faster to the lower layers of the storage, thus temperature of bottom increases considerably. The temperature profiles resemble very much the temperature profiles observed down to 32 cm deep of the storage media of higher aspect ratio.

6.1.2 Performance Parameters during Charging

Figure 6.5 thru 6.8 show the variations of performance parameters, ε and θ, during the charging period. Effectiveness, ε, of the storage unit continually decreases and hence heat removal should be started at the time just steady-state is achieved. Observation of downward variation of ε shows an interesting recession during 60-120 min of some of the experiments performed at $A = 0.26$. This almost constant effectiveness interval is not observed in the experiments performed at $A = 0.16$. The physical cause of this recession could not be explained yet.

The variation of dimensionless bulk temperature in the first half of the charging period is quite high and slows down in the second half and converges to a constant value. In some of the experiments, e.g. Exp. 8, the value at the end of the charging period is slightly lower than the limiting value of θ. The definition of θ involves the timewise variation of charging temperature, T_i, and in some of the experiments, electricity potential of METU increased in the afternoon causing unavoidable 1-1.5°C increases in the charging water temperature towards the end of charging period. The criterion for determination of the end of charging period in all of the experiments was convergence of mean bulk temperature, T_b, to a steady value.

Limiting values of ε and θ are presented in Table 6.1. The most influential parameter affecting the limiting performance parameters is found to be the initial

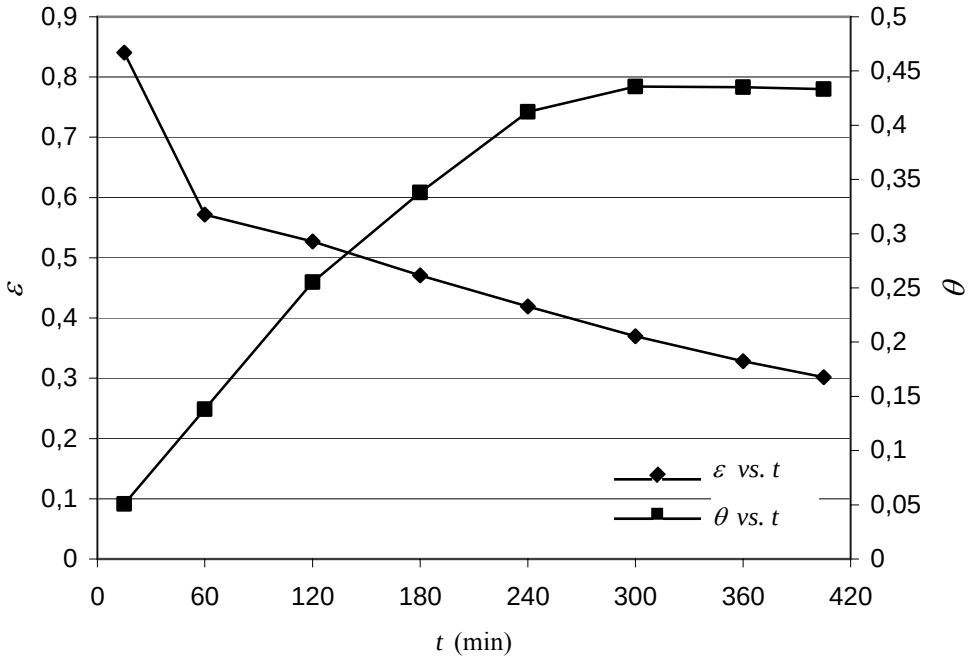

Figure 6.5 Development of Performance Parameters during Charging (Exp. 8, $A = 0.26$)

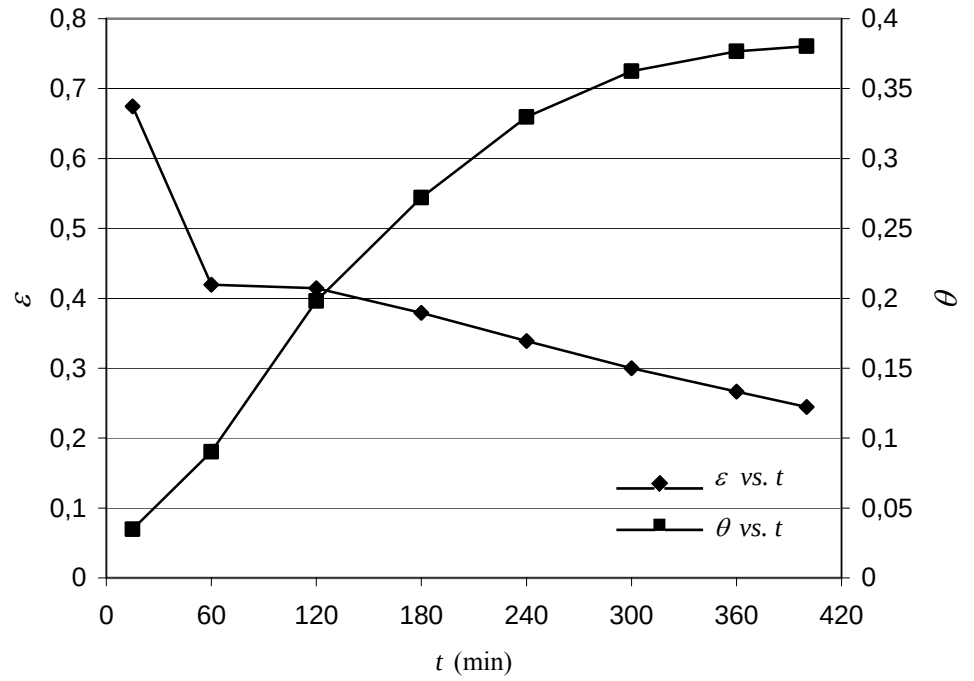

Figure 6.6 Development of Performance Parameters during Charging (Exp. 4, $A = 0.26$)

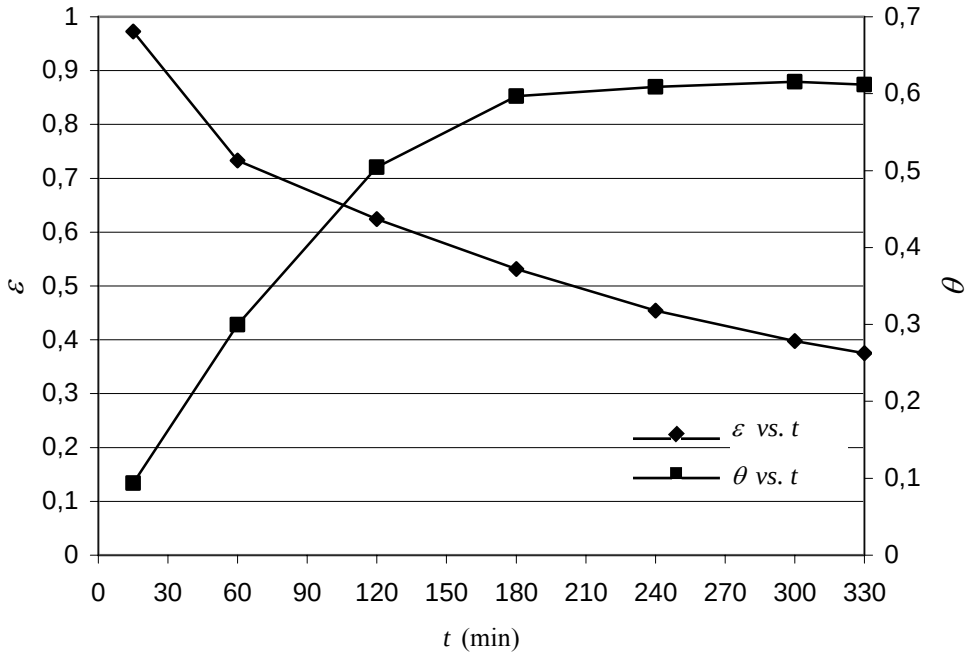

Figure 6.7 Development of Performance Parameters during Charging (Exp. 20, $A = 0.16$)

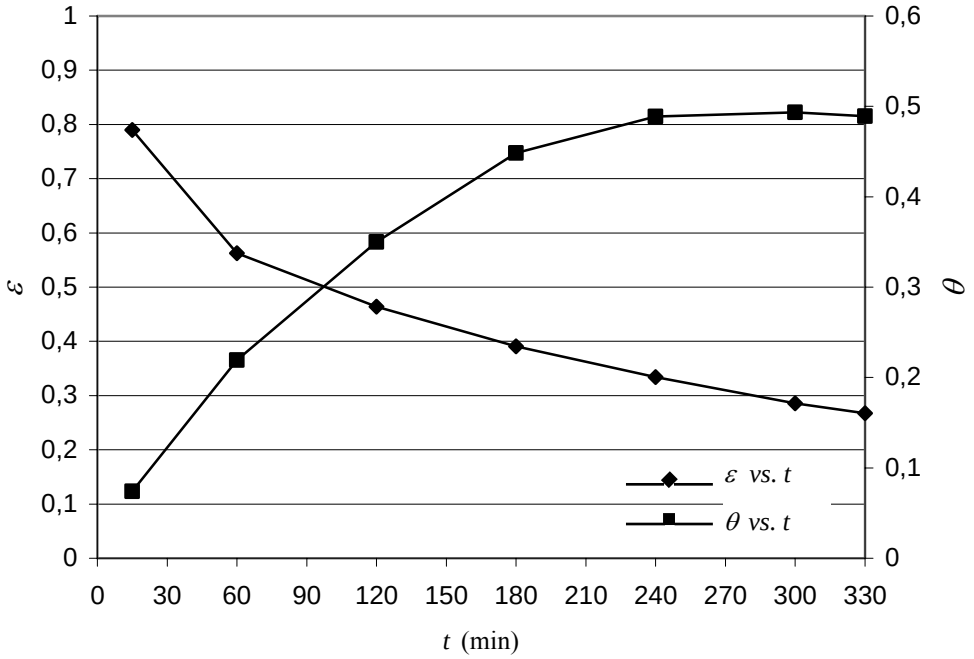

Figure 6.8 Development of Performance Parameters during Charging (Exp. 22, $A = 0.16$)

temperature, T_0, of the storage medium, in fact Table 6.1 is constructed with respect to increasing T_0. As the initial temperature of the storage unit increases, limiting values of performance parameters decreases. Lower aspect ratio gives better limiting performance values.

6.2 Analysis of Heat Removal Period

6.2.1 Heat Removal with Charging

Temperature profile developments during heat removal with charging of the storage are presented in Figure 6.9 thru 6.11 for A = 0.26 and in Figure 6.12 and 6.13 for A = 0.16.

The important observations are as follows:

- Heat removal affects the layers below the heat removal tubes more than it affects the layers above the heat removal tubes.
- The most affected region is around 10 cm below the tubes in all of the experiments.
- Only a few cm's of layer above the tubes is affected. Beyond, there is no effect of heat removal at all.
- The effect at the bottom of the storage unit for A = 0.26 is insignificant.
- Temperature profiles converge to a steady-state profile when heat removal rate and total heat losses equal the net enthalpy input to the storage medium.
- The time to reach this steady-state temperature profile from the starting of heat removal is around 260-285 min for A = 0.26, and 180-210 min for A=0.16 (Table 6.2).

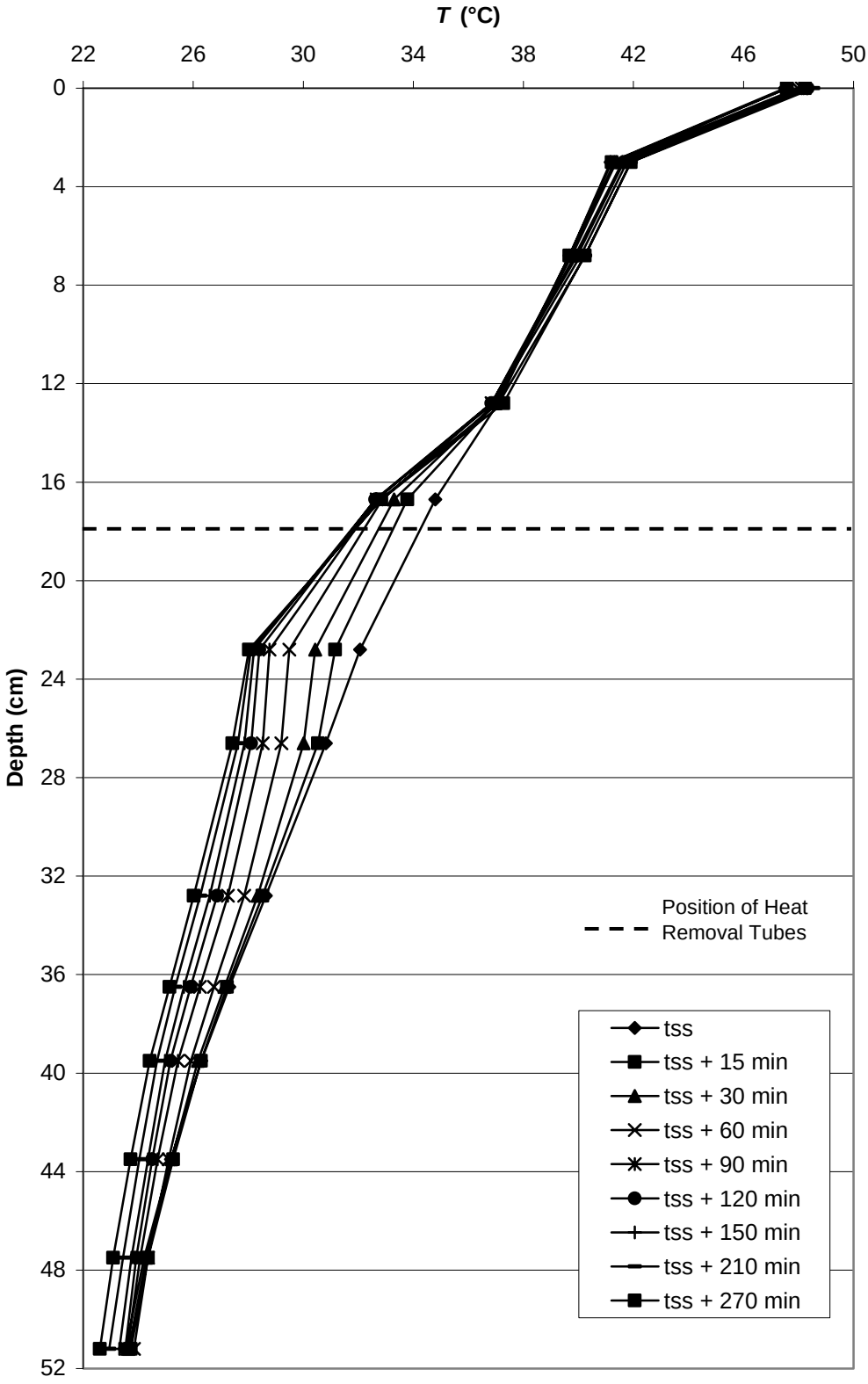

Figure 6.9 Development of Vertical Temperature Profile within the Storage Unit during Heat Removal (Exp. 1, $A = 0.26$, with Charging)

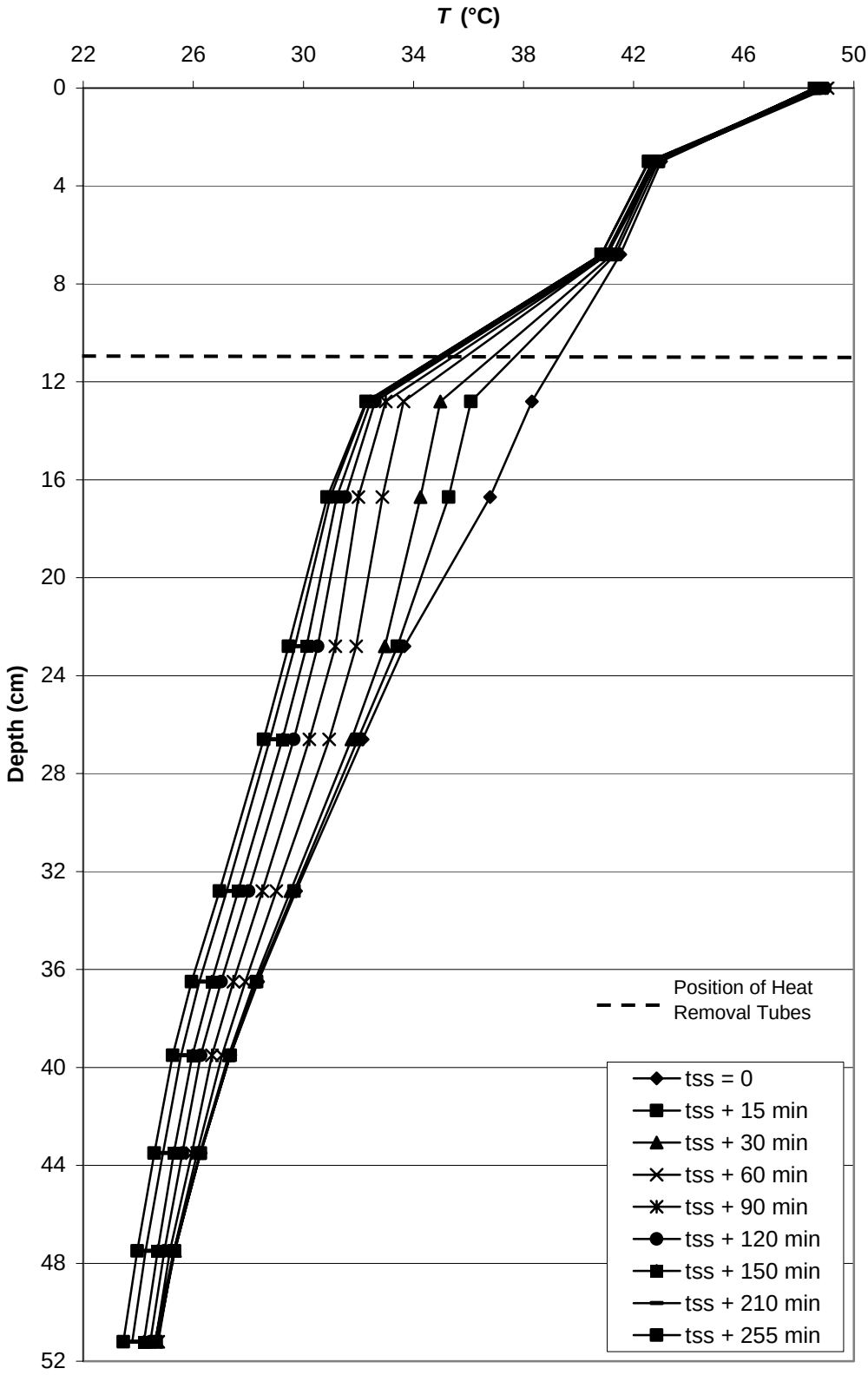

Figure 6.10 Development of Vertical Temperature Profile within the Storage Unit during Heat Removal (Exp. 4, A = 0.26, with Charging)

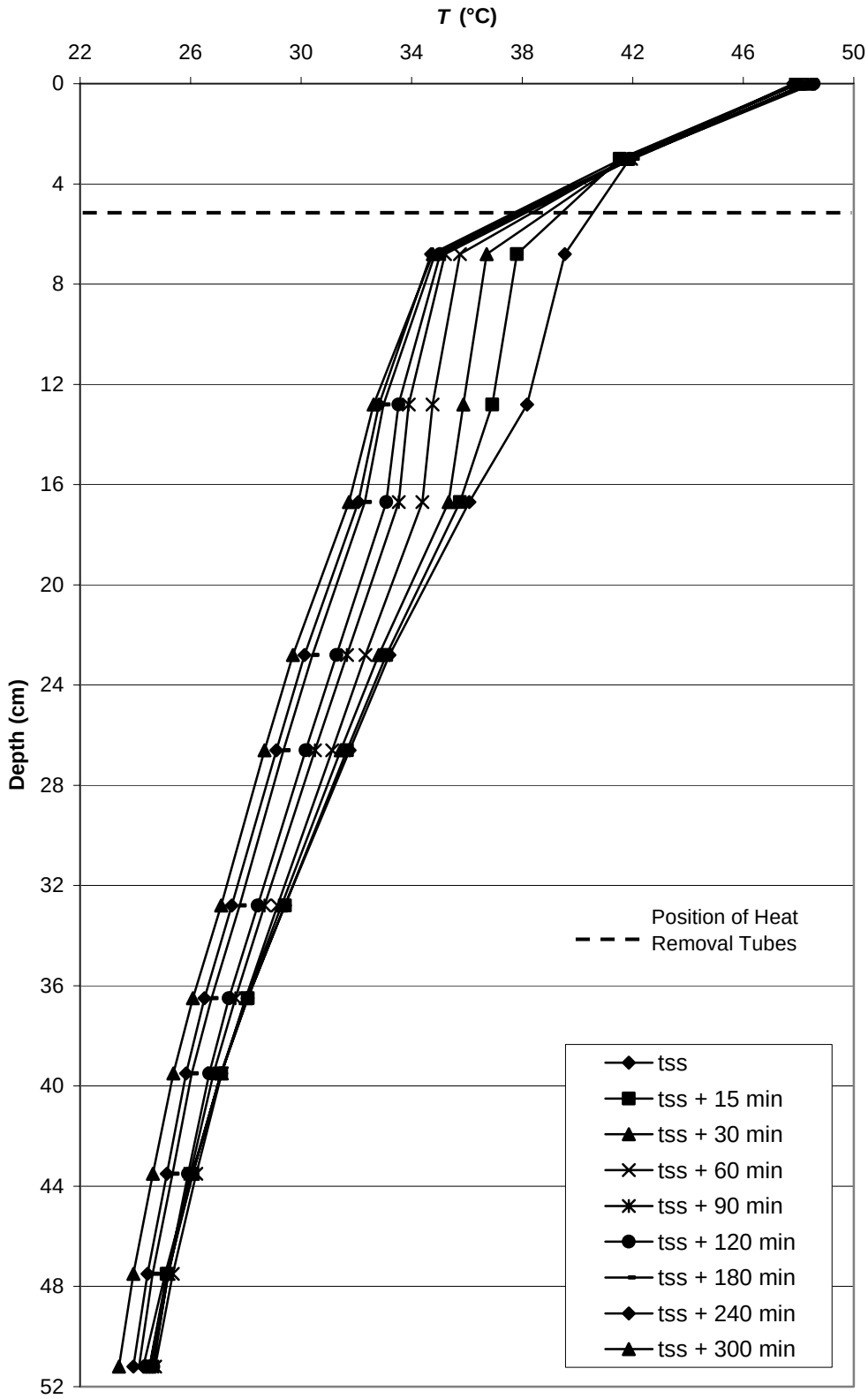

Figure 6.11 Development of Vertical Temperature Profile within the Storage Unit during Heat Removal (Exp. 7, $A = 0.26$, with Charging)

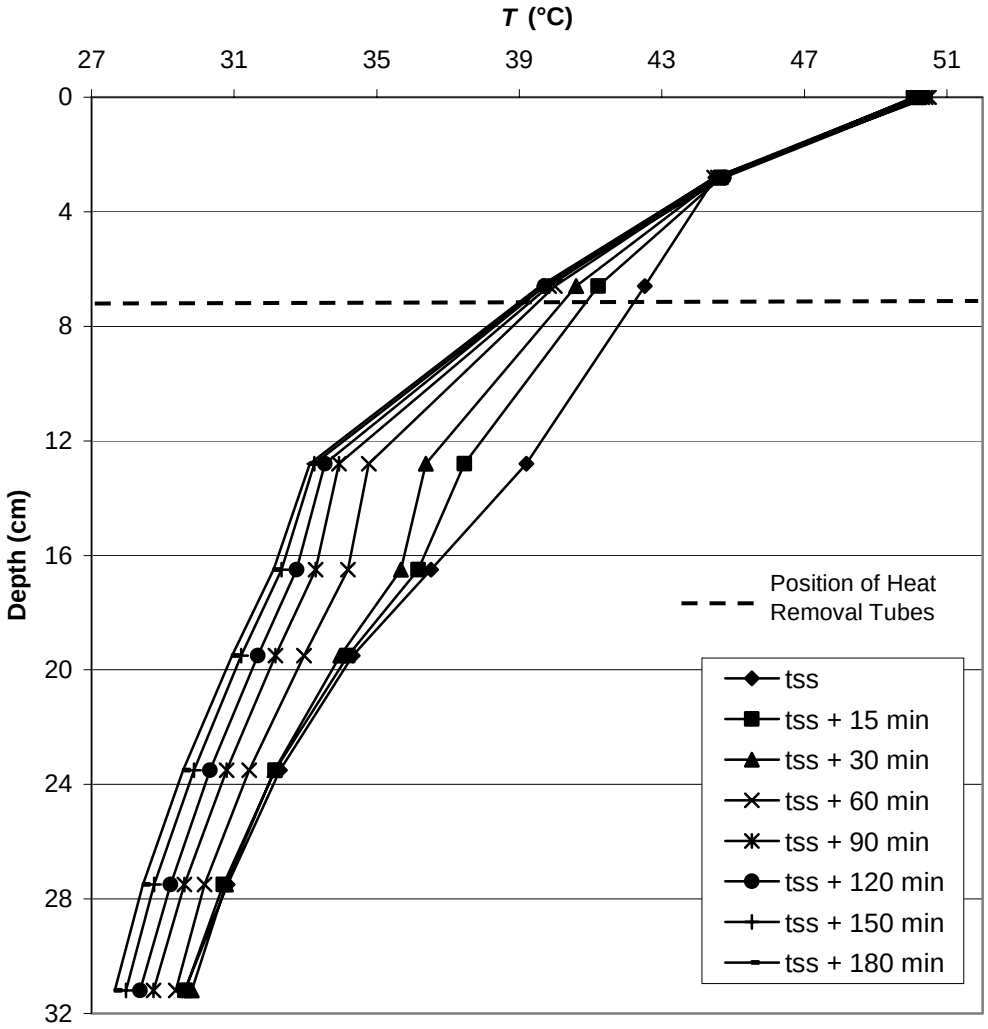

Figure 6.12 Development of Vertical Temperature Profile within the Storage Unit during Heat Removal (Exp. 16, $A = 0.16$, with Charging)

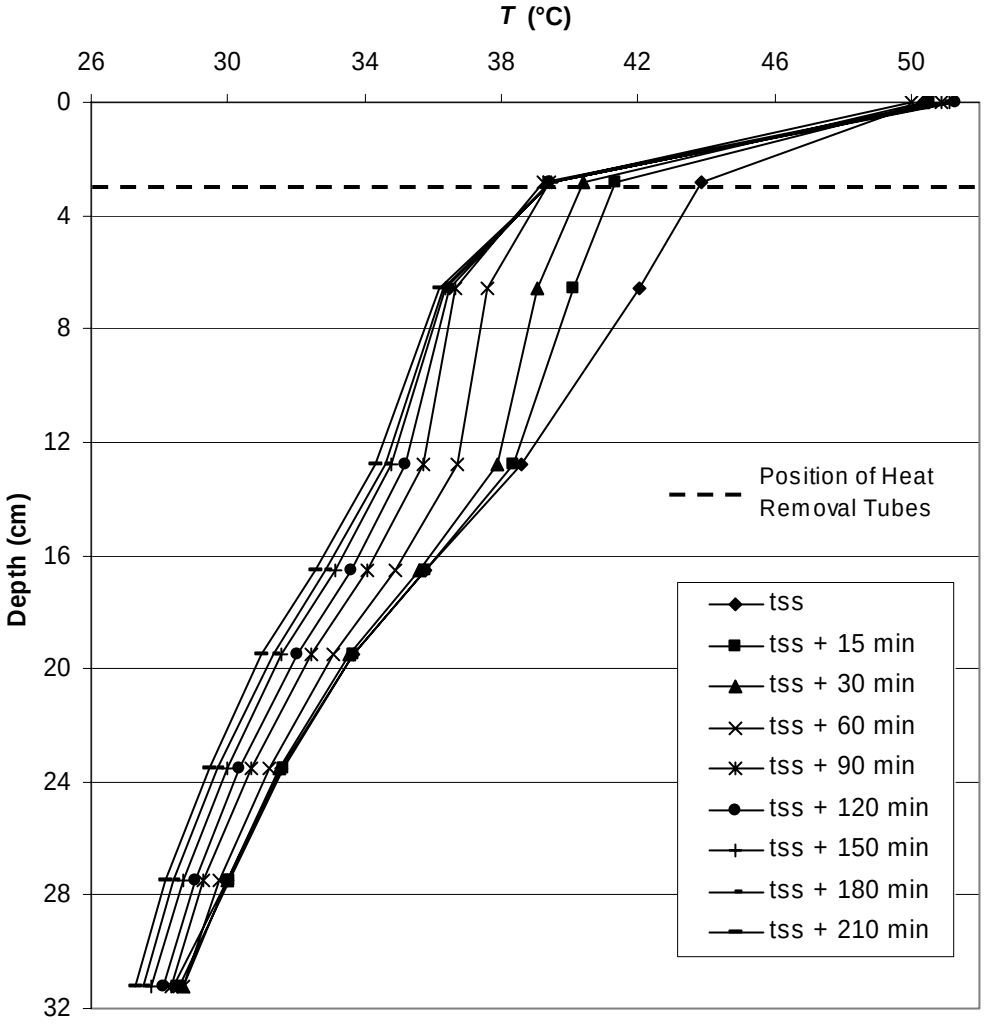

Figure 6.13 Development of Vertical Temperature Profile within the Storage Unit during Heat Removal (Exp. 18, A = 0.16, with Charging)

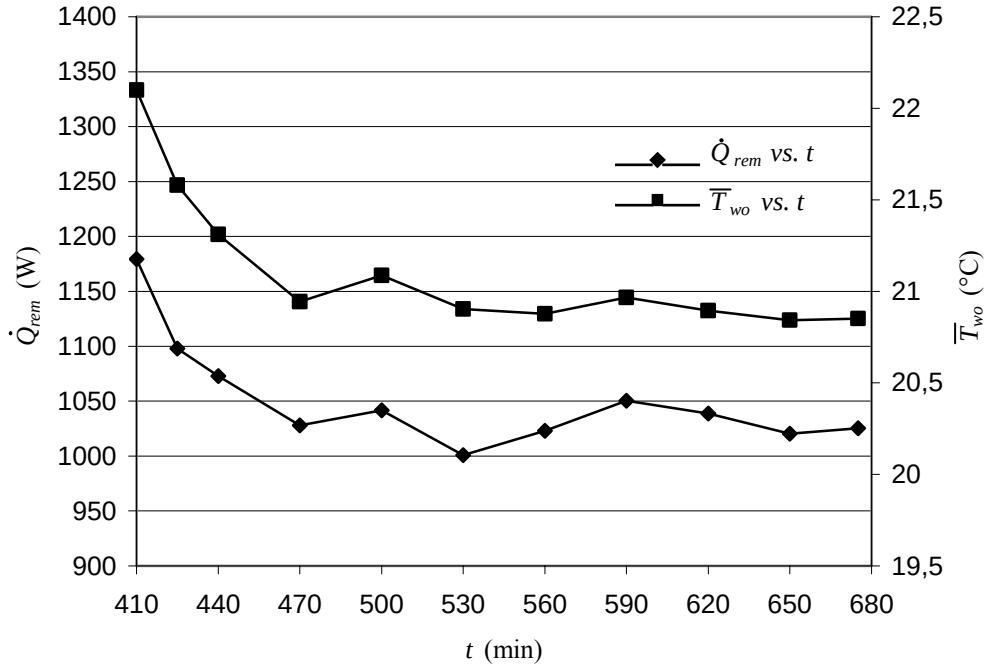

Figure 6.14 Variations of $\dot{Q}_{rem}$ and $\overline{T}_{wo}$ during Heat Removal
(Exp. 1, $A = 0.26$, $T_{wi} \cong 15.6°C$, with Charging)

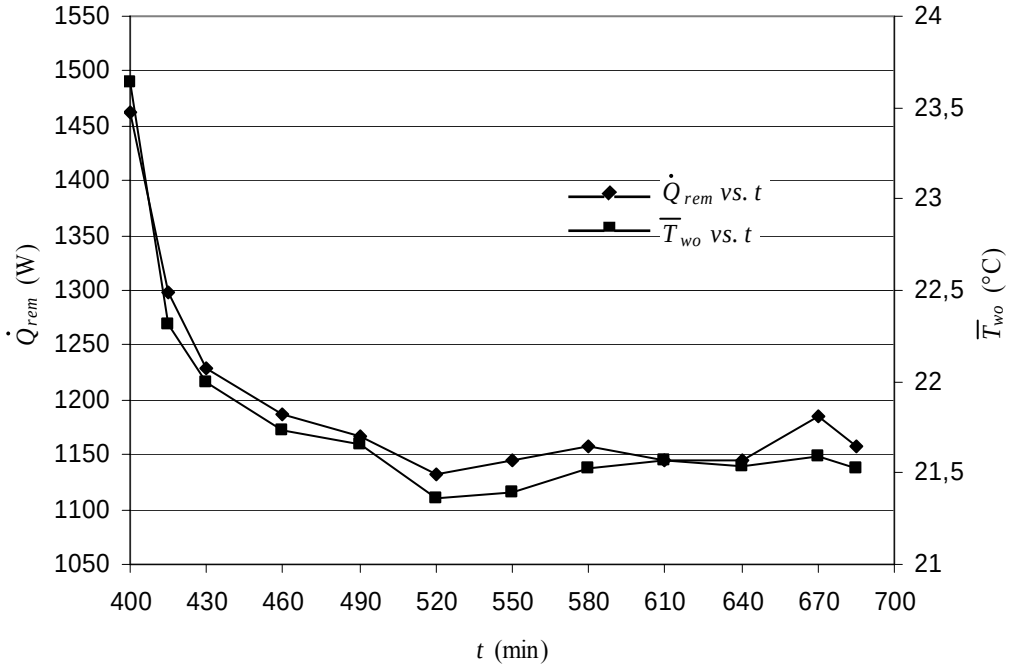

Figure 6.15 Variations of $\dot{Q}_{rem}$ and $\overline{T}_{wo}$ during Heat Removal
(Exp. 2, $A = 0.26$, $T_{wi} \cong 15.5°C$, with Charging)

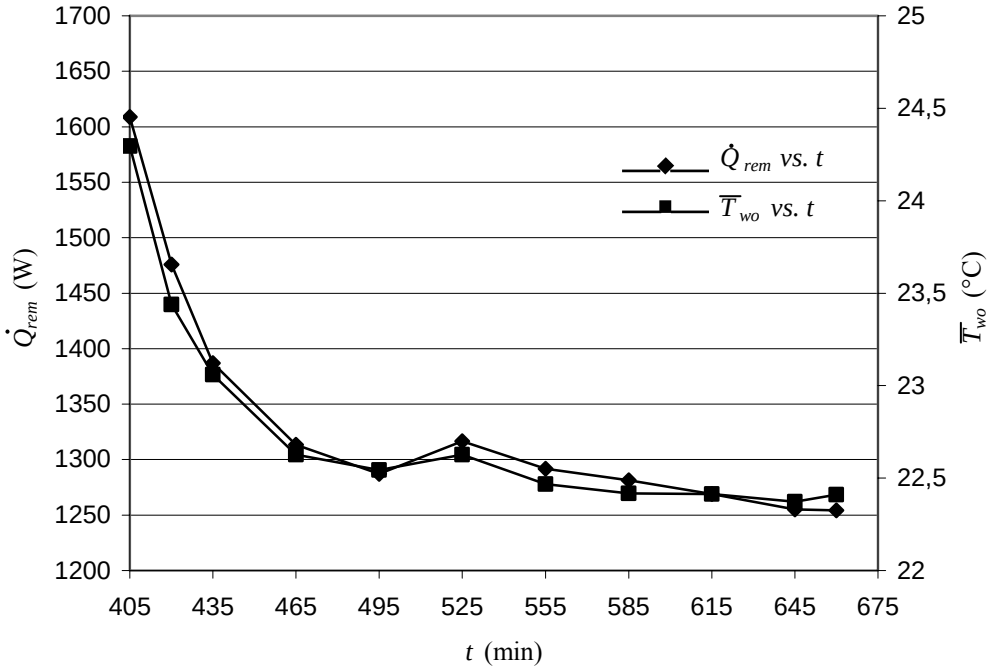

Figure 6.16 Variations of $\dot{Q}_{rem}$ and $\overline{T}_{wo}$ during Heat Removal
(Exp. 4, $A = 0.26$, $T_{wi} \cong 16.0°C$, with Charging)

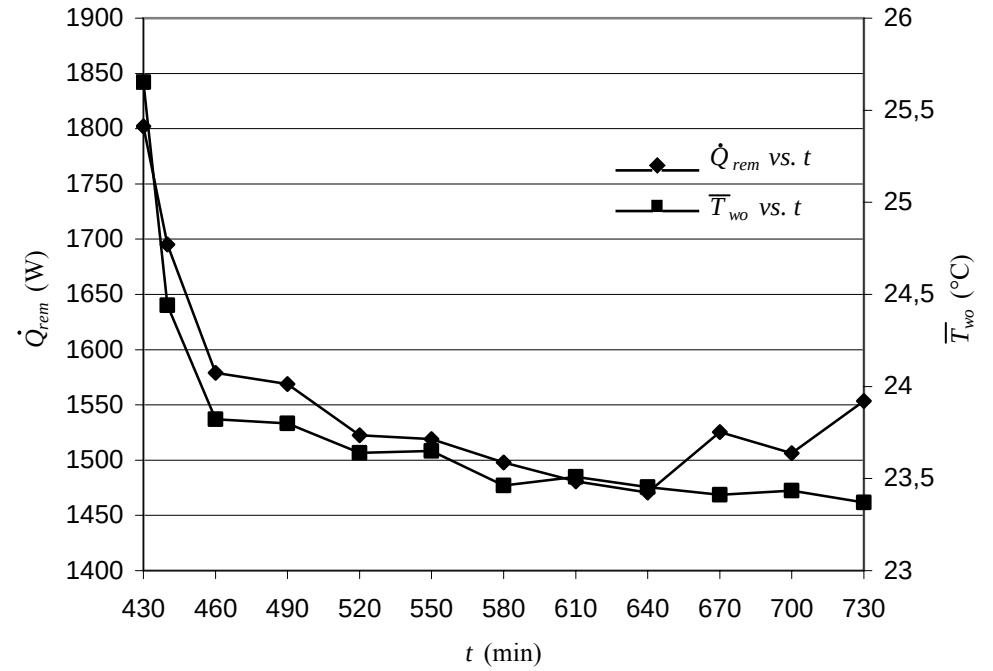

Figure 6.17 Variations of $\dot{Q}_{rem}$ and $\overline{T}_{wo}$ during Heat Removal
(Exp. 7, $A = 0.26$, $T_{wi} \cong 16.2°C$, with Charging)

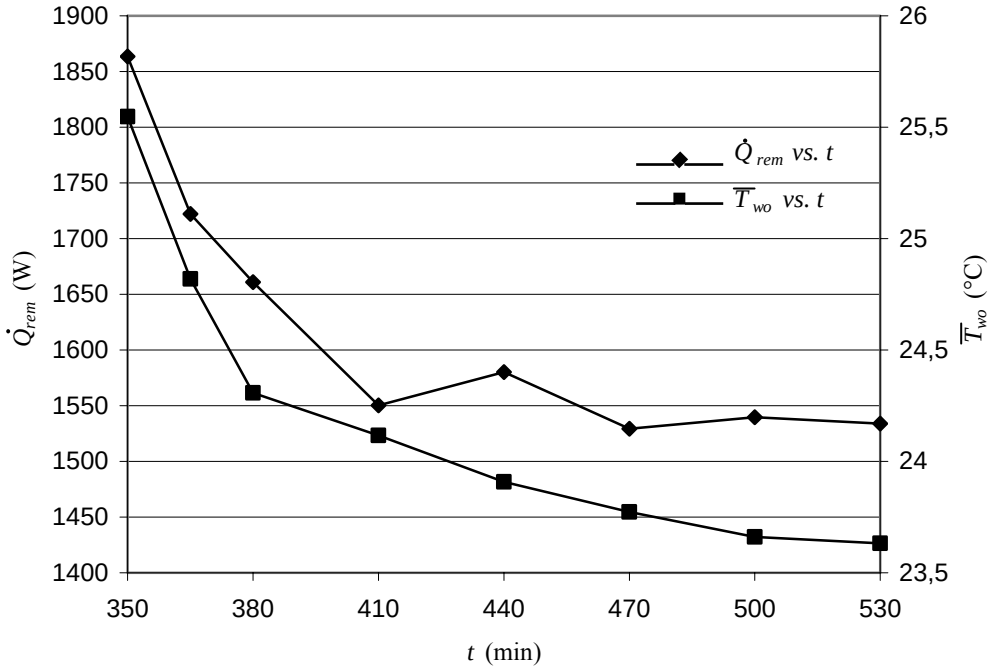

Figure 6.18 Variations of $\dot{Q}_{rem}$ and $\overline{T}_{wo}$ during Heat Removal
(Exp. 16, $A = 0.16$, $T_{wi} \cong 16.2°C$, with Charging)

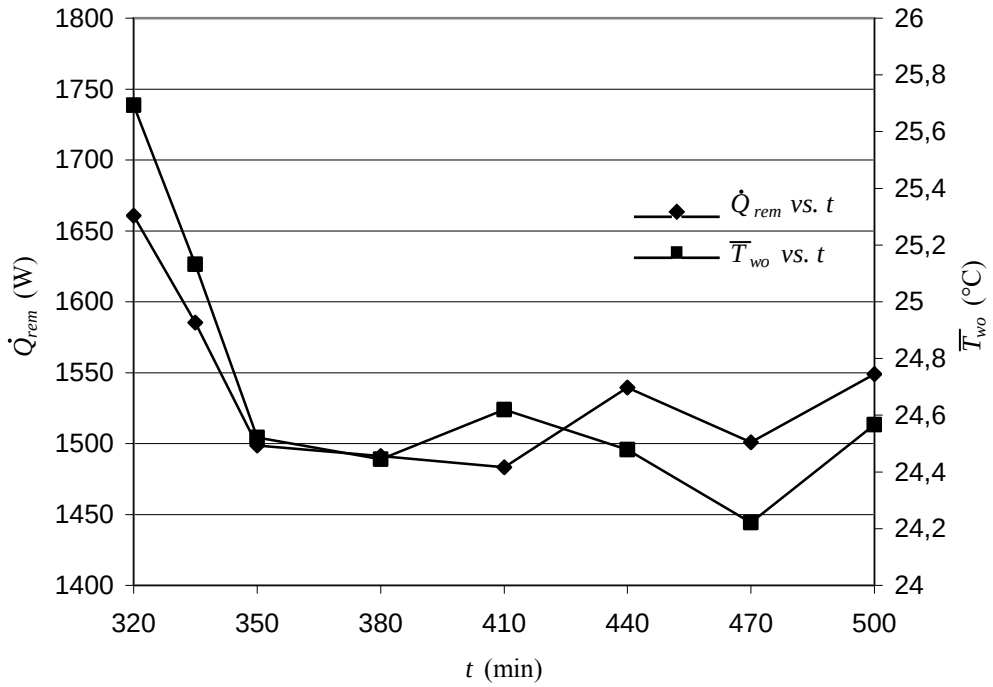

Figure 6.19 Variations of $\dot{Q}_{rem}$ and $\overline{T}_{wo}$ during Heat Removal
(Exp. 17, $A = 0.16$, $T_{wi} \cong 16.5°C$, with Charging)

Figure 6.14 thru 6.17 show the variations of heat removal rate, $\dot{Q}_{rem}$, and the arithmetic mean temperature of water at the outlet sections of the heat removal tubes, $\overline{T}_{wo}$, for A = 0.26, and Figure 6.18 and 6.19 for A = 0.16.

Both $\dot{Q}_{rem}$ and $\overline{T}_{wo}$ converge to steady-state values meaning that the storage unit can supply an almost steady heat output at the specified temperature as its operation is continued.

For A = 0.26, it can be concluded that the steady values of $\dot{Q}_{rem}$ increases as the heat removal tubes are located closer to the upper layers of the storage medium. For A = 0.16, this conclusion fails due to lack of adequate experimental data.

The area below the $\dot{Q}_{rem}$ *vs. t* curve gives the total heat removed from the system. These cumulative heat removal items are calculated for a time interval of 180 min starting from the beginning of heat removal period of the experiments and presented in Table 6.2. For A = 0.26, heat removed from the system in 180 min increases as heat removal is from a higher elevation. Another observation is that heat removed at the same depth for the two aspect ratios is comparable.

Variations of performance parameters both during the charging and heat removal periods are presented in Figure 6.20 thru 6.25. The decrease rate of ε increases as heat removal from the system is commenced. θ drops down from its maximum steady value at the end of the charging period and converges to another steady value at the end of the heat removal period.

Figure 6.26 and 6.27 show the variations of net enthalpy input to the system, net stored energy within the system, heat removed from the system, and heat loss items for A = 0.26 and A = 0.16 respectively.

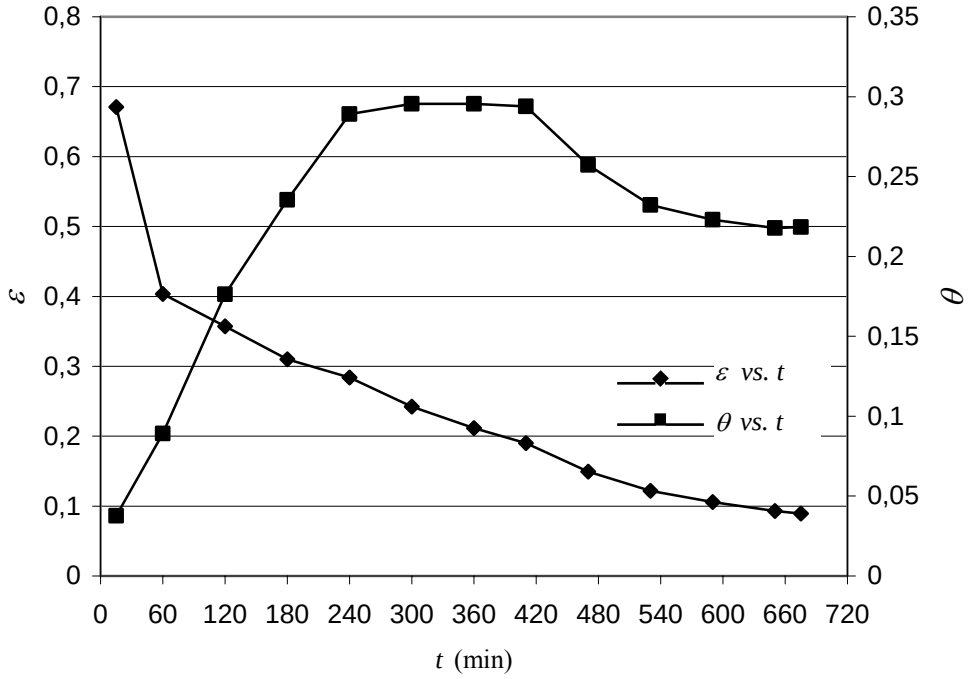

Figure 6.20 Variations of ε and θ (Exp. 1, $A = 0.26$)

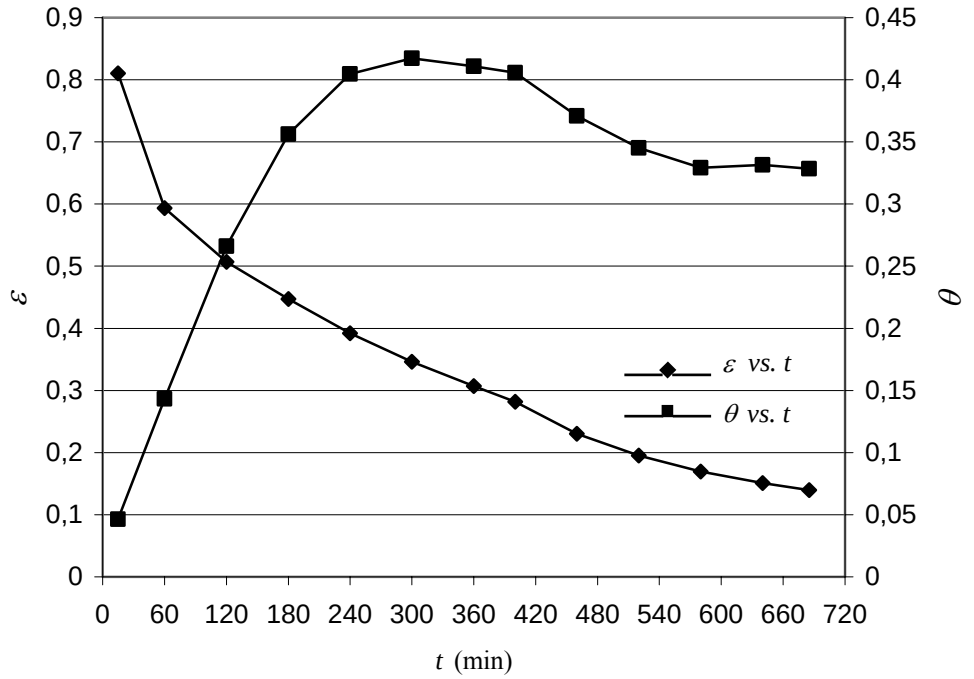

Figure 6.21 Variations of ε and θ (Exp. 2, $A = 0.26$)

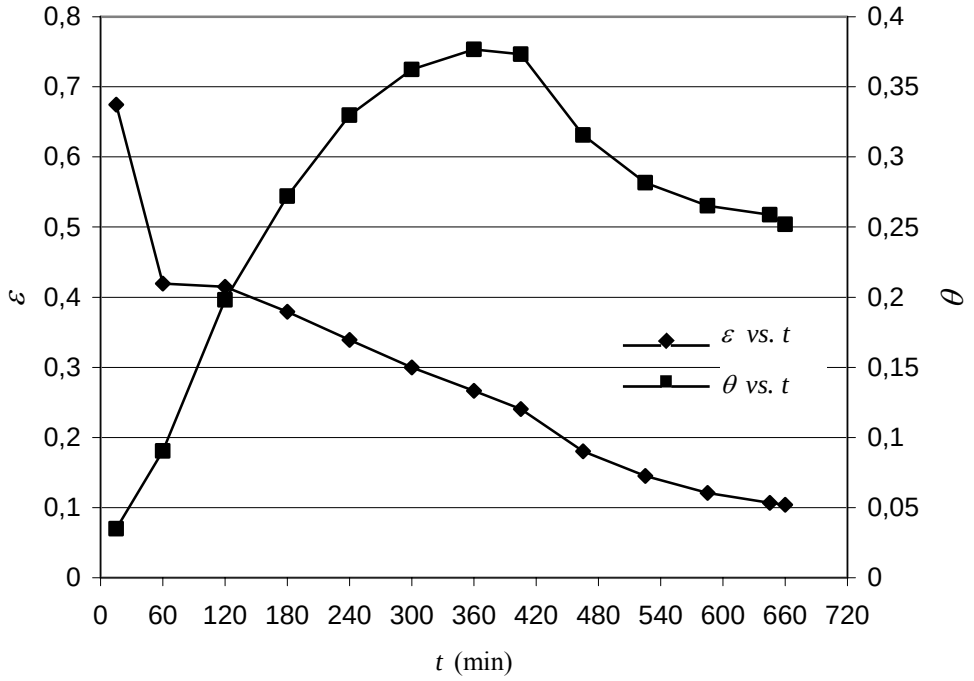

Figure 6.22 Variations of ε and θ (Exp. 4, $A = 0.26$)

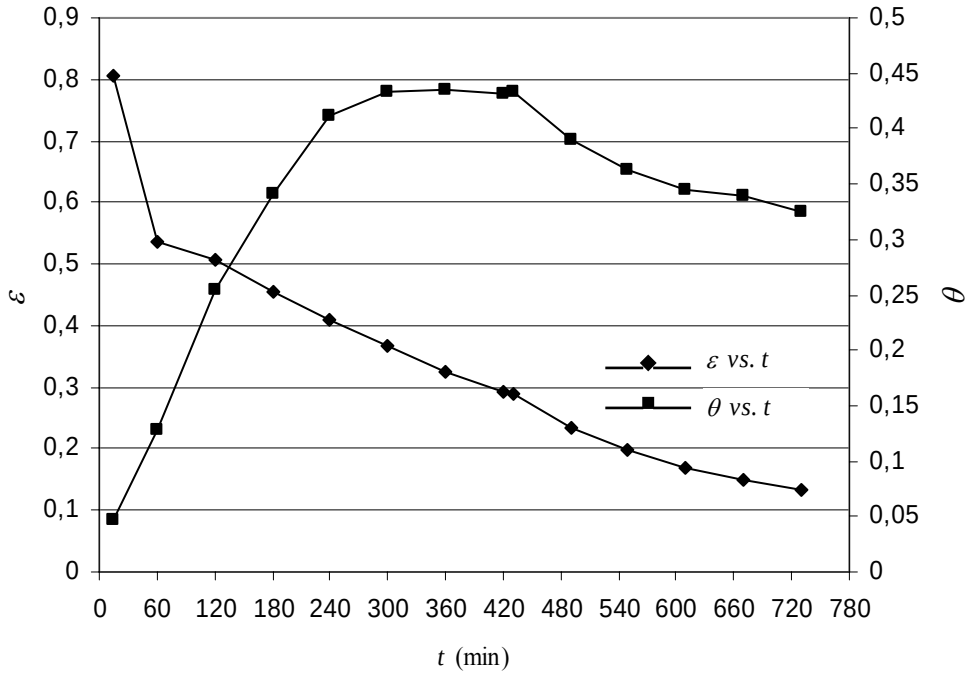

Figure 6.23 Variations of ε and θ (Exp. 7, $A = 0.26$)

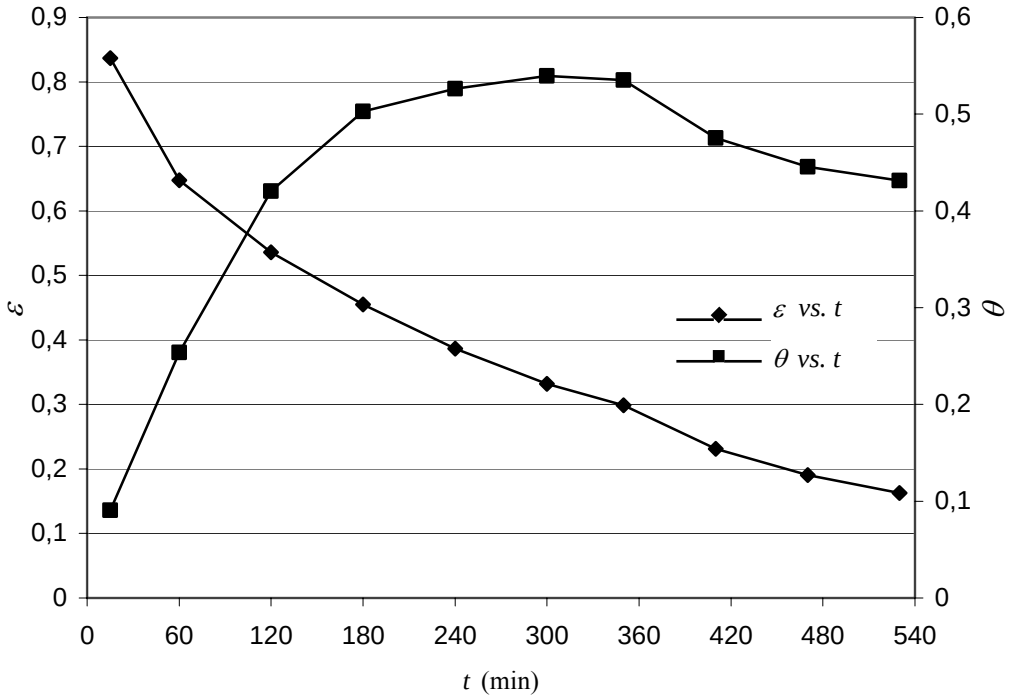

Figure 6.24 Variations of ε and θ (Exp. 16, $A = 0.16$)

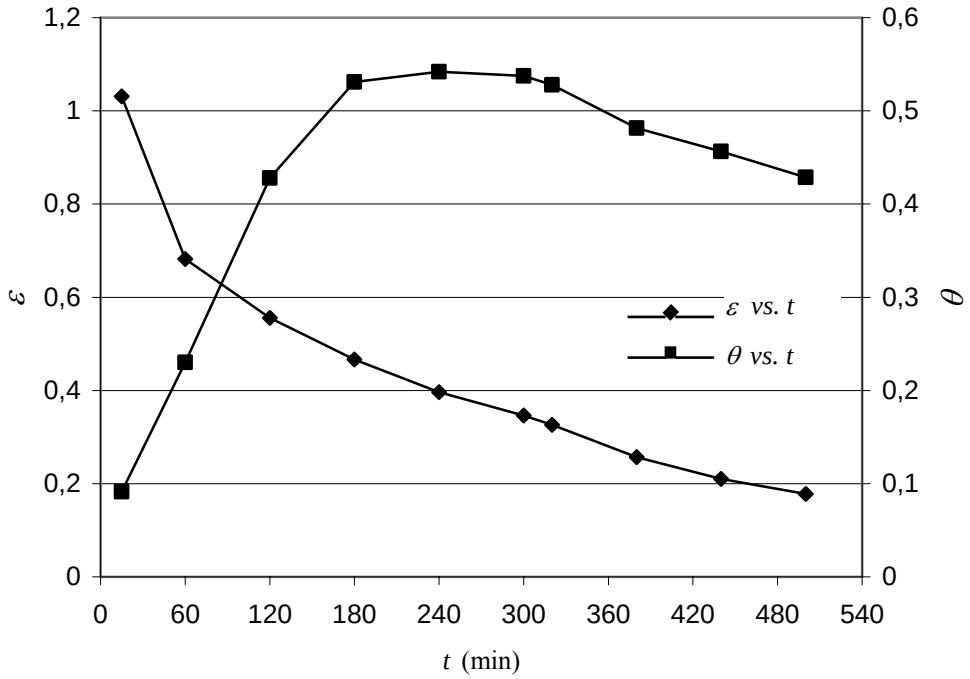

Figure 6.25 Variations of ε and θ (Exp. 17, $A = 0.16$)

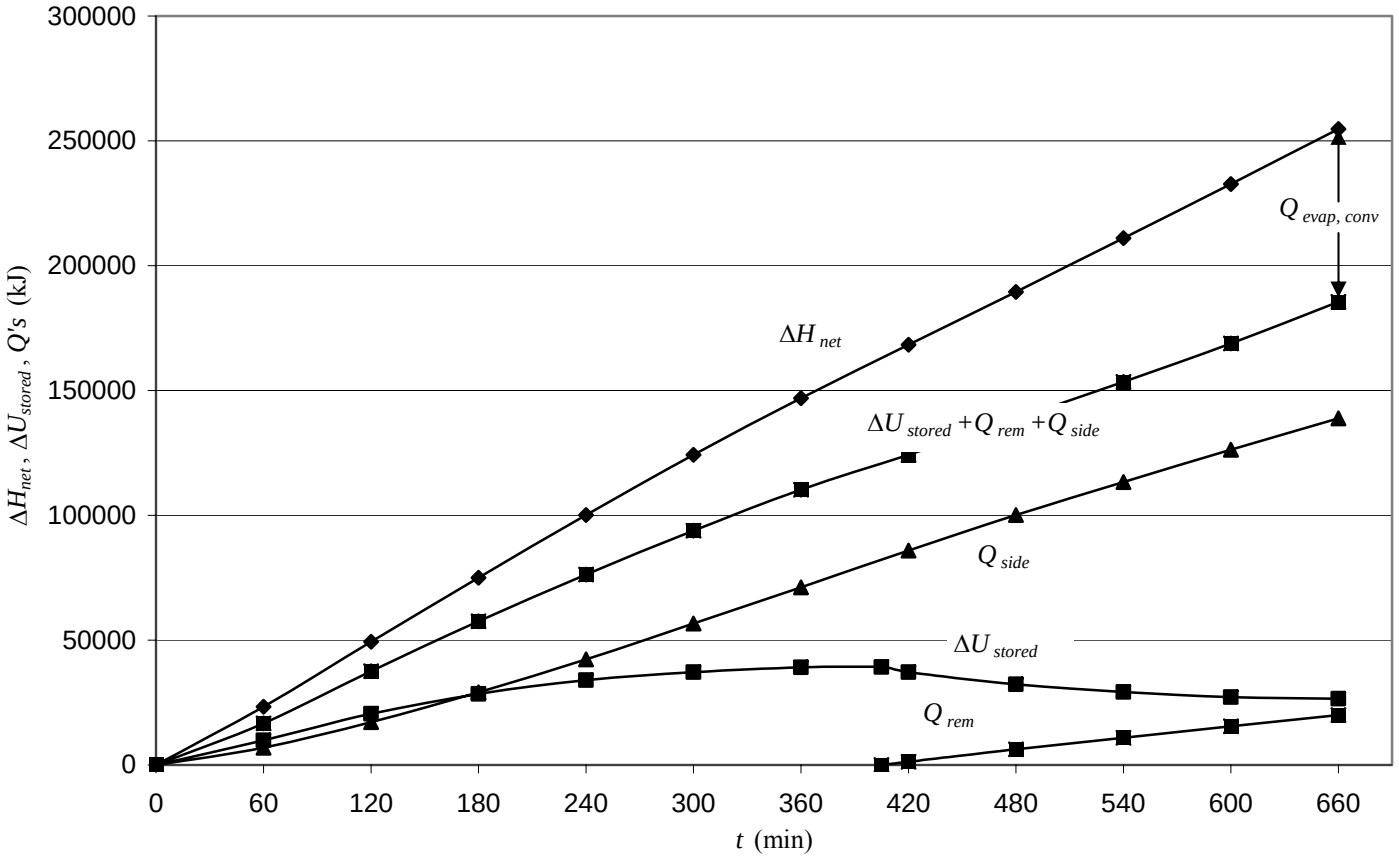

Figure 6.26 Variations of ΔH_{net}, ΔU_{stored}, Q_{rem}, and Q_{side} (Exp. 4, $A = 0.26$)

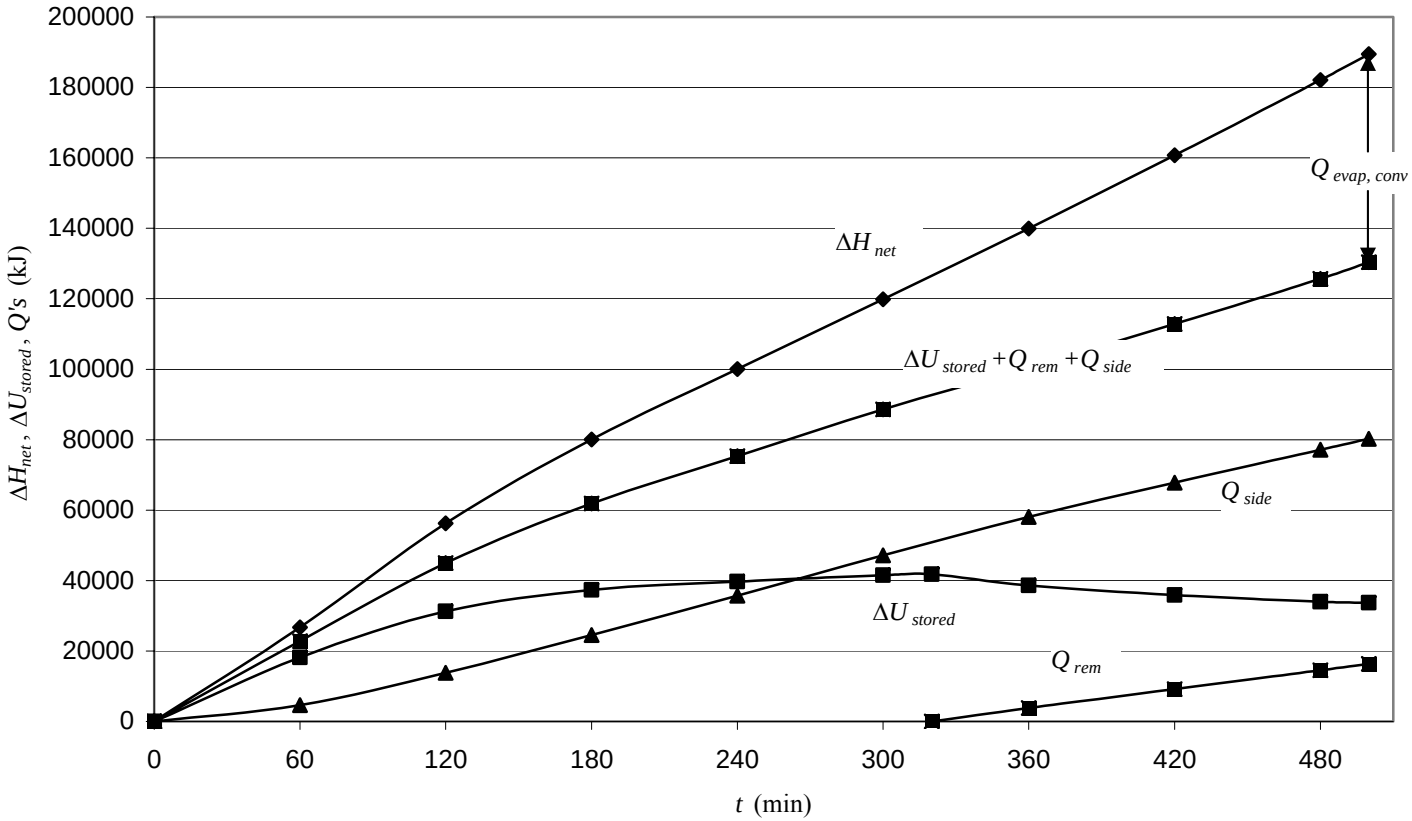

Figure 6.27 Variations of ΔH_{net}, ΔU_{stored}, Q_{rem}, and Q_{side} (Exp. 17, $A = 0.16$)

Table 6.2 Summary of Experimental Results (Heat Removal with Charging)

Exp. No	*A*	$\dot{m}_w$ (kg/hr)	T_i (°C)	T_{amb} (°C)	*Heat Removal Period* (min)	$\dot{m}_{w_{rem}}$ (kg/hr)	*d* (cm)	Q_{rem} *in* 180 *min* (MJ)
1	0.26	206	47.5	24	270	165	18	11.1
2		214	48.4	23.5	285	165	15	12.8
3		230	45.8	25	270	198	13	14.4
4		219	48.4	25	255	171	11	14.3
5		216	47.7	24.5	285	164	9	14.4
6		222	48.5	25	280	169	7	15.6
7		226	47.0	25	300	176	5	16.6
16	0.16	231	49.3	24	180	171	7	17.1
17		227	49.1	22	180	162	5	16.2
18		229	49.8	21.5	210	162	3	17.2

For $A = 0.26$, variation of net enthalpy input to the system, ΔH_{net}, is linear since charging water temperature varies slightly throughout an experiment and also the variation in the discharged water temperature for this aspect ratio is insignificant. The fraction of ΔU_{stored} within ΔH_{net} is maximum at the beginning of the experiment and starts to decrease towards the end of charging period. After the start of heat removal, the magnitude of $\Delta U_{stored} + Q_{rem}$ remains almost constant, hence looses its ratio from the whole energy input. After 660 min, ΔU_{stored} is expected to remain constant while Q_{rem} continues to rise with the same rate.

Fraction of Q_{side} in the total loss items is minimum during the beginning of the charging period. Q_{side} increases parabolically until around half of the charging period and then the increase turns to be a linear growth. Fraction of heat loss through the free surface in the heat loss items is maximum at the beginning of the

charging period and decreases as the rate of side loss increases. The rate of heat loss by combined evaporation and convection through the free surface is almost constant during an experiment since surface temperature and ambient conditions vary slightly.

The trend of ΔH_{net} *vs.* t changes for the lower aspect ratio. The slope of the curve is steeper up to around 120 min of the charging period and starts to decrease gradually to a constant value around 180 min. This is a direct consequence of the temperature development at the bottom of the storage unit from where discharged water drained.

Heat loss from the free surface is more compatible with the side heat loss for the lower aspect ratio since lower aspect ratio results smaller side loss area while the free surface has the same area for the two aspect ratios.

6.2.2 Heat Removal without Charging

Vertical temperature profile developments during heat removal without charging of the storage unit are presented in Figure 6.28 thru 6.30 for $A = 0.26$ and in Figure 6.31 and 6.32 for $A = 0.16$.

The important observations are as follows:

- Temperature drop within the upper layers is more rapid than the lower layers due to high heat loss from the relatively warmer surface.
- Heat removal enhances the decay rate of temperature field near the heat removal tubes.
- Thermal stratification eventually dies out. Only weak thermal stratification remains in the region above the heat removal tubes ($A = 0.26$).
- The temperature at the bottom of the storage unit is affected more for the lower aspect ratio since the heat removal tubes and free surface are closer to the bottom.

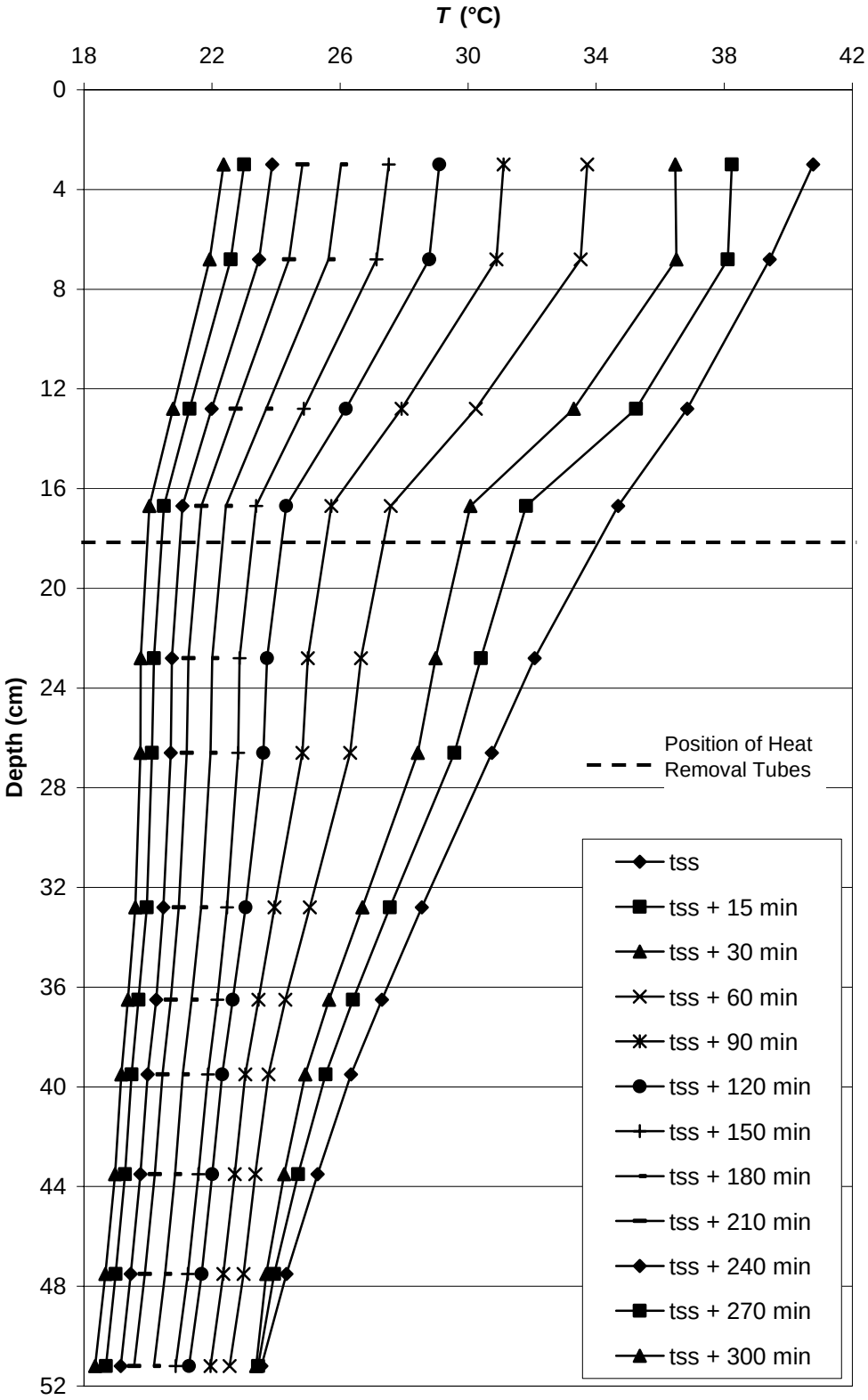

Figure 6.28 Development of Vertical Temperature Profile within the Storage Unit during Heat Removal (Exp. 8, $A = 0.26$, without Charging)

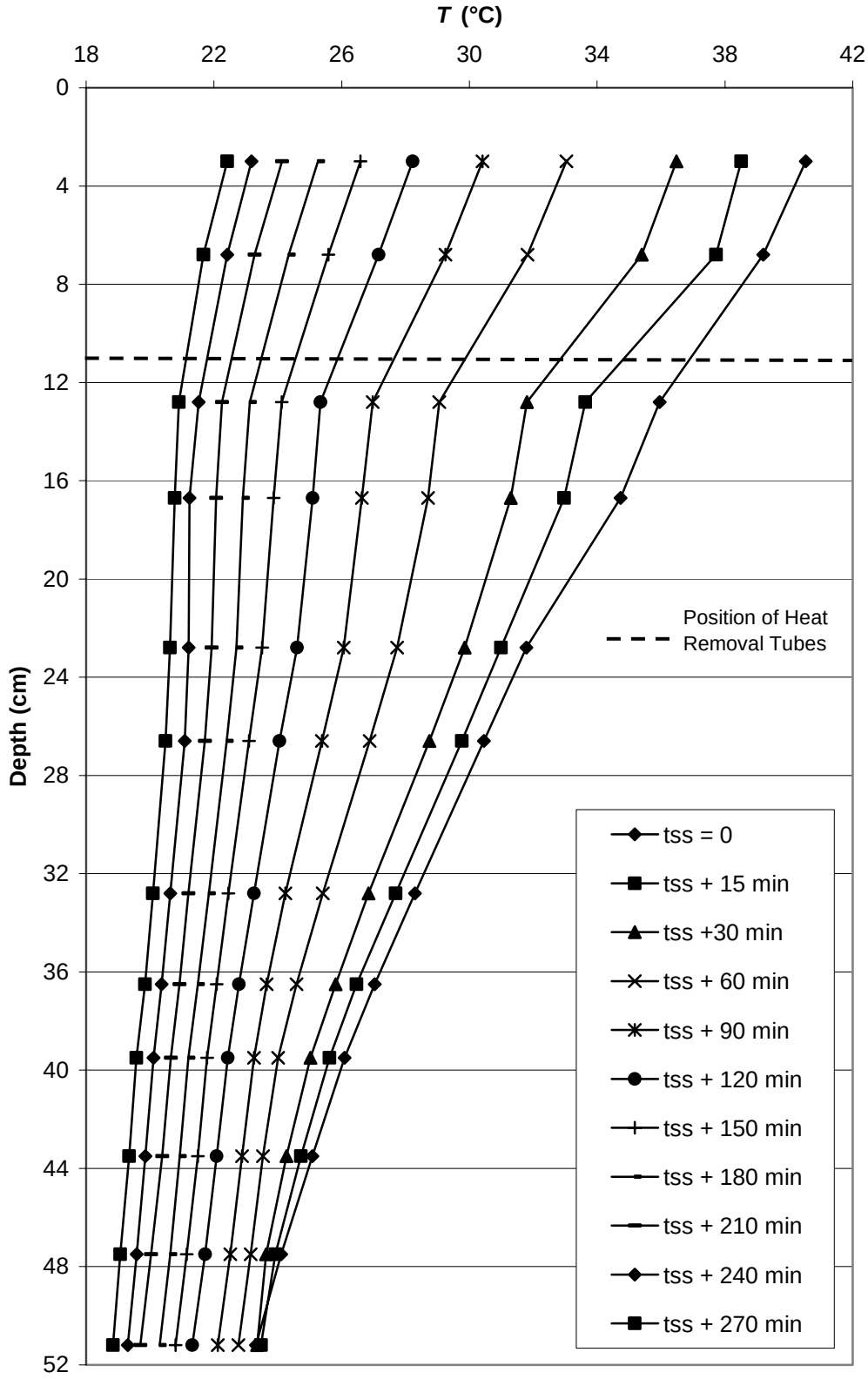

Figure 6.29 Development of Vertical Temperature Profile within the Storage Unit during Heat Removal (Exp. 11, $A = 0.26$, without Charging)

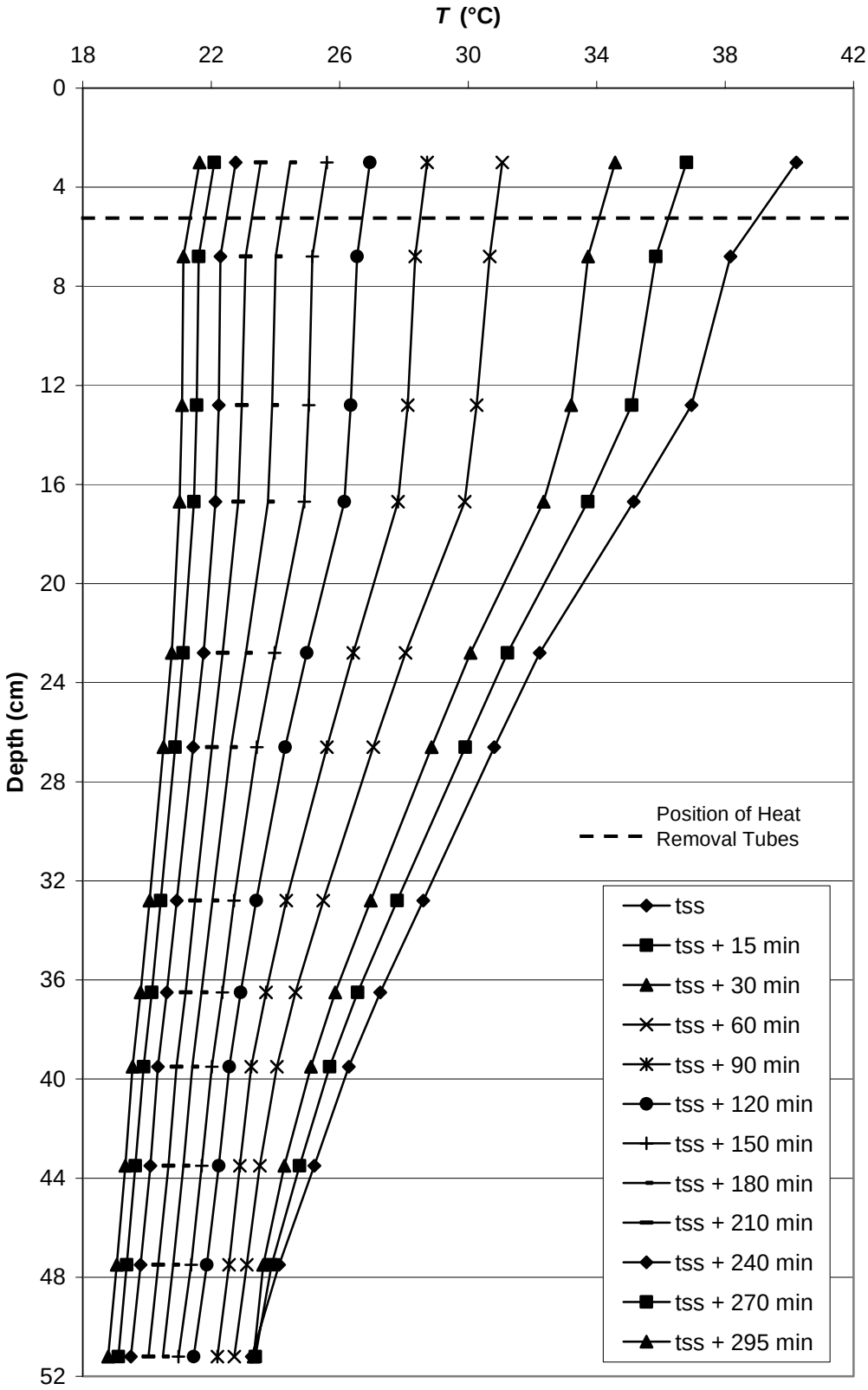

Figure 6.30 Development of Vertical Temperature Profile within the Storage Unit during Heat Removal (Exp. 14, $A = 0.26$, without Charging)

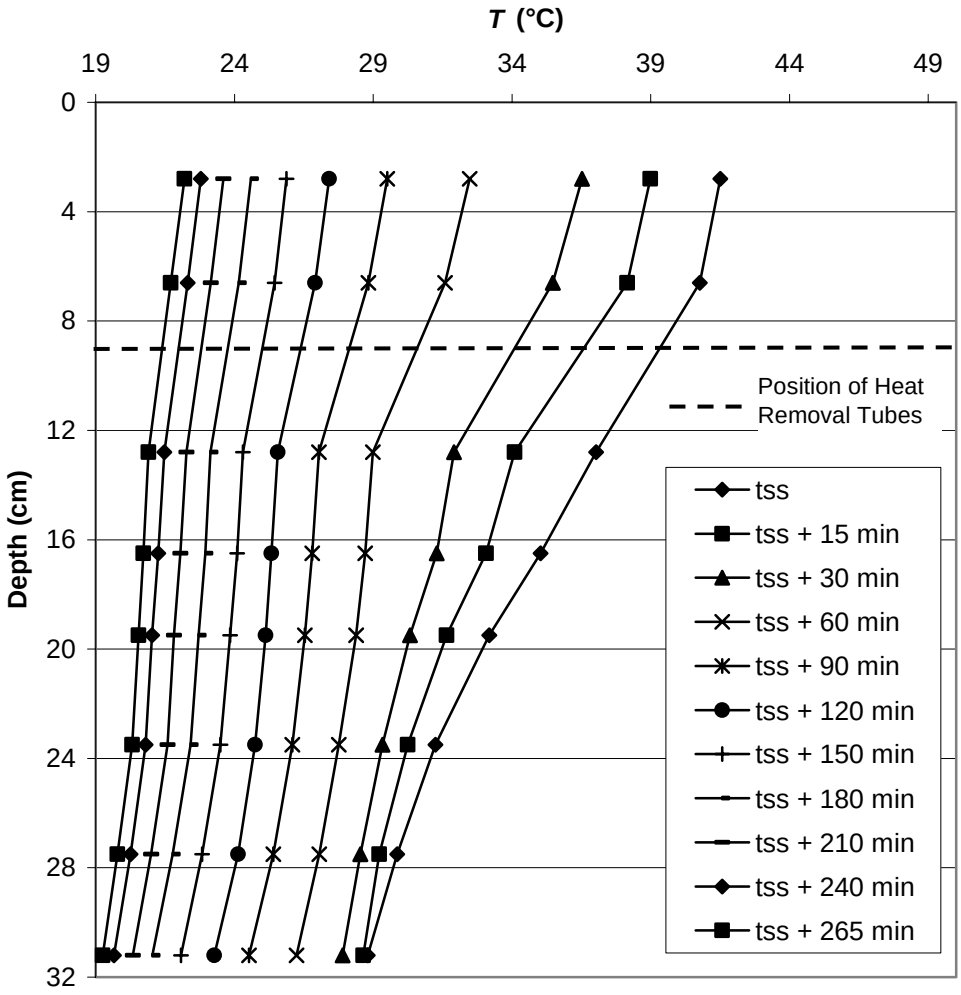

Figure 6.31 Development of Vertical Temperature Profile within the Storage Unit during Heat Removal (Exp. 19, A = 0.16, without Charging)

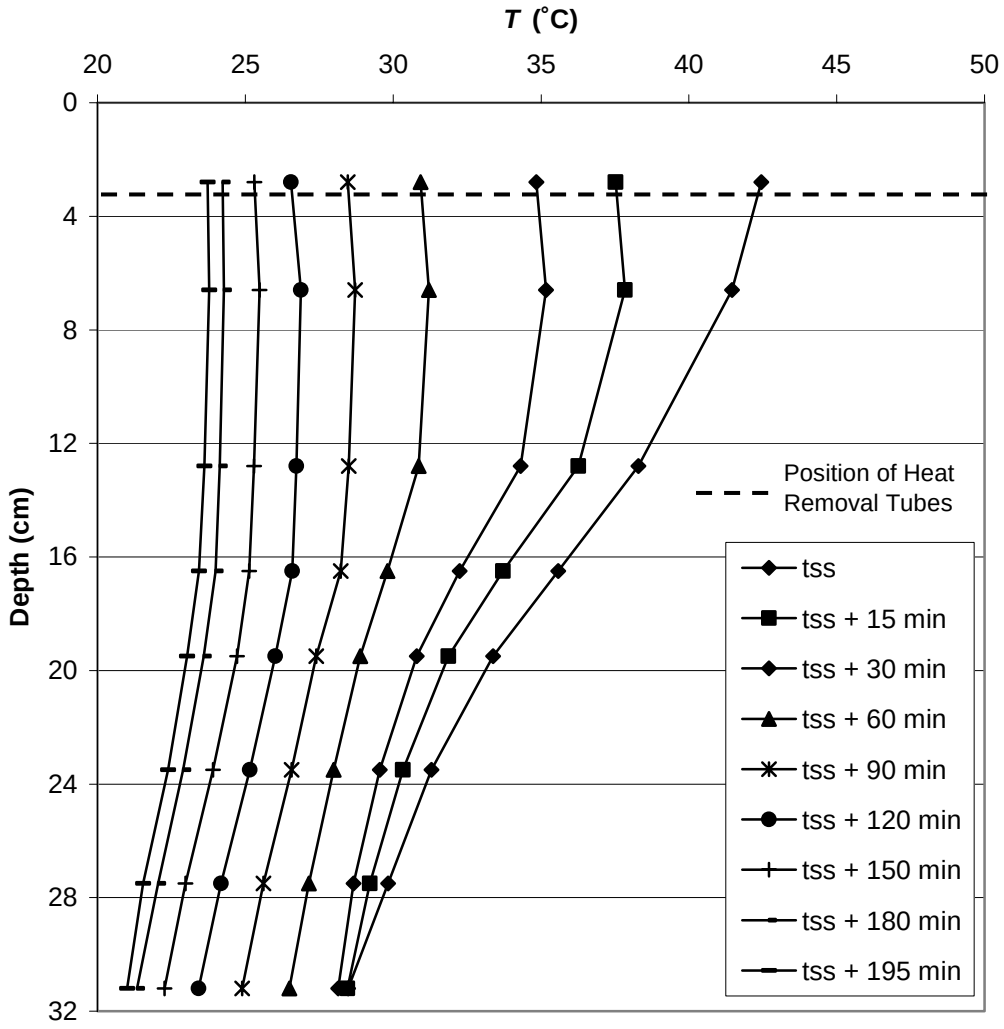

Figure 6.32 Development of Vertical Temperature Profile within the Storage Unit during Heat Removal (Exp. 22, A = 0.16, without Charging)

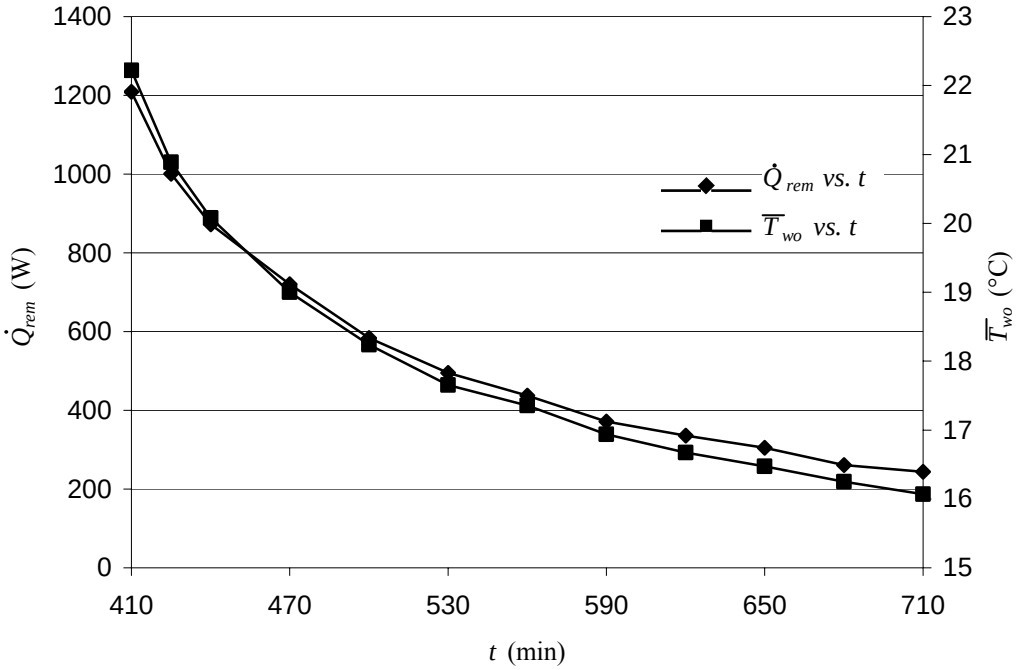

Figure 6.33 Variations of $\dot{Q}_{rem}$ and $\overline{T}_{wo}$ during Heat Removal
(Exp. 8, $A = 0.26$, $T_{wi} \cong 15.1°C$, without Charging)

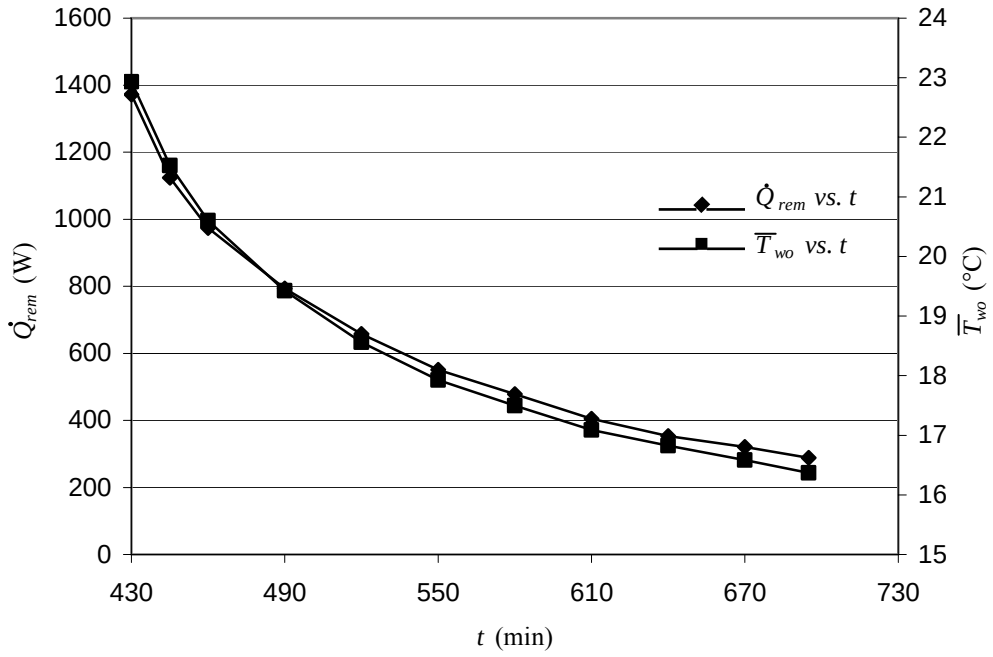

Figure 6.34 Variations of $\dot{Q}_{rem}$ and $\overline{T}_{wo}$ during Heat Removal
(Exp. 10, $A = 0.26$, $T_{wi} \cong 15.1°C$, without Charging)

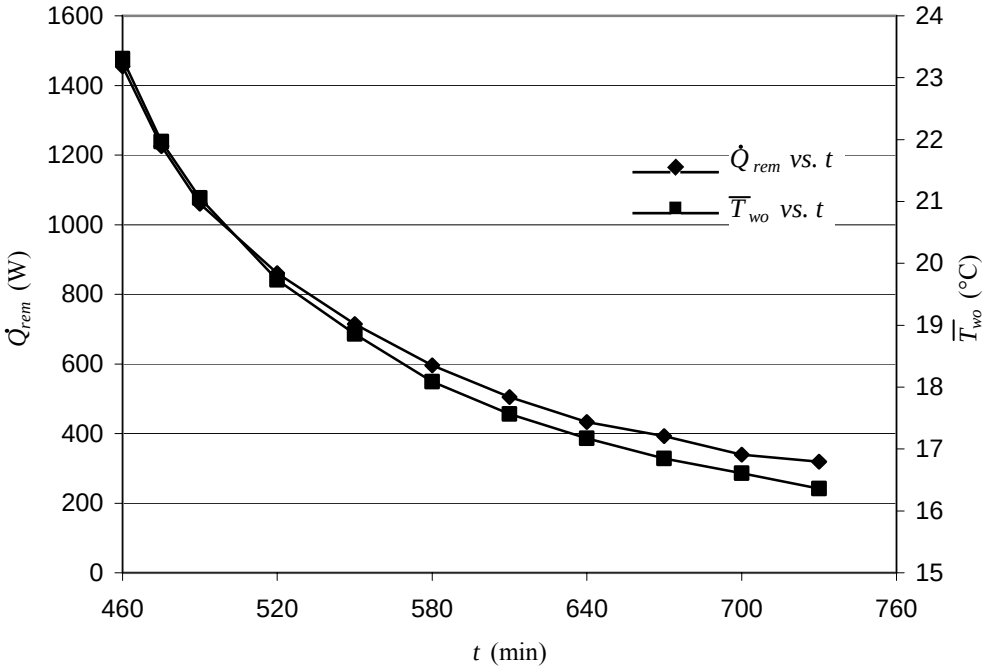

Figure 6.35 Variations of $\dot{Q}_{rem}$ and $\overline{T}_{wo}$ during Heat Removal
(Exp. 11, $A = 0.26$, $T_{wi} \cong 15.1°C$, without Charging)

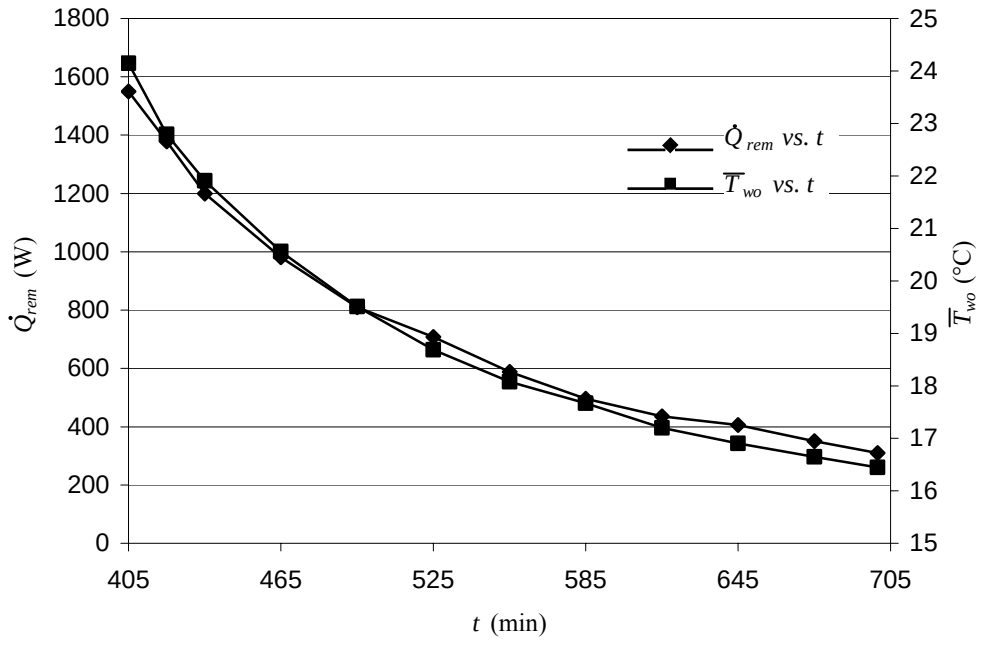

Figure 6.36 Variations of $\dot{Q}_{rem}$ and $\overline{T}_{wo}$ during Heat Removal
(Exp. 13, $A = 0.26$, $T_{wi} \cong 15.2°C$, without Charging)

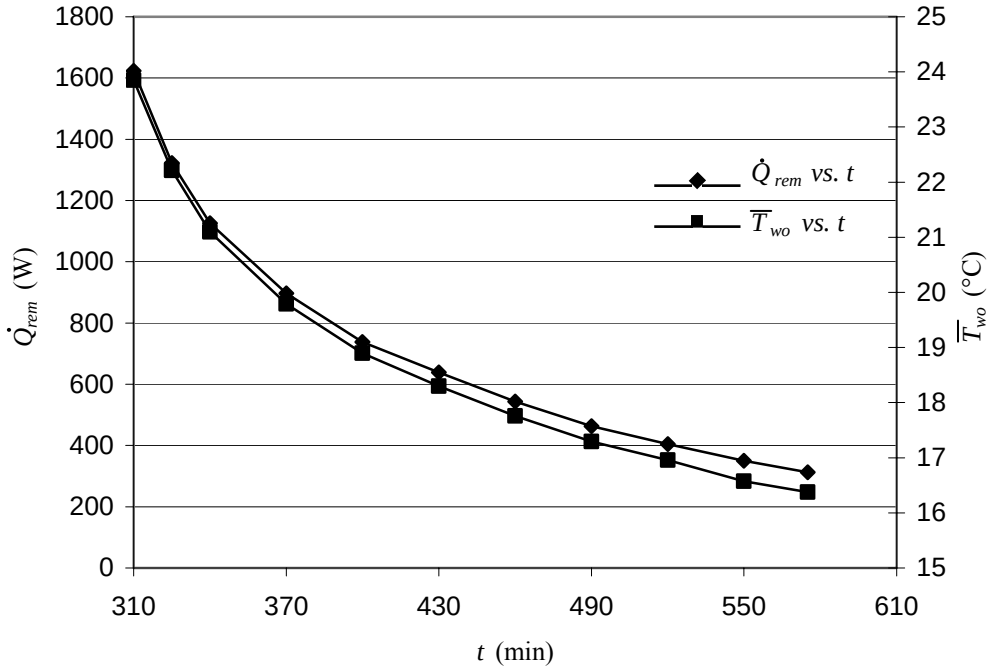

Figure 6.37 Variations of $\dot{Q}_{rem}$ and $\overline{T}_{wo}$ during Heat Removal
(Exp. 19, $A = 0.16$, $T_{wi} \cong 15.2°C$, without Charging)

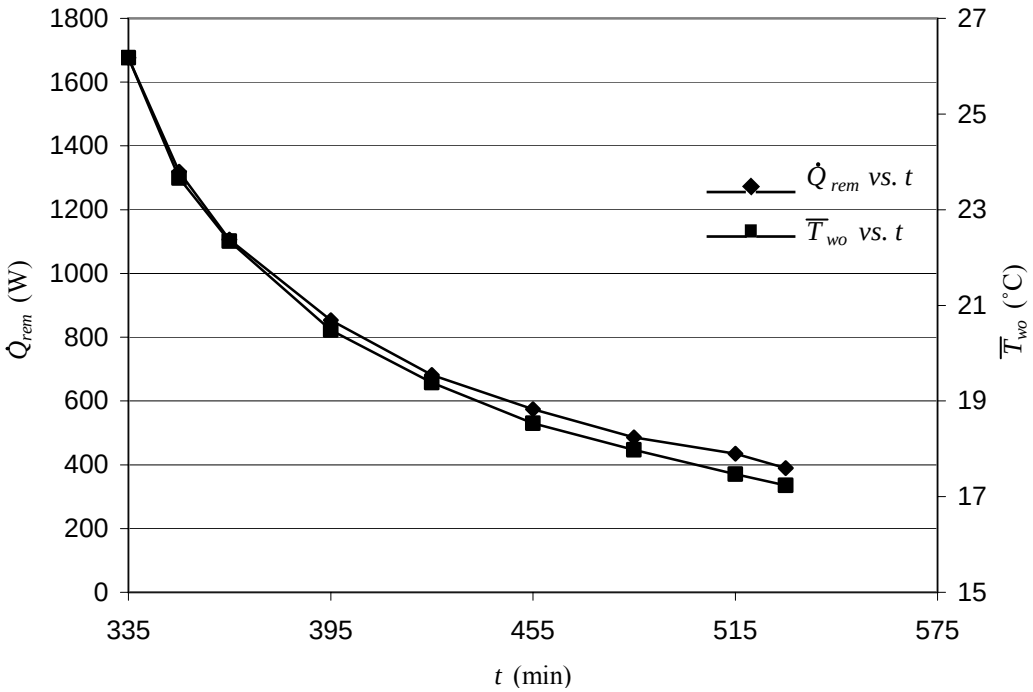

Figure 6.38 Variations of $\dot{Q}_{rem}$ and $\overline{T}_{wo}$ during Heat Removal
(Exp. 22, $A = 0.16$, $T_{wi} \cong 15.5°C$, without Charging)

Table 6.3 Summary of Experimental Results (Heat Removal without Charging)

Exp. No	*A*	T_{amb} (°C)	$\dot{m}_{w_{rem}}$ (kg/hr)	*d* (cm)	Q_{rem} *in* 180 *min* (MJ)
8	0.26	23.5	168	18	7.1
9		23.5	168	15	7.6
10		23	167	13	7.9
11		23	168	11	8.5
12		23.5	143	9	8.8
13		24	168	7	9.7
14		24.5	184	5	10.1
19	0.16	21.5	178	9	9.0
20		24.5	176	7	10.0
21		22	172	5	9.9
22		21.5	154	3	8.6

Figure 6.33 thru 6.38 show the variations of $\dot{Q}_{rem}$ and $\overline{T}_{wo}$. Both $\dot{Q}_{rem}$ and $\overline{T}_{wo}$ drop rapidly during the heat removal period due to the decrease of the available stored energy within the storage. Heat removed from the storage unit during the first 180 min of the heat removal period for different experiments are presented in Table 6.3. For the higher aspect ratio, total heat removed increases as the heat removal is from higher layers of the storage medium. Total heat removed in 180 min from the same depth for the two aspect ratios are comparable.

Figure 6.39 thru 6.44 show the variations of net energy stored within the storage unit, ΔU_{stored}, and mean bulk temperature of the storage, T_b. For a given aspect ratio, maximum values of mean bulk temperature vary only slightly. Lower aspect ratio results in higher maximum mean bulk temperature. Net energy stored within the storage during charging is higher when initial temperature of the storage, T_0,

is lower. Higher T_0 is a result of higher stored energy during the start of experiments and this energy could be consumed during heat removal resulting negative ΔU_{stored} values towards the end of heat removal period.

Figure 6.45 and 6.46 show the variations of ΔU_{stored}, Q_{rem}, and loss items for the two aspect ratios during the heat removal period. The increases in both Q_{rem} and Q_{side} slow gradually as the ΔU_{stored} within the storage decreases. At the end of heat removal period, two thirds of net stored energy at the beginning was lost through the side walls while the last third shared almost equally by Q_{rem} and $Q_{evap,conv}$ for A = 0.26. For the lower aspect ratio, less than half of the available net stored energy was lost through the side walls while the rest shared again almost equally by Q_{rem} and $Q_{evap,conv}$.

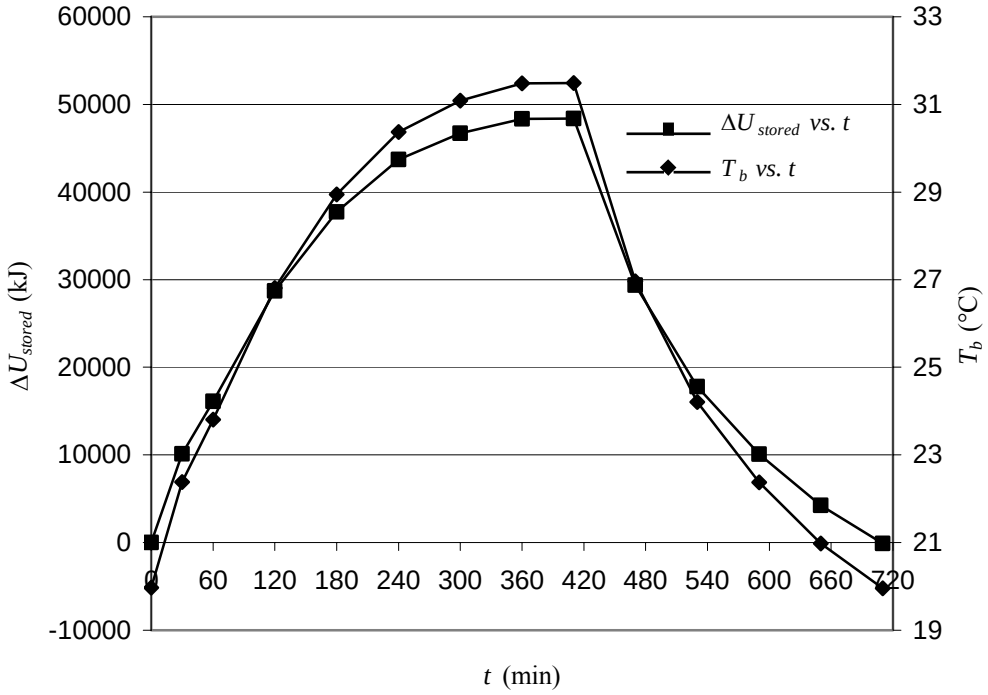

Figure 6.39 Variations of ΔU_{stored} and T_b (Exp. 8, $A = 0.26$)

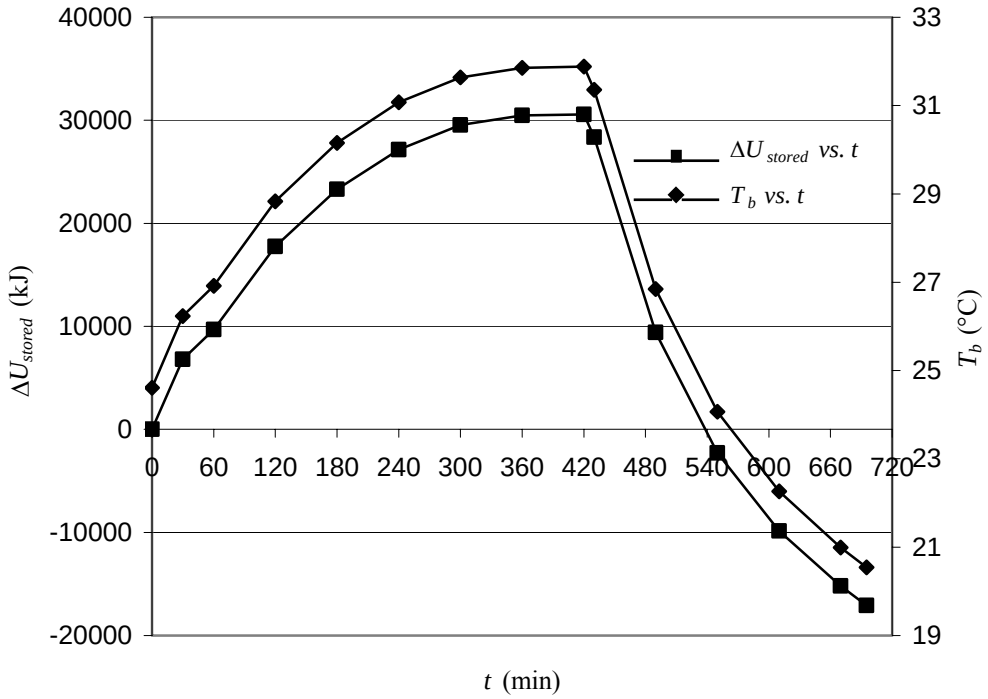

Figure 6.40 Variations of ΔU_{stored} and T_b (Exp. 10, $A = 0.26$)

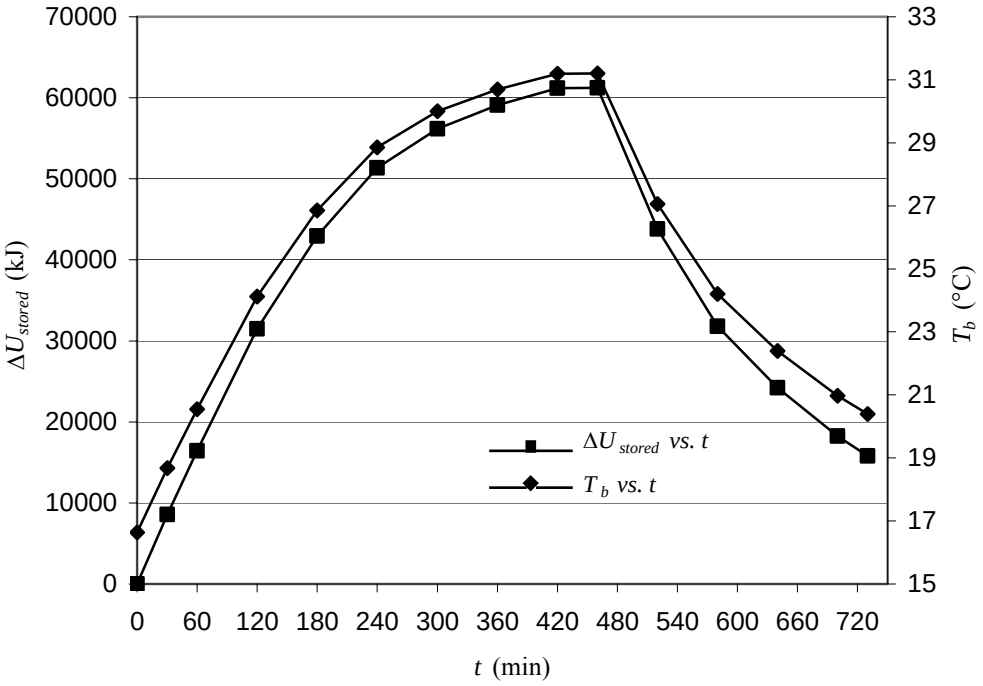

Figure 6.41 Variations of ΔU_{stored} and T_b (Exp. 11, $A = 0.26$)

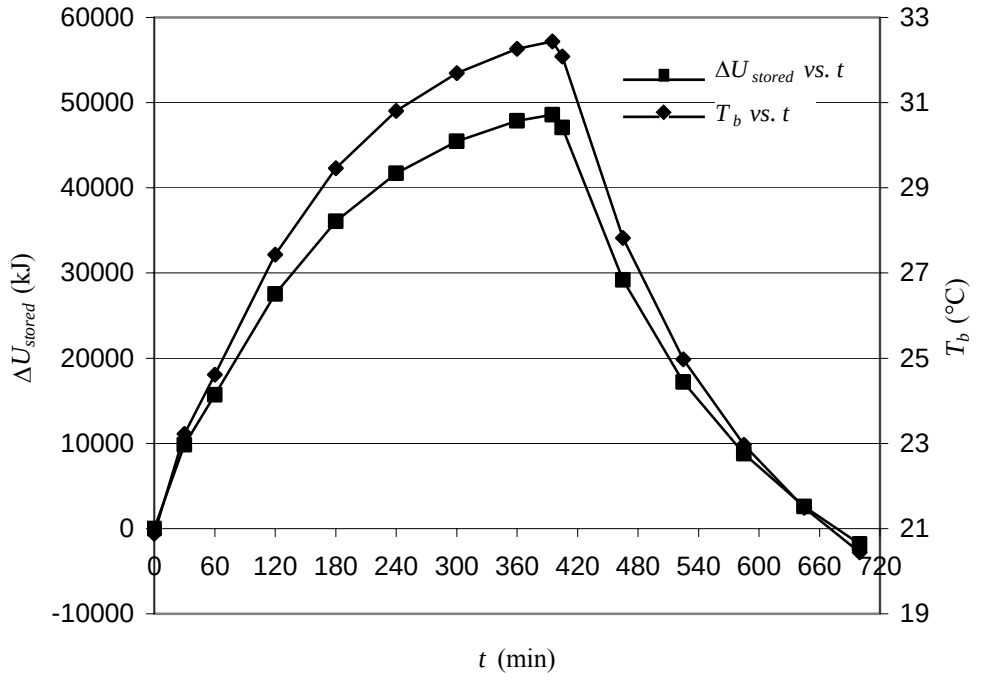

Figure 6.42 Variations of ΔU_{stored} and T_b (Exp. 13, $A = 0.26$)

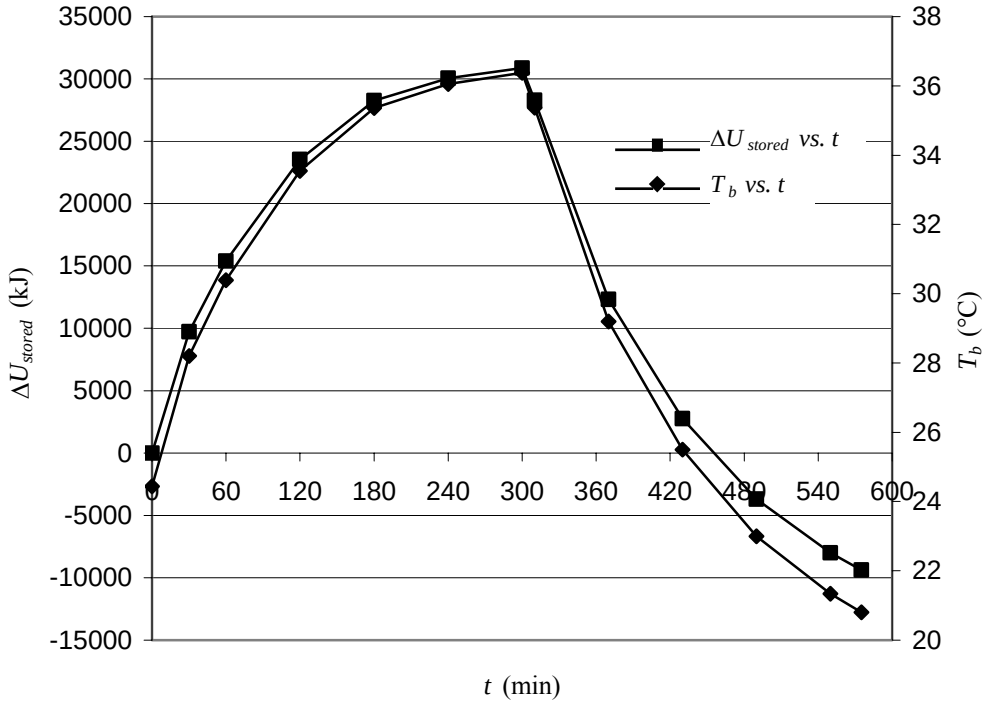

Figure 6.43 Variations of ΔU_{stored} and T_b (Exp. 19, $A = 0.16$)

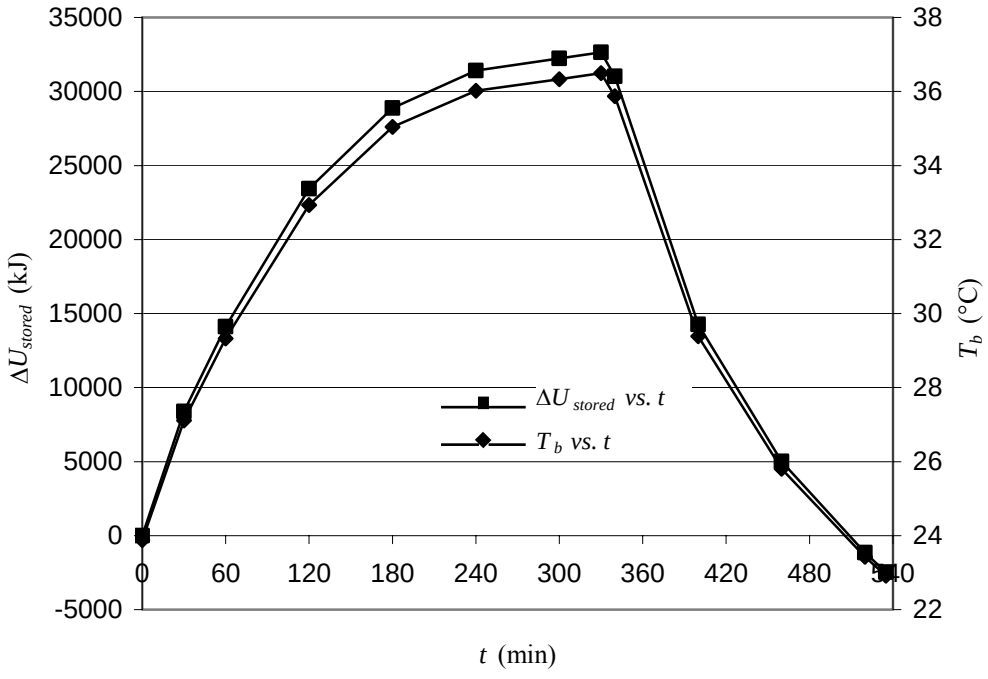

Figure 6.44 Variations of ΔU_{stored} and T_b (Exp. 22, $A = 0.16$)

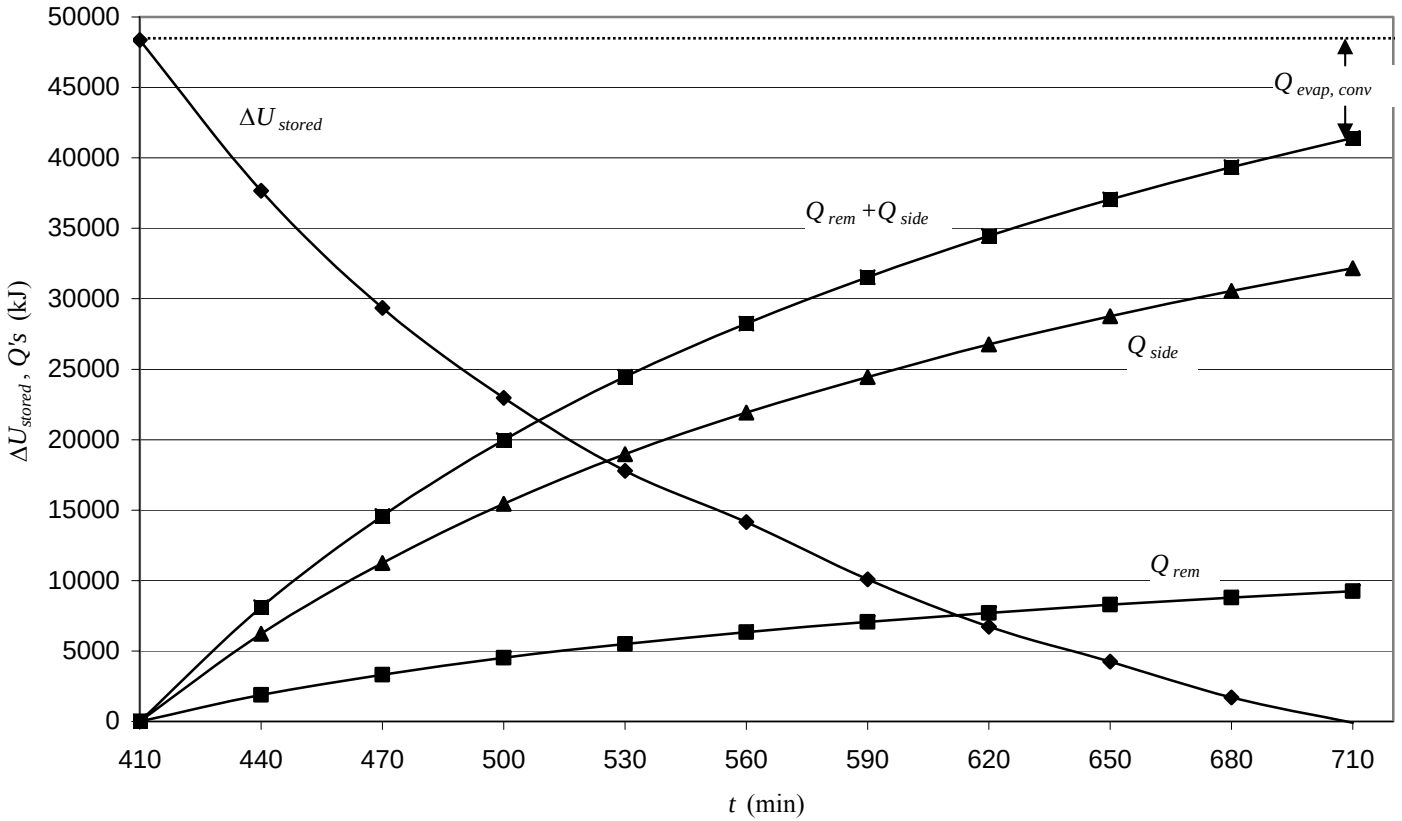

Figure 6.45 Variations of ΔU_{stored}, Q_{rem}, and Q_{side} (Exp. 8, $A = 0.26$)

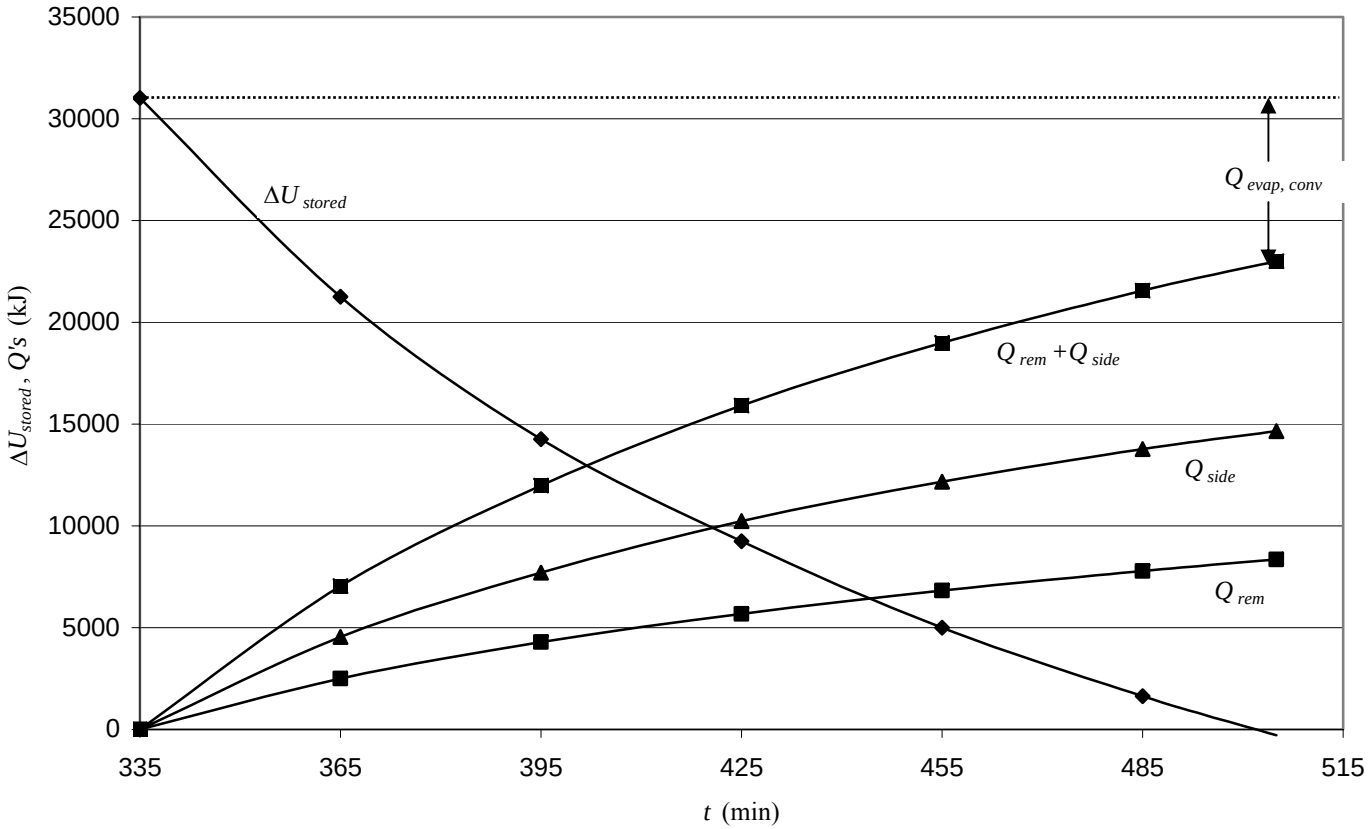

Figure 6.46 Variations of ΔU_{stored}, Q_{rem}, and Q_{side} (Exp. 22, $A = 0.16$)

CHAPTER 7

CONCLUSIONS

A preliminary experimental study was performed in order to investigate the charging and heat removal characteristics of the warm water storage. The emphasis of the study was on observing the heat removal outputs from different elevations of the storage medium for the two different heat removal configurations, one involving simultaneous heat removal from and charging of a previously loaded storage, and the other one involving the heat removal from a previously loaded storage. In all of the experiments, similar storage medium at the end of the charging period (beginning of the heat removal period) was intended by keeping the boundary conditions as similar as possible.

In all of the experiments, thermal stratification could be achieved within the storage medium in the vertical direction. Thermal stratification could not be disturbed considerably by the present heat removal tubes and mass flow rates of water passing through the tubes provided that charging of the storage unit was continuous.

It can be concluded that higher heat removal outputs can be obtained as the heat extraction is from upper and upper layers of the stratified medium, although the close proximity of the free surface was avoided for heat extraction. Heat removal outputs for the two aspect ratios from same elevations were found to be comparable.

Steady-state heat removal outputs could be obtained from the storage while charging is continuous. These low grade outputs could be used for preheating of a successive process.

The measurement of the mass flow rate of water passing through the heat removal tubes was problematic and this caused the largest error in the experiments. The mean outlet temperature of the tubes was assumed to be the arithmetic mean of the outlet temperatures of the four tubes presuming that all the flow rates were equal. It was not the real situation and in some of the experiments these flow rates differed considerably. Manual interference sometimes worsened the situation. The result was timewise fluctuations in the calculated heat removal outputs. Also in some of the experiments water flow rate from the campus grid varied considerably during the long experiments. The solution could be utilizing seperate reservoirs with the same and constant head for the tubes and overfeeding the reservoirs from campus grid letting the excess water thrown away. Digital measurement of all of the mass flow rates (charging mass flow rate, seperate mass flow rates through the tubes, mass flow rates through the water jackets) can decrease the errors occuring during the measurements, can improve the response of experimental data to the fluctuations in these items during experiments, and can lighten the workload of the experimenter.

Heat removal tubes of the set-up were very primitive. Different geometries and/or fins could be utilized in order to enhance heat removal from the storage unit. Further analysis can be performed at higher charging mass flow rates and variable charging temperatures. Accuracy, repeatability, and reliability of the experimental work could be improved.

REFERENCES

[1] Kakaç S., Paykoç E., and Yener Y., Storage of Solar Thermal Energy, *Energy Storage Systems: Fundamentals & Applications,* ASI Proceedings, 1988.

[2] Oberkampf W. L. and Crow L. I., Numerical study of the velocity and temperature fields in a flow-through reservoir, *J. Heat Transfer,* Vol. 98, pp. 353-359, 1976.

[3] Lavan Z. and Thompson J., Experimental study of thermally stratified hot water storage tanks, *Solar Energy,* Vol. 19, pp. 519-524, 1977.

[4] Çömez F., Large Scale Energy Storage, M. S. Thesis, ME Department of Middle East Technical University, 1981.

[5] Jaluria Y. and Gupta S. K., Decay of thermal stratification in a water body for solar energy storage, *Solar Energy,* Vol. 28, No. 2, pp. 137-143, 1982.

[6] Jaluria Y. and O'Mara B. T., Thermal field in a water body for solar energy storage and extraction due to a buoyant two-dimensional surface water jet, *Solar Energy,* Vol. 43, No. 3, pp. 129-138, 1989.

[7] Yoo H. and Pak E.-T., Theoretical model of the charging process for stratified thermal storage tanks, *Solar Energy,* Vol. 51, No. 6, pp. 513-519, 1993.

[8] Safi M. J. and Loc T. P., Development of thermal stratification in a two-dimensional cavity: a numerical study, *Int. J. Heat Mass Transfer,* Vol. 37, No. 14, pp. 2017-2024, 1994.

[9] Eames P. C. and Norton B., The effect of tank geometry on thermally stratified sensible heat storage subject to low Reynolds number flows, *Int. J. Heat Mass Transfer,* Vol. 41, No. 14, pp. 2131-2142, 1998.

[10] Spall R. E., A numerical study of transient mixed convection in cylindrical thermal storage tanks, *Int. J. Heat Mass Transfer,* Vol. 41, No. 13, pp. 2003-2011, 1998.

[11] Hahne E. and Chen Y., Numerical study of flow and heat transfer characteristics in hot water stores, *Solar Energy,* Vol. 64, Nos 1-3, pp. 9-18, 1998.

[12] Alizadeh S., An experimental and numerical study of thermal stratification in a horizontal cylindrical solar storage tank, *Solar Energy,* Vol. 66, No. 6, pp. 409-421, 1999.

[13] Yoo H., Kim C.-J., and Kim C. W., Approximate analytical solutions for stratified thermal storage under variable inlet temperature, *Solar Energy,* Vol. 66, No. 1, pp. 47-56, 1999.

[14] Bouhdjar A. and Harhad A., Numerical analysis of transient mixed convection flow in storage tank: influence of fluid properties and aspect ratios on stratification, *Renewable Energy,* Vol. 25, pp. 555-567, 2002.

[15] Shin M.-S., Kim H.-S., Jang D.-S., Lee S.-N., Lee Y.-S., and Yoon H.-G., Numerical and experimental study on the design of a stratified thermal storage system, *Applied Thermal Engineering,* Vol. 24, pp. 17-27, 2004.

[16] *Operating Instructions Model 3702,* MOLYTEK Inc., 1986.

[17] Incropera F. P. and DeWitt D. P., *Fundamentals of Heat and Mass Transfer,* Chap. 9, John Wiley & Sons, 1996.

APPENDIX A

SAMPLE DATA AND CALCULATION

A.1 Sample Data

Sample data is presented from Exp. 2, at $t = 0$ and $t = 600$ min. $t = 600$ min corresponds to 200 min after the start of heat removal process.

Table A.1 Temperature Probe Measurements

Depth (cm)	51.2	47.5	43.5	39.5	36.5	32.8	26.6
T.C. #	1	2	3	4	5	6	7
$T\|_{t=0}$ **(°C)**	20.8	20.9	21.1	21.2	21.4	21.5	21.6
$T\|_{t=600}$ **(°C)**	23.4	23.9	24.5	25.2	25.9	26.8	28.2
Depth (cm)	22.8	16.7	12.8	6.8	3	0	
T.C. #	8	9	10	11	12	29	
$T\|_{t=0}$ **(°C)**	21.7	21.7	21.7	21.7	21.7		
$T\|_{t=600}$ **(°C)**	28.9	30.5	37.0	40.9	42.6	48.9	

There is no thermocouple junction at the surface of the storage unit. Charging water temperature is assumed to be aproximately equal to the surface temperature.

Charging of the storage unit and recirculation of cooling water through the water jackets are started $t \geq 0$ virtually, giving no temperature reading at $t = 0$ in Table A.2.

Table A.2 Rest of the Thermocouple Readings

	T_{wi}	T_{wo1}	T_{wo2}	T_{wo3}	T_{wo4}	
T.C. #	20	21	22	23	24	
***t* = 0**						
***t* = 600 min**	15.5ºC	21.7ºC	21.4ºC	21.3ºC	21.9ºC	
	T_{wj1i}	T_{wj1o}	T_{wj2i}	T_{wj2o}	T_i	T_e
T.C. #	25	26	27	28	29	30
***t* = 0**						
***t* = 600 min**	14.3ºC	16.1ºC	14.3ºC	16.3ºC	48.9ºC	23.8ºC

Table A.3 Sample Data for Mass Flow Rate, Ambient Temperature, Ambient Pressure and Relative Humidity

	$\dot{m}_w$ (kg/hr)	$\dot{m}_{w_{rem}}$ (kg/hr)	$\dot{m}_{w_{waterjackets}}$ (kg/hr)	T_{amb} (°C)	P_{amb} (mmHg)	ϕ
***t* = 0**				23.5	679	0.53
***t* = 600 min**	211.2	165.1	1620	24	678	0.53

A.2 Sample Calculation

A.2.1. Calculation of Heat Removal Rate $\dot{Q}_{rem}$, Side Loss Rate $\dot{Q}_{side}$ and Enthalpy Input Rate $\dot{H}_{net}$ at t = 600 min

$$\dot{Q}_{rem} = \dot{m}_{w_{rem}} c_p (\bar{T}_{wo} - T_{wi})$$

where $c_p \cong 4.18\,\text{kJ/kgK}$

$$\bar{T}_{wo} = \frac{T_{wo1} + T_{wo2} + T_{wo3} + T_{wo4}}{4} = 21.6°\text{C}$$

heat removal rate becomes;

$$\dot{Q}_{rem} = 1.169\,\text{kW}$$

$$\dot{Q}_{side} = \dot{m}_{w_{waterjackets}} c_p (\overline{T}_{we_{waterjackets}} - \overline{T}_{wi_{waterjackets}})$$

where $\overline{T}_{we_{waterjackets}} = \dfrac{T_{wj1o} + T_{wj2o}}{2} = 16.2°\text{C}$

$$\overline{T}_{wi_{waterjackets}} = \frac{T_{wj1i} + T_{wj2i}}{2} = 14.3°\text{C}$$

Side heat loss rate becomes;

$$\dot{Q}_{side} = 3.5739\,\text{kW}$$

$$\dot{H}_{net} = \dot{m}_w c_p (T_i - T_e) = 6.155\,\text{kW}$$

A.2.2. Calculation of ΔU_{stored} and T_b

$$\Delta U_{stored} = \rho c_v BL \int_0^H \left[T(z,t) - T_0\right] dz$$

where $B = 97.5\,\text{cm}$ and $L = 199\,\text{cm}$

The integral is evaluated by summing up each trapezoidal area obtained by the two consecutive thermocouple readings and their respective depth diffence:

$$\int_0^{H=52\,\text{cm}} \left[T(z, t = 600\,\text{min}) - T_0\right] dz \cong (52 - 51.2)\cdot 23.4 + (51.2 - 47.5)(\frac{23.4 + 23.9}{2})$$
$$+(47.5 - 43.5)(\frac{23.9 + 24.5}{2}) + (43.5 - 39.5)(\frac{24.5 + 25.2}{2}) + (39.5 - 36.5)(\frac{25.2 + 25.9}{2})$$
$$+(36.5 - 32.8)(\frac{25.9 + 26.8}{2}) + (32.8 - 26.6)(\frac{26.8 + 28.2}{2}) + (26.6 - 22.8)(\frac{28.2 + 28.9}{2})$$
$$+(22.8 - 16.7)(\frac{28.9 + 30.5}{2}) + (16.7 - 12.8)(\frac{30.5 + 37.0}{2}) + (12.8 - 6.8)(\frac{37.0 + 40.9}{2})$$
$$(6.8 - 3)(\frac{40.9 + 42.6}{2}) + (3 - 0)(\frac{42.6 + 48.9}{2}) - 52\cdot 21.4 = 485.2\,\text{cm}\,°\text{C}$$

In the above calculation, temperature at the bottom 0.8 cm portion of the storage unit is assumed to be equal to first thermocouple reading. Also, T_0 is assumed to be constant. Total internal energy stored within the storage unit in 600 min becomes:

$$\Delta U_{stored} = 39233\,\text{kJ}$$

Mean bulk temperature is simply;

$$T_b = \frac{1}{H}\int_0^H \left[T(z,t) - T_0\right]dz + T_0 = 30.7^\circ\text{C}$$

A.2.3. Calculation of ε and θ

Net enthalpy input, ΔH_{net} can be calculated as;

$$\Delta H_{net} = \sum_{1}^{600\,\text{min}/\,\Delta t} \dot{H}_{net}\Delta t = 235832\,\text{kJ}$$

$\Delta t = 5\,\text{min}$, which is the temperature recording interval during the experiments. Corresponding $\dot{H}_{net}$ values are calculated individually.

Effectiveness at t = 600 min is then;

$$\varepsilon\big|_{t=600\,\text{min}} = \frac{\Delta U_{stored}}{\Delta H_{net}} = 0.166$$

and dimensionless bulk temperature is;

$$\theta\big|_{t=600\,\text{min}} = \frac{T_b - T_0}{T_i - T_0} = 0.338$$

APPENDIX B

ENERGY BALANCE FOR THE STORAGE UNIT

In Exp. 2, at t = 685 min, a steady-state temperature distribution was achieved after a heat removal period of 285 min. At this time, $\frac{dU}{dt} = 0$ for the storage unit and Equation 5.6 becomes:

$$\dot{Q}_{rem} + \sum \dot{Q}_{loss} = \dot{H}_{net}$$

The terms in the above equation are calculated as follows;

Evaporative heat loss rate from the free water surface is:

$T_s := 48.4 \cdot oC$ $T_{amb} := 24 \cdot oC$ $T_f := \frac{T_s + T_{amb}}{2}$ $T_f = 36.2\ oC$

air properties at T_f $\rho_a = 1.141 \frac{kg}{m^3}$ $k_a = 0.027 \frac{W}{m \cdot K}$ $\nu_a = 1.662 \times 10^{-5} \frac{m^2}{s}$

$\alpha_a = 2.342 \times 10^{-5} \frac{m^2}{s}$ $Pr_a = 0.711$ $\beta := \frac{1}{T_f + 273 \cdot K}$

$H := 0.52 \cdot m$ $B := 0.975 \cdot m$ $L := 1.99 \cdot m$

$A_{freesurface} := B \cdot L$ $P_{freesurface} := 2 \cdot (B + L)$

$L_{ch} := \frac{A_{freesurface}}{P_{freesurface}}$ $L_{ch} = 0.327\ m$

$Ra := \frac{g \cdot \beta \cdot (T_s - T_{amb}) \cdot L_{ch}^{3}}{\nu_a \cdot \alpha_a}$ $Ra = 6.964 \times 10^{7}$

$Nu := 0.15 \cdot Ra^{\frac{1}{3}}$ $Nu = 61.7$

$h_{conv} := Nu \cdot \frac{k_a}{L_{ch}}$ $h_{conv} = 5.061 \frac{W}{m^2 \cdot K}$

$$\frac{h_{conv}}{h_m} = \rho_a \cdot c_p \cdot \left(\frac{\alpha}{D_{aw}} \right)^{1-n} \qquad n := \frac{1}{3} \qquad D_{aw} := 26 \cdot 10^{-6} \cdot \frac{m^2}{s}$$

$$P_{air} := 678 \cdot mmHg \qquad T_{amb} = 24 \cdot oC \qquad \phi := 0.52 \qquad w := 10.5 \cdot \frac{gm}{kg}$$

$$c_p := 1003 \cdot \frac{J}{kg \cdot K} + 1805 \cdot \frac{J}{kg \cdot K} \cdot w \qquad c_p = 1.022 \ \frac{kJ}{kg \cdot K}$$

$$h_m := \frac{h_{conv}}{\rho_a \cdot c_p \cdot \left(\frac{\alpha_a}{D_{aw}} \right)^{1-n}} \qquad h_m = 4.651 \times 10^{-3} \ \frac{m}{s}$$

$$Q_{evap} = h_m \cdot A_{freesurface} \cdot \left(\rho_{ws\_atTsurface} - \rho_{ws\_atTamb} \right) \cdot h_{fg}$$

$$\rho_{ws\_atTsurface} = 0.076 \ \frac{kg}{m^3} \qquad \rho_{ws\_atTamb} = 0.021 \ \frac{kg}{m^3} \qquad h_{fg\_atTs} = 2.387 \times 10^3 \ \frac{kJ}{kg}$$

$$m_{evap} := h_m \cdot A_{freesurface} \cdot \left(\rho_{ws\_atTsurface} - \phi \cdot \rho_{ws\_atTamb} \right)$$

$$m_{evap} = 5.854 \times 10^{-4} \ \frac{kg}{s}$$

$$Q_{evap} := m_{evap} \cdot h_{fg\_atTs} \qquad Q_{evap} = 1397 \ W$$

Convective heat loss from the free water surface

$$Q_{conv} := h_{conv} \cdot A_{freesurface} \cdot \left(T_s - T_{amb} \right) \qquad Q_{conv} = 240 \ W$$

Heat loss rate from the side jackets:

$$m_{waterjackets} := 0.449 \cdot \frac{kg}{s} \qquad T_{wi\_jackets} := 14.3 \cdot oC \qquad T_{wo\_jackets} := 16.1 \cdot oC$$

$$c_{p\_water\_jackets} = 4.186 \times 10^3 \ \frac{J}{kg \cdot K}$$

$$Q_{sideloss} := m_{waterjackets} \cdot c_{p\_water\_jackets} \cdot \left(T_{wo\_jackets} - T_{wi\_jackets} \right)$$

$$Q_{sideloss} = 3383 \ W$$

Heat removal rate from the storage unit:

$$m_{w\_rem} := 165.1 \cdot \frac{kg}{hr} \qquad T_{wi} := 15.5 \cdot oC \qquad T_{wo} := 21.5 \cdot oC$$

$$c_{p\_water\_rem} = 4.183 \times 10^{3} \frac{J}{kg \cdot K}$$

$$Q_{rem} := m_{w\_rem} \cdot c_{p\_water\_rem} \cdot \left(T_{wo} - T_{wi}\right)$$

$$Q_{rem} = 1151\ W$$

Heat loss rate through the glass surfaces:

$$T_{glass\_avg} := 35 \cdot oC \qquad T_{f\_glass} := \frac{T_{glass\_avg} + T_{amb}}{2} \qquad T_{f\_glass} = 29.5\ oC$$

$$\rho_a = 1.168 \frac{kg}{m^3} \qquad k_a = 0.026 \frac{W}{m \cdot K} \qquad \beta := \frac{1}{T_{f\_glass} + 273 \cdot K} \qquad \nu_a = 1.599 \times 10^{-5} \frac{m^2}{s}$$

$$Pr_a = 0.712 \qquad \alpha_a = 2.259 \times 10^{-5} \frac{m^2}{s}$$

$$Ra_{glass} := \frac{g \cdot \beta \cdot \left(T_{glass\_avg} - T_{amb}\right) \cdot H^3}{\nu_a \cdot \alpha_a} \qquad Ra_{glass} = 1.388 \times 10^{8}$$

A suitable correlation for external free convection flow over a vertical plate is used:

$$Nu_H := 0.68 + \frac{0.670 \cdot Ra_{glass}^{\frac{1}{4}}}{\left[1 + \left(\frac{0.492}{Pr_a}\right)^{\frac{9}{16}}\right]^{\frac{4}{9}}} \qquad Nu_H = 56.5$$

$$h_H := Nu_H \cdot \frac{k_a}{H} \qquad h_H = 2.865 \frac{W}{m^2 \cdot K}$$

$$Q_{glass} := h_H \cdot (2 \cdot H \cdot L) \cdot \left(T_{glass\_avg} - T_{amb}\right) \qquad Q_{glass} = 65.2\ W$$

Total heat loss rate from the storage unit is:

$$Q_{total\_loss} := Q_{evap} + Q_{conv} + Q_{sideloss} + Q_{glass}$$

$$Q_{total\_loss} = 5085\ W$$

Net energy input rate to the storage unit:

$$m_w := 211.2 \cdot \frac{kg}{hr} \qquad T_i := 48.4 \cdot oC \qquad T_e := 23.3 \cdot oC$$

$$c_{p\_water\_charging} = 4.178 \times 10^3 \frac{J}{kg \cdot K}$$

$$H_{net} := m_w \cdot c_{p\_water\_charging} \cdot \left(T_i - T_e\right)$$

$$H_{net} = 6152\ W$$

$$Q_{total\_loss} + Q_{rem} = 6236\ W$$

Total heat transfer rate from the storage unit and net energy input to the storage unit are found to be close. Table B.1 shows the energy balance results for three other experiments.

Table B.1 Summary of Energy Balance Results

Exp. No	***t* (min)**	$\dot{Q}_{rem}$ **(W)**	$\sum \dot{Q}_{loss}$ **(W)**	$\dot{Q}_{rem} + \sum \dot{Q}_{loss}$ **(W)**	$\dot{H}_{net}$ **(W)**
1	675	1044	4909	5952	5943
4	660	1252	5154	6406	6219
16	530	1523	4298	5820	5901

APPENDIX C

STEADY-STATE, SPATIAL TEMPERATURE VARIATION IN THE STORAGE UNIT

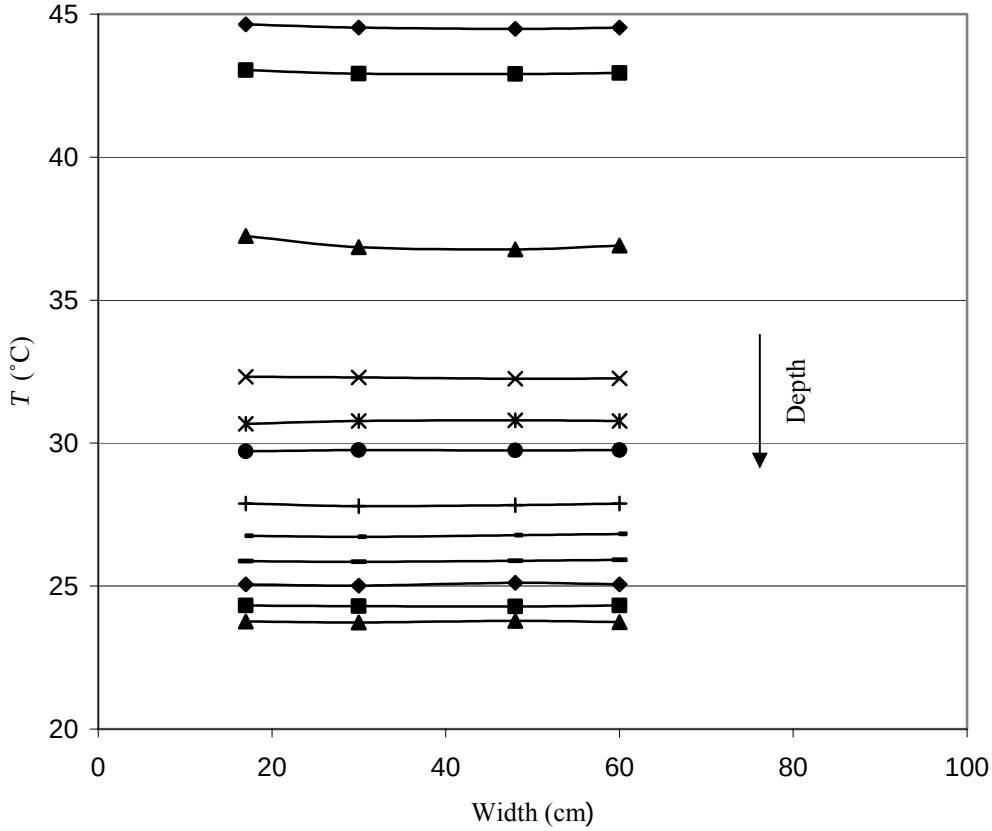

Figure C.1 Temperature Variation along the Width of the Storage Unit (from Exp. 26 at t = 685 min)

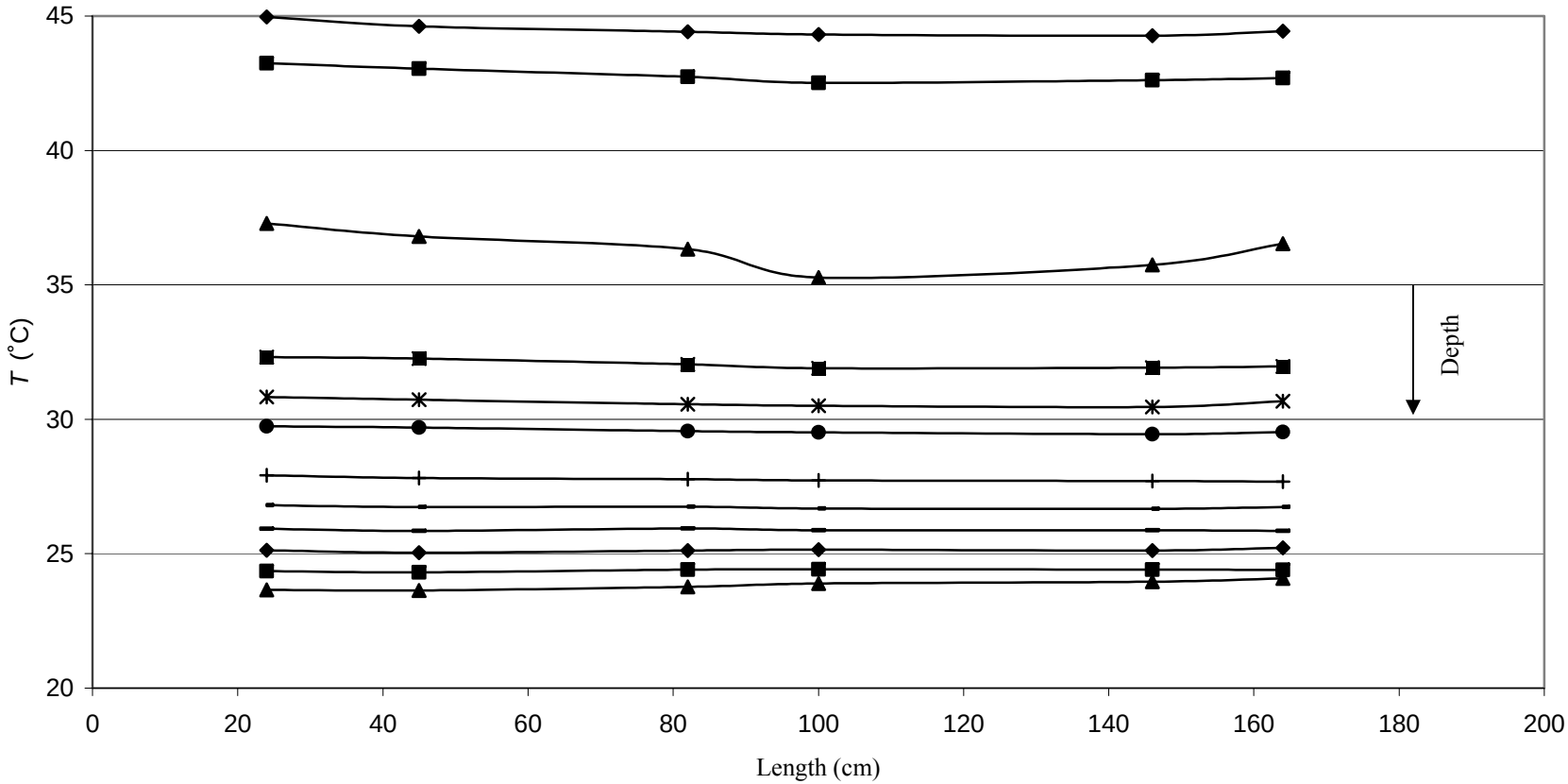

Figure C.2 Temperature Variation along the Length of the Storage Unit (from Exp. 26 at t = 685 min)